Investigating the interactions between paxillin, vinculin and talin in regulating the dynamics of cell-extracellular matrix adhesions.

Masters by Research

2019

Gabriella Laker

Acknowledgements

I would firstly like to thank my supervisor, Dr. Ben Goult, for his invaluable support and guidance throughout this project, and for continually inspiring me with his passion for science. I would also like to thank past and present members of the Goult, Geeves and Mulvihill lab for their friendship, assistance and encouragement.

Abstract

Focal adhesions provide a bi-directional, highly dynamic interface between the extracellular and intracellular environments. The abundance and diversity of proteins recruited to the adhesion sites enable focal adhesions to act as highly efficient mechanosensitive signalling hubs that regulate multiple aspects of cell behaviour including cell movement. Paxillin is one of the proteins identified to localise to focal adhesions. This study explored the interaction of paxillin with the focal adhesion-associated proteins talin, vinculin and focal adhesion kinase, and how such interactions are regulated. Biochemical characterisation using a suite of assays, including fluorescence polarisation, microscale thermophoresis, nuclear magnetic resonance, size exclusion chromatography and pulldowns, identified two novel interactions: 1) the paxillin LIM domains bind talin R9-R12, and 2) multiple paxillin LD motifs cooperatively bind to the head and talin domains of vinculin. We propose a model whereby talin facilitates the localisation of paxillin in proximity of vinculin at adhesions. Once recruited, paxillin functions to control the activation state of vinculin and thus regulate adhesion dynamics, influencing a whole host of cellular activities including cell migration and apopotosis.

Contents

List of figures and tables:

Abbreviations

[ ] : Denotes concentration

ECM : Extracellular matrix

FA : Focal adhesion

F-actin : Filamentous actin

FAK : Focal Adhesion Kinase

FAT : Focal adhesion targeting

FP : Fluorescence Polarisation

FRET : Fluorescence Resonance Energy Transfer

GST : Glutathione S-transferase

K_d : Dissociation constant

MST : Microscale Thermophoresis

NMR : Nuclear Magnetic Resonance

OD_{600} : Optical density at 600nm

PBS : Phosphate buffered saline

SDS-PAGE : Sodium dodecyl sulfate polyacrylamide gel electrophoresis

SEC-MALS : Size Exclusion Chromatography with Multi-Angle Light Scattering

VBS : Vinculin binding site

VD1 : Vinculin domain 1

VD2 : Vinculin domain 2

VD3 : Vinculin domain 3

VD4 : Vinculin domain 4

Vt : Vinculin tail domain

YFP : Yellow fluorescent protein

1. Introduction

1.1. Focal Adhesions

The ability of cells to attach to each other and to the extracellular matrix (ECM) is essential for multicellular existence. Focal adhesions (FAs) provide a bi-directional, highly dynamic interface between the extracellular chemical and physical environment and the intracellular scaffolding and signalling machinery. Cross-talk between the two environments is crucial for cellular decision-making in the cell-cycle, differentiation and death, and occurs with remarkable spatial and temporal precision. In addition to functioning as multi-protein signalling hubs, FAs serve to transmit mechanical force between the cytoskeleton and the cellular surroundings to drive tissue morphogenesis, cell movement and ECM remodelling (Kenneth M. Yamada et al., 2019).

Nascent FAs form at the leading edge of migrating cells as small (<250 nm) structures rich in integrin (see section 1.2), focal adhesion kinase (FAK) (see section 1.5) and paxillin (see section 1.6) (Choi et al., 2008). Adhesion maturation occurs in an actomyosin-dependent manner, generating adhesions several microns in length and 200 nm thick, organised into three distinct nano-domains each characterised by variations in protein localisation. FAK and paxillin localise at the distal tips within the membrane-proximal integrin signalling layer, actin-binding proteins including α-actinin and zyxin localise at the proximal tips approximately 50-60 nm from the plasma membrane in the actin regulatory layer, and the mechanosensitive rod domain of talin (see section 1.3) localises to the force transduction layer that spans between the integrin signalling layer and actin regulatory layer (Kanchanawong et al., 2010) (figure 1).

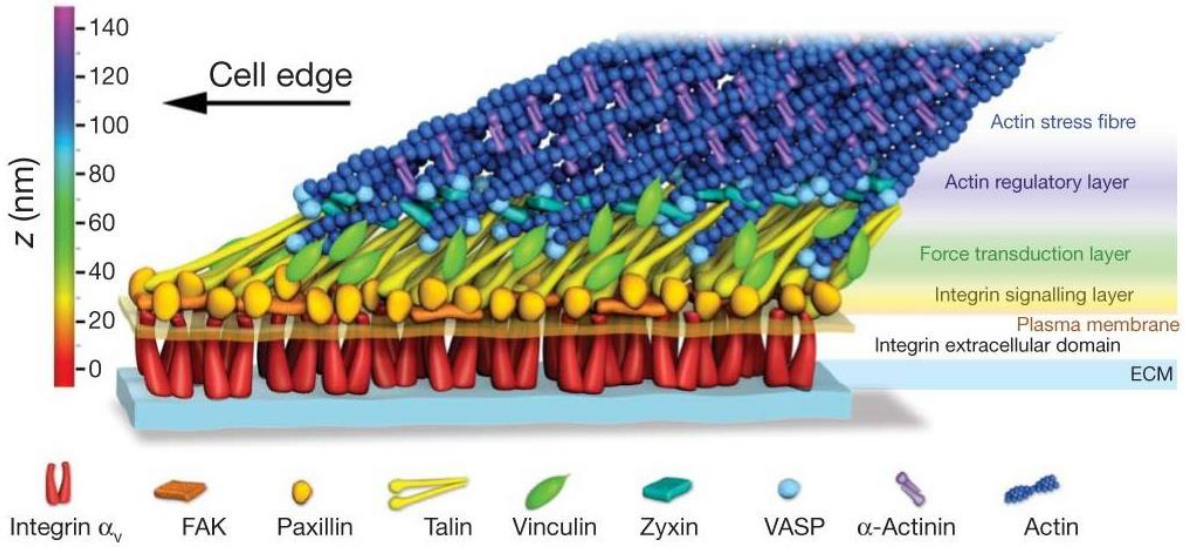

Figure 1. Nanoscale architecture of focal adhesions (Kanchanawong et al., 2010).

The diverse functionality of FAs is reflected in their biochemical complexity. Analysis of the 'integrin adhesome' using mass spectrometry has identified a network of > 240 proteins involved in focal adhesion formation and regulation (Horton et al., 2016). The abundance and diversity of these proteins enables FAs to act as highly efficient, mechanosensitive signalling hubs that regulate multiple aspects of cell behaviour involving biochemical and physical interactions between the cell and its environment.

1.2. Integrin

Integrins are heterodimeric membrane spanning adhesion receptors, central to focal adhesion formation. They are comprised of a noncovalently associated α and β subunit, each containing a large 80-150 kDa extracellular ectodomain, a single transmembrane-spanning α-helix and a largely unstructured cytoplasmic tail, 10-70 residues in length (Wegener & Campbell, 2008) (figure 2). Within mammals, one of 18 α subunits heterodimerises with one of 8 β subunits to form 24 integrins, each showing distinct patterns of cell-type and tissue-specific expression and adhesion characteristics (Hynes, 2002). Integrins connect to the ECM via their ectodomains,

whilst simultaneously providing a scaffold for the assembly of large multiprotein complexes on the cytoplasmic tails. The ability to connect the cell interior to the extracellular environment allows integrins to function in creating both a structural connection and a bi-directional signalling pathway across the cell membrane.

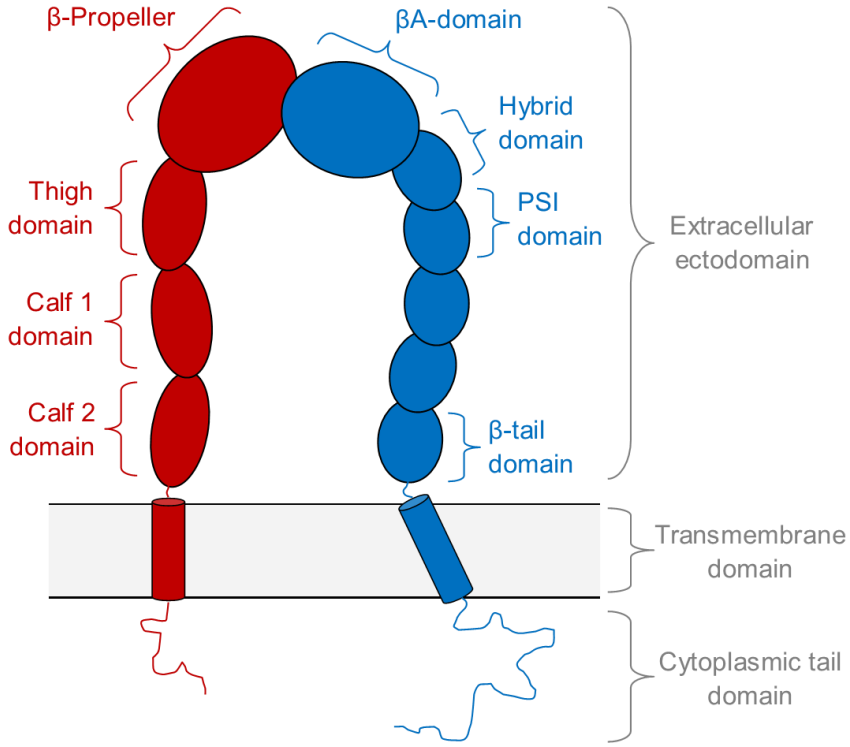

Figure 2. Structural model of integrin. The β-Propeller domain of the α subunit (red) and the βA-domain of the β subunit (blue) assemble to form the extracellular ligand binding site.

Integrins are highly dynamic regulators of cell function and are capable of driving fundamental cellular responses including cell spreading, migration, proliferation and apoptosis (Durrant, van den Bosch, & Hers, 2017). Such cellular processes are dependent on the conformational state, and thus the activation state of integrin, a process which is tightly regulated to reflect the activation state of the cell. The integrin ectodomain can exist in three conformations; 1) a low-affinity closed conformation, 2) an activated intermediate conformation and 3) an activated and ligand occupied open conformation. The crystal structure of the extracellular ectodomain of αVβ3 integrin in

its closed conformation was published in 2001 (figure 3). The structure reveals that a deadbolt exists at the interface between the membrane-proximal β-tail domain and the ligand-binding βA domain of the β subunit (Xiong et al., 2001). Consequently, the binding site formed by the β-Propeller domain of the α subunit and the βA-domain of the β subunit has little affinity for extracellular ligands. In this conformation, the transmembrane helices of the α and β subunits interact to form a right-handed coiled coil, bringing the cytoplasmic tails of the two subunits into close spatial proximity (Adair & Yeager, 2002) (figure 3).

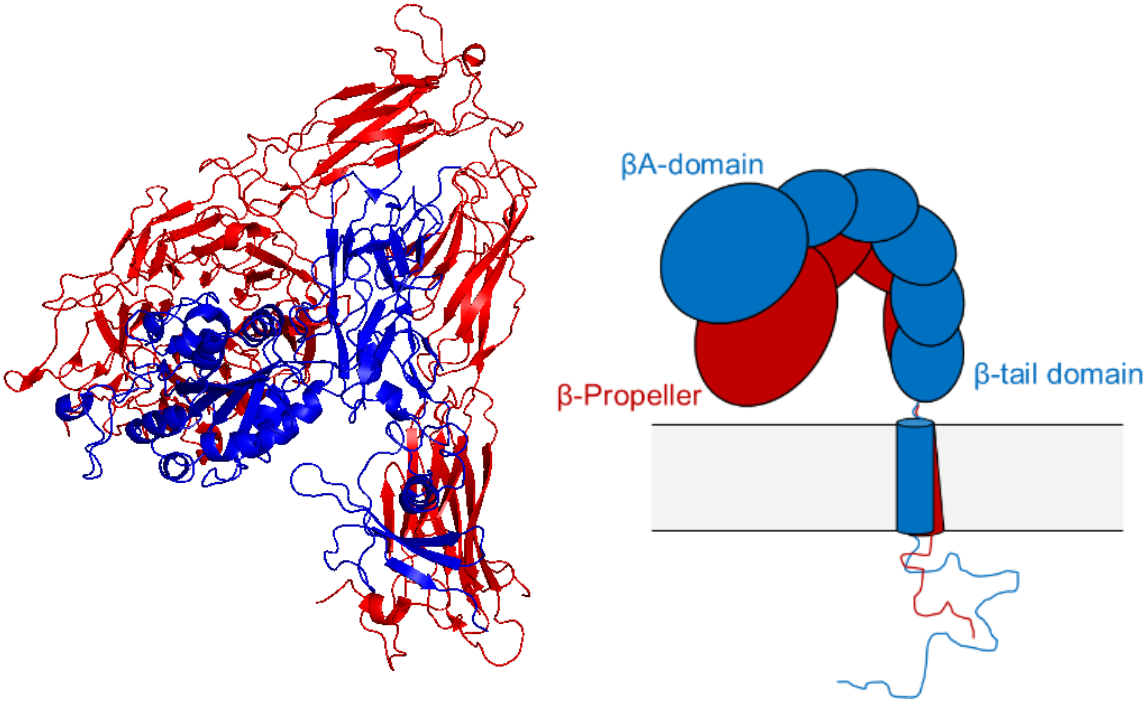

Figure 3. Structural model of inactive integrin. Crystal structure of the extracellular ectodomain of integrin αVβ3 in its closed conformation (Xiong et al., 2001) (left panel). The α and β subunits are coloured red and blue, respectively. Schematic arrangement of the inactive integrin showing the transmembrane helices and cytoplasmic tails in the closed conformation (right panel).

The bidirectionality of integrin-mediated signalling across the cell membrane can occur via either “outside-in” or “inside-out” mechanisms. Outside-in signalling resembles traditional receptor signalling and involves engagement of extracellular matrix ligands

by the ectodomain of integrin, triggering conformational changes in the cytoplasmic regions which result in downstream signalling events including cytoskeletal reorganisation, kinase cascade activation and cell cycle modulation (K M Yamada & Geiger, 1997). In contrast, inside-out signalling involves binding of intracellular activators to the cytoplasmic β-tail, triggering tail separation and propagation of conformational changes to the extracellular ectodomain which release the deadbolt between the β-tail domain and the ligand-binding βA domain of the β subunit, increasing ligand affinity and thus activating integrin (Anthis et al., 2009) (figure 4).

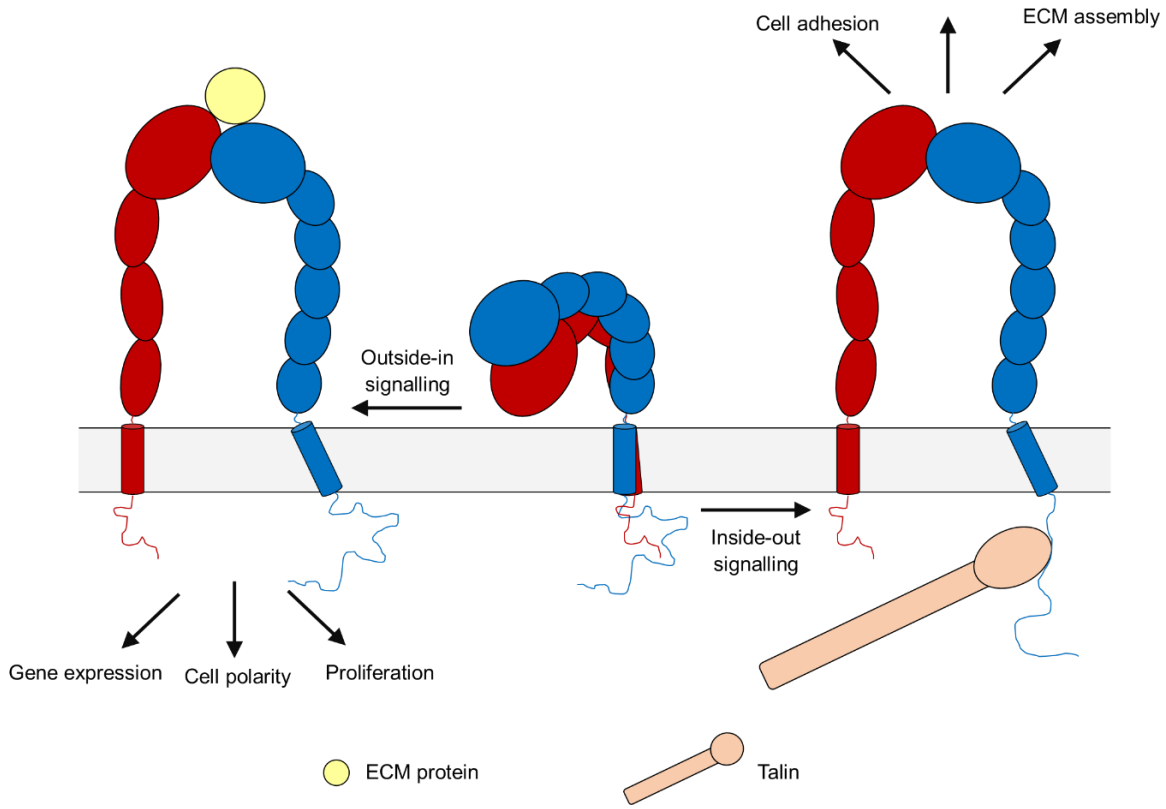

Figure 4. Integrin activation via outside-in and inside-out signalling mechanisms. Image adapted from (Shattil, Kim, & Ginsberg, 2010).

Of the many cytoplasmic proteins that bind to the integrin tail during inside-out signalling, talin is central to integrin activation, focal adhesion formation and mechanotransduction.

1.3. Talin

Talin was first identified as a 270 kDa cytoplasmic protein concentrated at regions of cell-substratum contact (Burridge & Connell, 1983). Talin comprises an N-terminal FERM (4.1 protein, ezrin, radixin, moesin) domain (the head, F0-F3), connected to an elongated series of 62 α-helices arranged into 13 helical bundles (the rod, R1-R13) by an 82-residue unstructured linker. The FERM domain is atypical in structure, comprising four subdomains arranged linearly rather than the more traditional three-lobed cloverleaf seen in other FERM proteins. Full length talin exists as a dimer, facilitated by the C-terminal dimerization domain (DD) (Bate et al., 2012; Elliott et al., 2010; Goult et al., 2013) (figure 5).

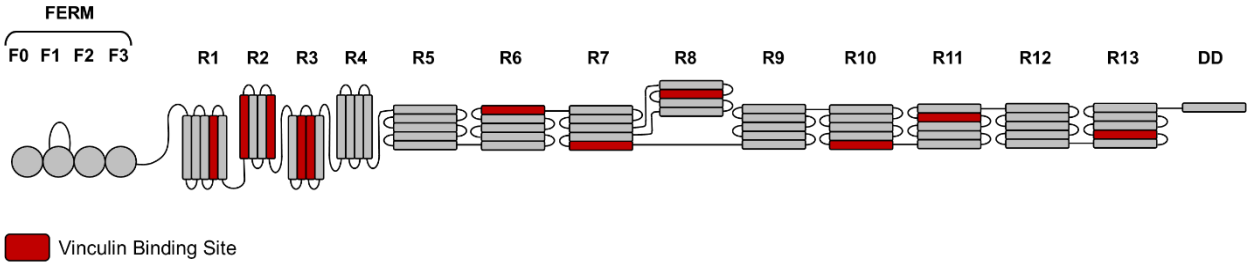

Figure 5. Structural model of talin. The N-terminal head comprising F0-F3 and the rod domains R1-R13 are shown. Vinculin binding sites are shown in red. DD; dimerization domain. Image adapted from (Gough & Goult, 2018).

Talin has been shown to activate integrin directly via an interaction between the phosphotyrosine binding F3 domain of the talin head and the membrane-proximal NPxY motif within the cytoplasmic β-tail (Calderwood et al., 1999). This interaction sterically interferes with the α/β cytoplasmic interface, inducing conformational changes that are propagated through the transmembrane domains to the ligand-binding extracellular ectodomains.

The ability of talin to activate integrin is dependent on the conformational state of talin itself. Autoinhibition of talin is mediated via the interaction between F3 in the head domain and R9 in the rod domain. In this conformation, talin is maintained in a compact globular state within the cytosol, and the integrin-binding site within F3 is masked (Goksoy et al., 2008b; Goult et al., 2009) (figure 6). Phosphatidylinositol 4,5-bisphosphate (PIP2) has been shown to relieve this autoinhibition by sterically displacing the inhibitory R9 rod domain to expose the integrin binding site within F3 (Goksoy et al., 2008b).

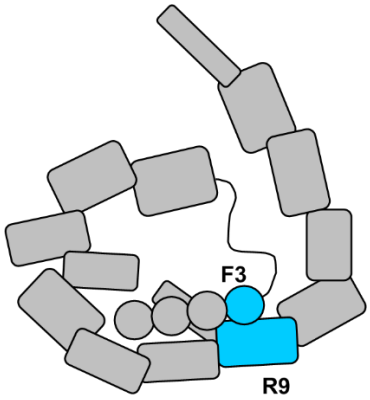

Figure 6. Autoinhibition of talin. F3 of the head domain and R9 of the rod domain, both shown in blue, interact directly to hold talin in a compact autoinhibited conformation. For clarity, only one talin monomer is shown. Image adapted from (Gough & Goult, 2018).

In addition to binding integrin via the head domain, talin binds to the actin cytoskeleton via R4-R8 (Hemmings et al., 1996) and R13-DD (Gingras et al., 2008; McCann & Craig, 1997) of the rod domain, through which a physical linkage is established between the intracellular cytoskeleton and the extracellular matrix.

As a series of helical bundles, the talin rod is sensitive to mechanical force and can transition between folded and unfolded conformations accordingly (Goult, Yan, & Schwartz, 2018; Yao et al., 2015) (figure 7). Consequently, binding sites across the length of the rod domain are not accessible at all times but are instead both masked

and revealed in response to different cellular cues. Ligands that bind to folded talin, including actin, RIAM and KANK, are therefore lost during force-induced unfolding, and cryptic binding sites are revealed. Once talin has captured both the ECM and the actin cytoskeleton, force exerted on the rod domain, initially by actin retrograde flow and then by actomyosin contractility, drives structural transitions of each helical bundle (Gough & Goult, 2018).

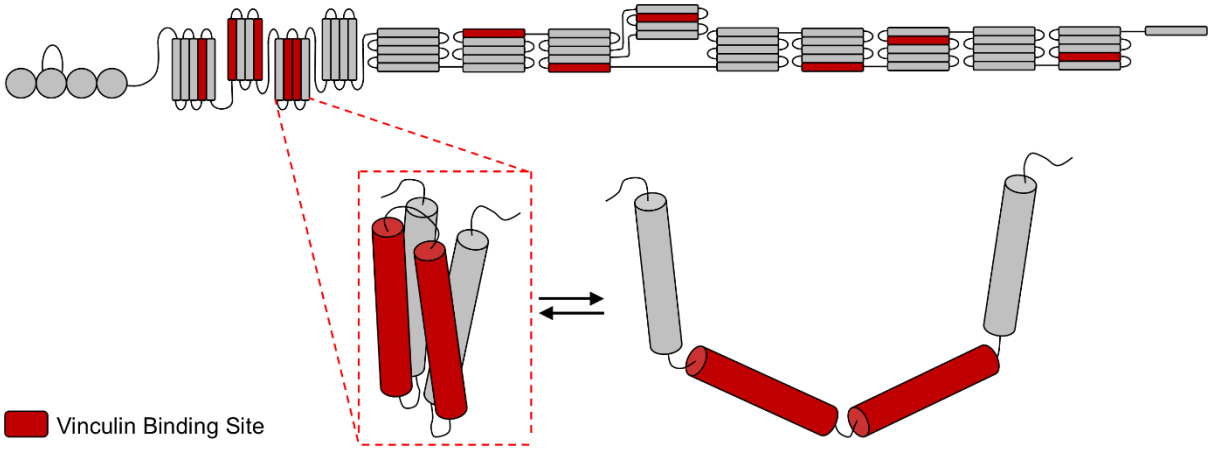

Figure 7. The talin rod domains are mechanosensitive. The helical talin rod domains unfold in response to force, starting with the initial mechanosensor, R3 (Yao et al., 2016). Domain unfolding exposes cryptic vinculin-binding sites required for adhesion maturation. Image adapted from (Goult et al., 2018).

A key protein known to bind to the talin rod domain following force-induced exposure of cryptic binding sites is the cytoplasmic protein vinculin, required for adhesion maturation and strengthening.

1.4. Vinculin

Vinculin was first isolated from chicken gizzard smooth muscle as an intracellular protein that co-purified with the actin-binding protein α-actinin (Benjamin Geiger, 1979). Further characterisation revealed that vinculin localised to specialised regions where microfilament bundles terminate at membrane attachment sites (Burridge &

Feramisco, 1980; B Geiger, Tokuyasu, Dutton, & Singer, 1980), giving rise to the Latin name *vinculum*, meaning “bond”.

Vinculin is a globular 116-kDa cytoplasmic protein comprised of eight antiparallel α-helical bundles organised into a 90-kDa N-terminal head domain (VD1-4) connected to a 27-kDa C-terminal tail domain (Vt) by a flexible proline-rich linker (Bakolitsa et al., 2004). VD1, 2 and 3 each contain two four-helix bundles connected by a long, centrally shared α-helix. The three subdomains are organised in a trilobed planner arrangement and associate with the four-helix VD4 bundle (figure 8). The proline-rich linker is flexible and allows for global conformational changes that regulate the activation state of vinculin.

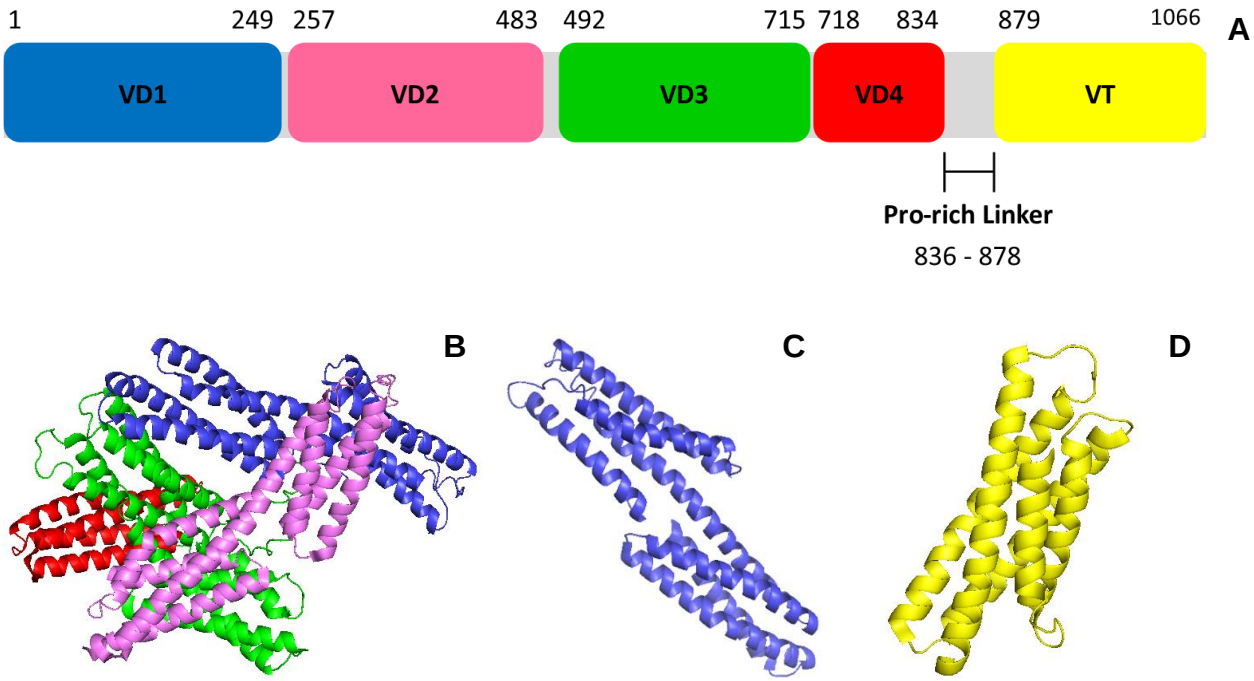

Figure 8. Domain structure of vinculin. (A) Domain organisation of full-length vinculin. Domain boundaries are indicated. **(B)** VD1 (blue), VD2 (pink), VD3 (green) and VD4 (red) associate to form the globular N-terminal head domain. **(C)** VD1 is comprised of two four-helix bundles connected by a long, centrally shared α-helix. **(D)** The C-terminal tail domain (yellow) is a five-helix bundle.

Vinculin is a dynamic focal adhesion-associated protein that undergoes remarkable conformational changes upon ligand binding. Such conformational changes are facilitated by both the flexibility of the linker region and by the plasticity of the helical bundles. The head domain, tail domain and proline-rich linker all provide distinct binding platforms in their own right, and function cooperatively to control many aspects of cell-ECM adhesion including the assembly, turnover, strength and force-transmission of focal adhesions.

1.4.1. Vinculin Binding Sites.

The rod domain of talin contains 11 putative vinculin binding sites (VBS) (Patel et al., 2006). Each VBS is defined by hydrophobic residues along one side of the helix, which are buried within the helical bundle in the absence of mechanical force (Roberts & Critchley, 2009). In response to actomyosin contraction, the talin domains unfold (figure 7) and the exposed VBS helices bind vinculin by inserting into a hydrophobic groove between helices 1 and 2 of VD1 (Izard et al., 2004). Talin binding functions to recruit vinculin to adhesion sites, bringing vinculin into proximity with the actin cytoskeleton.

The five-helix vinculin tail domain contains two spatially separate actin binding sites, each contacting a different actin monomer along the filament (Janssen et al., 2006). F-actin binding triggers activation of a cryptic dimerization site within the vinculin tail, enabling vinculin to crosslink actin bundles and thus provide mechanical stability required for adhesion durability (figure 9).

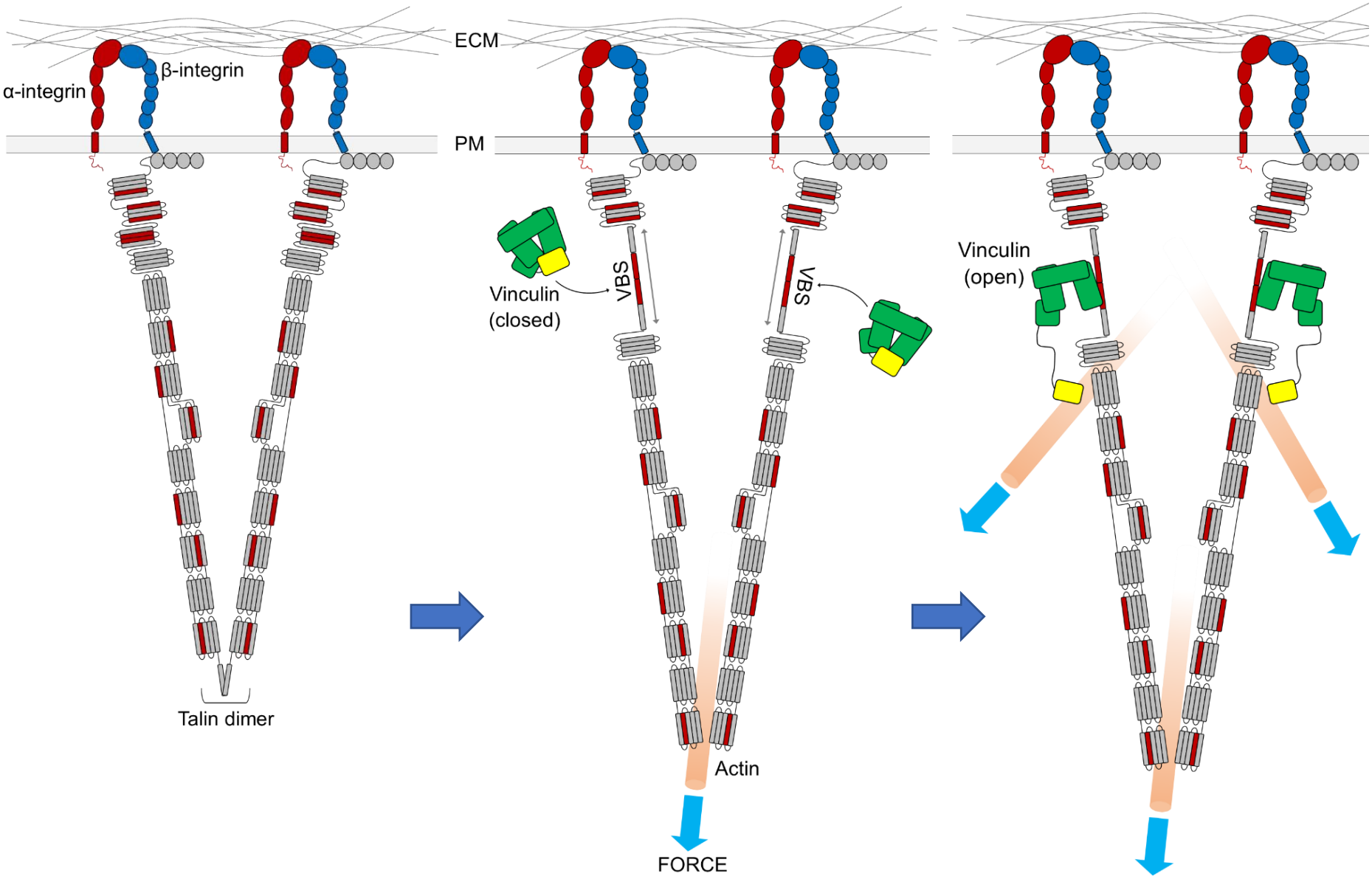
α-integrin
β-integrin
Talin dimer
ECM
PM
Vinculin
(closed)
VBS
VBS
Actin
FORCE
Vinculin
(open)

Figure 9. Engagement of multiple vinculin domains by both talin and F-actin facilitates FA robustness. F3 of the talin head domain switches integrin to a high affinity state by binding directly to the cytoplasmic β-tail. Once talin has engaged integrin, actin binding to the rod domain exerts a pulling force sufficient to unfold the mechanosensitive bundles and thus expose cryptic VBS (red). Vinculin is recruited to the adhesion site once the VBS becomes accessible. Binding of the vinculin head domain (green) to the VBS and binding of the vinculin tail domain (yellow) to actin filaments, synergistically outcompetes the autoinhibitory head-to-tail interaction and thus switches vinculin to an open conformation. Actin binding via the vinculin tail domain triggers activation of a cryptic dimerization site, resulting in bundling of actin filaments and increased mechanical stability. Image adapted from (Klapholz & Brown, 2017).

In addition to binding talin and actin, vinculin has been shown to bind the focal adhesion adapter protein, paxillin (see section 1.8). Full-length vinculin can be cleaved within the proline-rich linker by digestion with *Staphylococcus aureus* V8 protease to yield isolated head and tail domains. Coomassie staining of the V8-digested vinculin followed by transfer to nitrocellulose and coating with radioiodinated paxillin determined that the ^{125}I-paxillin bound to full-length vinculin and to the 27 kDa tail domain, but not the 90 kDa head domain (figure 10) (C E Turner, Glenney, & Burridge, 1990).

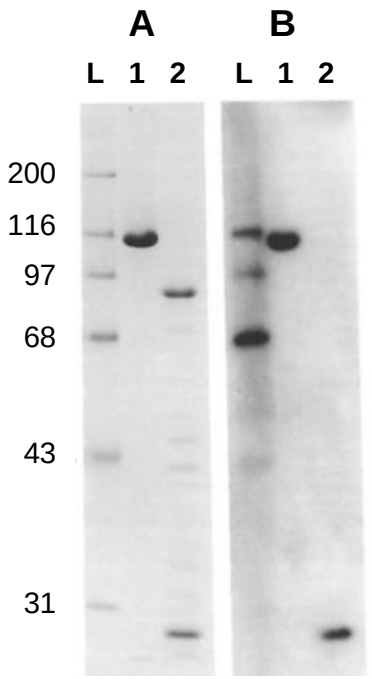

Figure 10. The C-terminal vinculin tail domain binds paxillin. *Staphylococcus aureus* V8 protease-digested vinculin was coelectrophoresed with full-length vinculin. **(A)** Coomassie stained SDS-PAGE gel showing intact vinculin (lane 1) and 90 kDa and 27 kDa fragments following digestion (lane 2). **(B)** Identical samples were transferred to nitrocellulose and overlaid with radioiodinated paxillin. ^{125}I-paxillin bound to full-length vinculin (lane 1) and to the 27 kDa vinculin fragment (lane 2). L; ladder (kDa) (C E Turner, Glenney, & Burridge, 1990).

The isolated vinculin head domain readily binds talin, however binding is significantly reduced in the full-length molecule. Similarly, the ability of the isolated vinculin tail domain to cross-link actin filaments are lost in the full-length assembly. Crystal structures of full-length chicken vinculin (Bakolitsa et al., 2004), full-length human vinculin (Borgon, Vonrhein, Bricogne, Bois, & Izard, 2004a) and residues 1-258 of the head domain in complex with residues 879-1066 of the tail domain (Izard et al., 2004) have been solved. These structures reveal that an interface exists between VD1 and Vt, maintained by hydrophobic interactions and hydrogen bonds, which holds vinculin in an autoinhibited head-to-tail conformation (Miller, Dunn, & Ball, 2001). This inactive conformation is also supported by polar contacts between the tail domain and VD3,

and by hydrogen bonds and electrostatic interactions between the tail domain and VD4 (Miller et al., 2001) (figure 11). These observations led to a model whereby vinculin exists in two conformations: 1) an autoinhibited conformation in which ligand binding sites are masked, and 2) an open conformation in which these binding sites are exposed (Bakolitsa et al., 2004) .

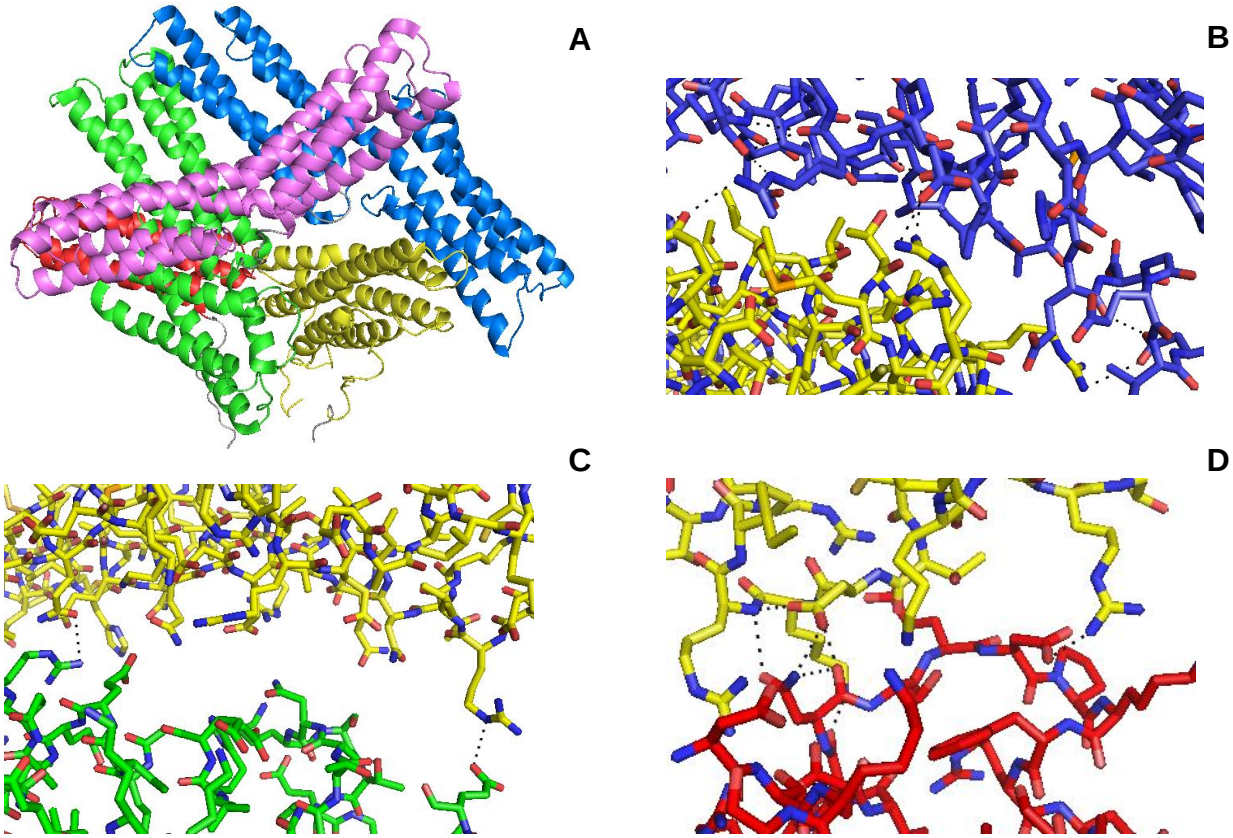

Figure 11. Vinculin exists in an autoinhibited head-to-tail conformation. (A) VD1 (blue), VD3 (green) and VD4 (red) interact with Vt (yellow) to restrain vinculin in a compact globular conformation. **(B)** VD1 binds Vt via hydrophobic interactions and hydrogen bonds. **(C)** VD3 binds Vt via polar contacts. **(D)** VD4 binds Vt via hydrogen bonds and electrostatic interactions. Polar contacts are represented as black dashed lines.

Vinculin has no enzymatic activity; consequently, activation results from conformational rearrangements of the helical bundles that disrupt the autoinhibited conformation. It has been proposed that two ligands are required to disrupt the head-tail interface, since no known ligands bind vinculin with an affinity comparable to the

head-tail interaction (< 1 nM) (Bakolitsa et al., 2004). F-actin and talin have together been shown to activate vinculin in a dose-dependent manner, with talin binding the VD1 interface and F-actin binding the Vt interface (Chen, Choudhury, & Craig, 2006).

1.5. Focal Adhesion Kinase (FAK)

Focal adhesion kinase (FAK) was first identified as a major integrin-dependent tyrosine phosphorylated 125 kDa protein in cells transformed by the v-Src oncogene (Guan, Trevithick, & Hynes, 1991; Kanner, Reynolds, Vines, & Parsons, 1990). Further characterisation revealed that it predominately localised to focal adhesions and was therefore named focal adhesion kinase (M. D. Schaller et al., 1992). FAK is comprised of an N-terminal FERM domain similar in structure to that of talin, a central kinase domain and a C-terminal domain containing the focal adhesion targeting (FAT) domain and two proline-rich docking sites for SH3 domain-containing proteins. Numerous sites of tyrosine phosphorylation have been identified throughout FAK, including the major autophosphorylation site Tyr397 (figure 12).

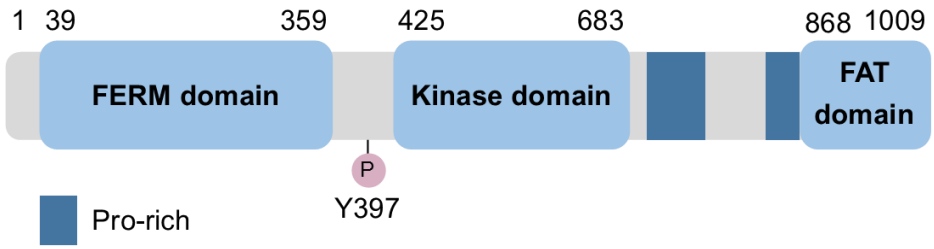

Figure 12. Domain structure of focal adhesion kinase (FAK). The domain boundaries are indicated. Tyrosine phosphorylation (P) at position 397 is essential for FAK activity. Proline-rich SH3 docking sites are indicated.

The crystal structure of FAK has been solved and reveals that FAK exists in an autoinhibited state in which the N-terminal FERM domain binds to the central kinase domain. F1 within the FERM domain binds to a linker segment containing Tyr397, and Phe596 within the kinase domain binds to a hydrophobic pocket within F2. In this

conformation, target ligands cannot access the catalytic cleft or the autophosphorylation site and thus intrinsic kinase activity is inhibited.

Autoinhibition of FAK is relieved by binding of the cytoplasmic β-integrin tail to the N-terminal FERM domain. Binding displaces the FERM domain and thus facilitates exposure and autophosphorylation of Tyr397. FAK can then bind to the SH2 domains of Src family kinases, which phosphorylate additional sites along FAK required for full activation. The SH2 and SH3-domain binding sites and the intrinsic kinase activity enable FAK to serve as both a scaffold protein and a non-receptor tyrosine kinase important for recruitment and activation of diverse signalling proteins involved in adhesion migration.

1.6. Paxillin

Paxillin was first identified as a 68-70 kDa phosphotyrosine-containing protein in Rous Sarcoma Virus-transformed cells (Glenney & Zokas, 1989). Further characterisation revealed that paxillin functions as a cytoskeletal component that localises to focal adhesions at the tips of actin stress fibres (figure 13). This idea of becoming tethered to the membrane resulted in the name paxillin after the Latin “paxillus”, meaning a small stake or peg (C E Turner et al., 1990).

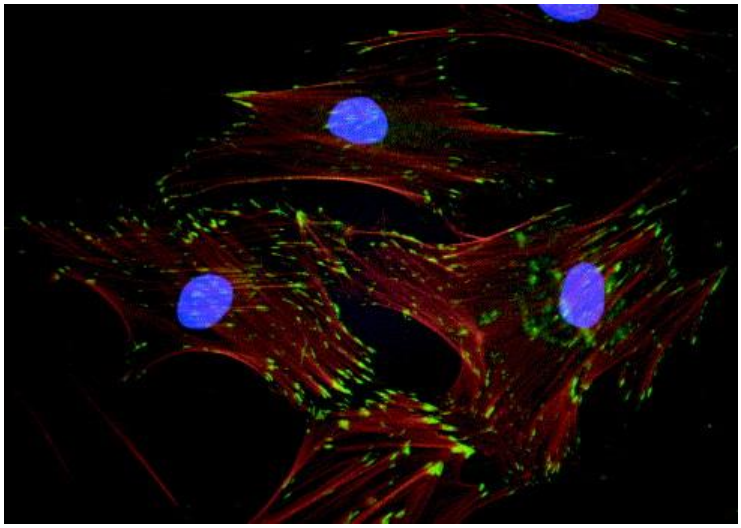

Figure 13. Subcellular localisation of paxillin. Paxillin (green) localises to focal adhesions at the ends of actin stress fibres (red). (Tumbarello, Brown, & Turner, 2002).

Paxillin was soon implicated in integrin-mediated signalling after tyrosine phosphorylation of paxillin was observed in response to integrin-dependent cell adhesion to extracellular matrix proteins (Burridge, Turner, & Romer, 1992). Together, these early studies provided our current view of paxillin; a focal adhesion-associated adaptor protein that functions as a scaffold to recruit diverse cytoskeletal and signalling proteins to adhesion sites and thus coordinate the transmission of downstream signals (Michael D Schaller, 2001).

Paxillin is comprised of 591 residues organised into two distinct domains (figure 14).

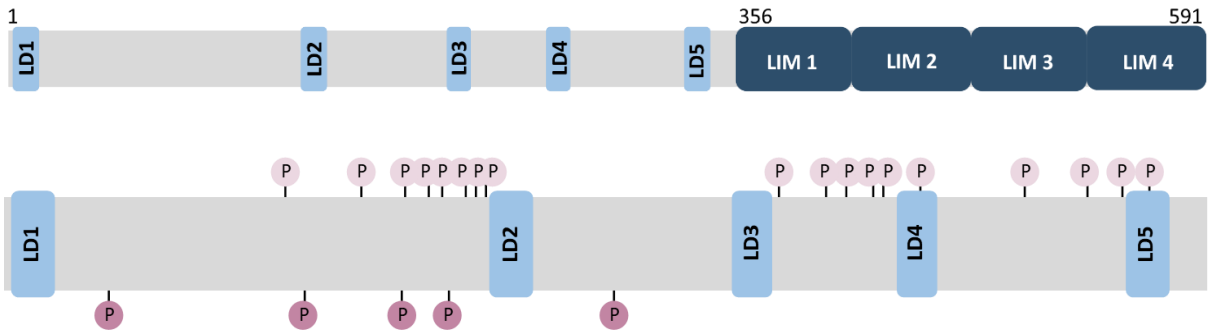

Figure 14. Domain structure of paxillin. (A) Domain organisation of full length paxillin. LD motifs are coloured light blue. LIM domains are coloured dark blue. **(B)** Phosphorylation sites located throughout the N-terminal LD domain. Tyrosine

phosphorylation sites are coloured purple. Serine phosphorylation sites are coloured pink.

The N-terminal domain (residues 1-355) is an unstructured region containing five highly conserved, leucine and aspartic acid-rich LD motifs (termed LD1-5), which share the consensus sequence LDXLLXXL (except LD3, where the LD is substituted by a VE) (figure 15).

	-2	-1	0	+1	+2	+3	+4	+5	+6	+7	+8	+9	+10	+11	+12
LD1	D	D	**L**	**D**	**A**	**L**	**L**	**A**	**D**	**L**	E	S	T	T	S
LD2	S	E	**L**	**D**	**R**	**L**	**L**	**L**	**E**	**L**	N	A	V	Q	H
LD3	P	S	V	E	**S**	**L**	**L**	**D**	**E**	**L**	E	S	S	V	P
LD4	R	E	**L**	**D**	E	**L**	M	A	S	**L**	S	D	F	K	M
LD5	S	Q	**L**	**D**	S	M	**L**	G	S	**L**	Q	S	D	L	N

Figure 15. Alignment of the five paxillin LD motifs. The LDXLLXXL consensus sequence begins at point 0. Residues belonging to the consensus sequence are in bold. Negatively charged residues are in red. Positively charged residues are in green. Residues predicted by CFSSP (Ashok Kumar, 2013) to form an α-helix are underlined.

The five LD motifs function as discrete binding platforms which engage multiple ligands, including vinculin (Glenney & Zokas, 1989) and the non-receptor tyrosine kinase FAK (C E Turner & Miller, 1994). Several tyrosine phosphorylation sites, conforming to SH2 domain-binding sites, and serine phosphorylation sites important in integrin-mediated signalling, are also located throughout the N-terminal domain of paxillin. Additionally, a fairly well conserved proline-rich region is located between LD1 and LD2 (figure 18), which may serve as an SH3 domain-binding site. Upon binding, the unstructured LD motifs form alpha helices which dock against hydrophobic interfaces and stabilise via electrostatic interactions and salt bridges (figure 16).

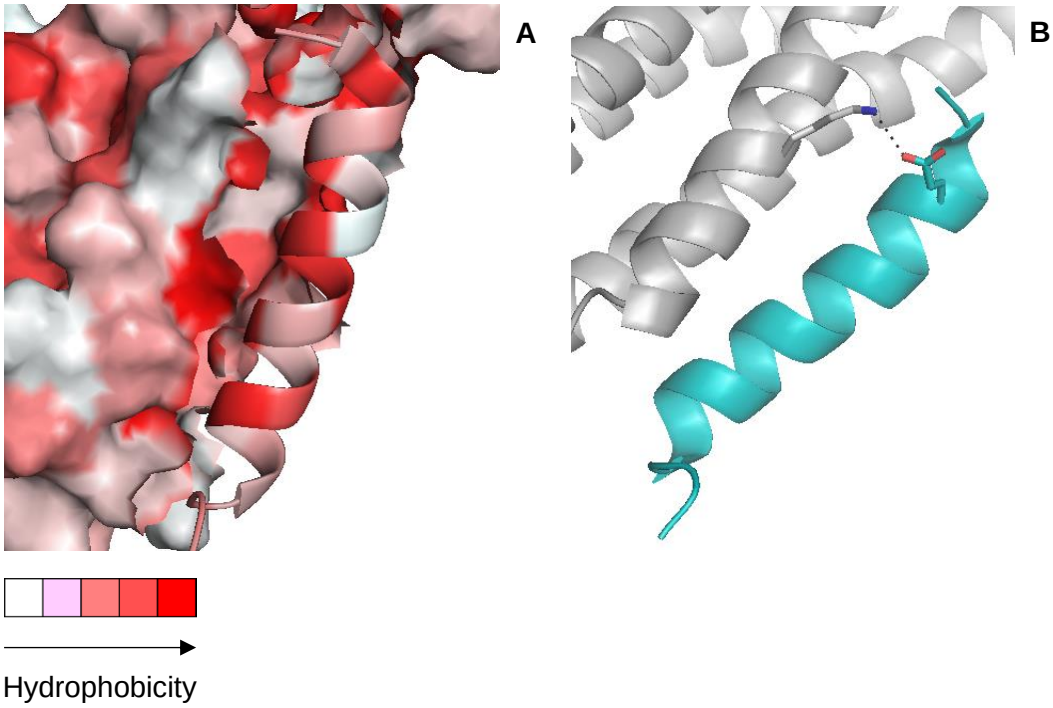

Figure 16. LD binding characteristics. (A) α-helical LD motifs dock against hydrophobic interfaces (hydrophobic residues are coloured red). **(B)** LD binding is stabilised by salt bridges (shown as a black dashed line) across the binding interface.

The C-terminal domain (resides 356-591) is comprised of four consecutive LIM domains, which are zinc-binding structures that resemble a double zinc finger domain (sequence motif C-X_2-C-X_{17-19}-H-X_2-C-X2-C-X2-C-X_{15-19}-C) (figure 17). LIM domains were first observed to possess conserved cysteine and histidine residues in the transcription factors *lin-11, Isl-1* and *mec-3* gene products, hence the name 'LIM' (Karlsson, Thor, Norberg, Ohlsson, & Edlund, 1990).

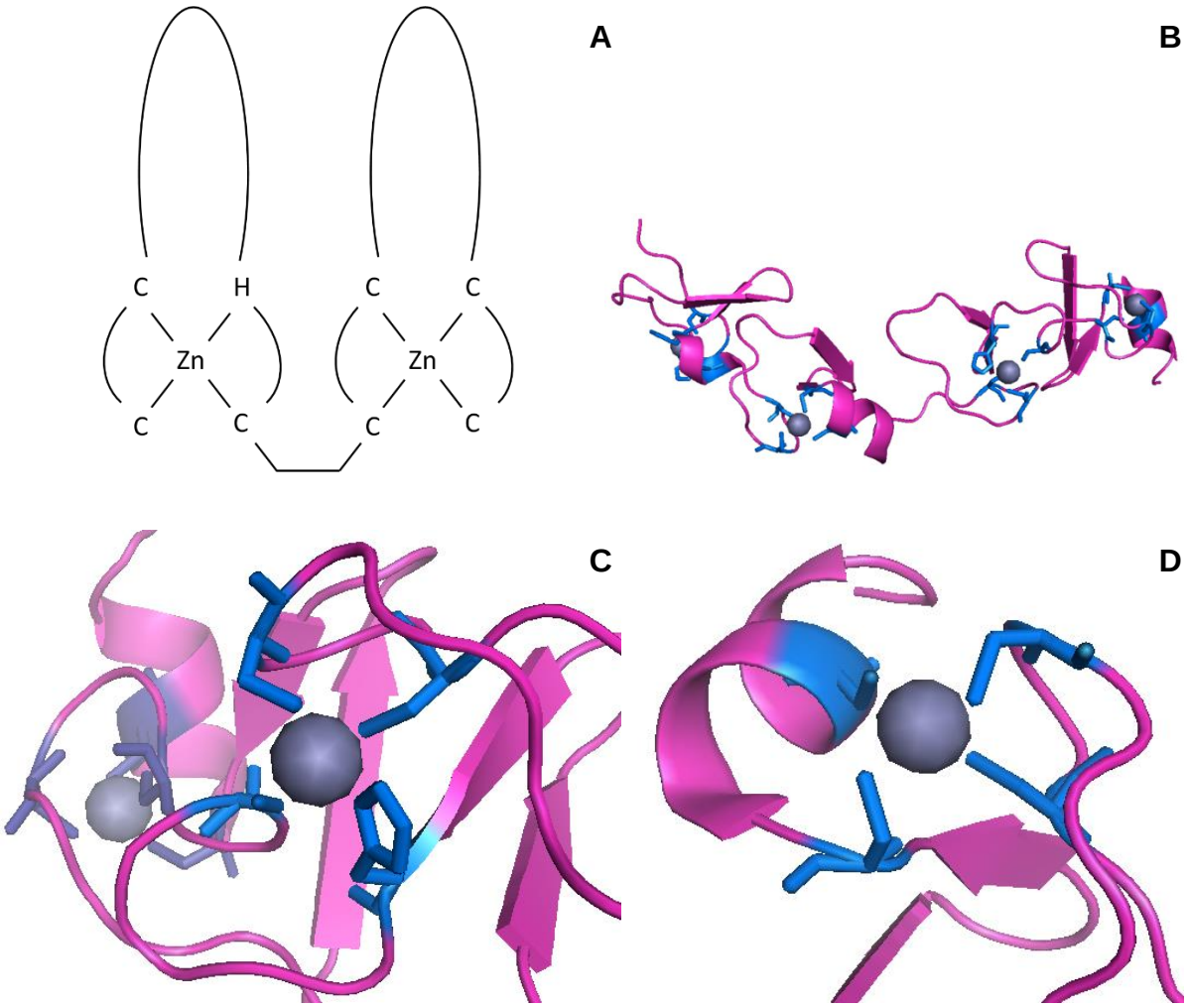

Figure 17. LIM domain structure. (A) Schematic diagram of a double zinc finger domain. **(B)** Crystal structure of LIM 2 and 3 of testin. Each LIM domain binds two zinc ions. **(C)** One zinc ion of LIM 3 of testin coordinated by three cysteine residues and one histidine residue. **(D)** The second zinc ion of LIM 3 of testin coordinated by four cysteine residues. Residues involved in zinc binding are shown as blue sticks. Zinc ions are shown as grey spheres.

Within paxillin, the four LIM domains are thought to function as a modular protein binding site, and are known to engage the tyrosine phosphatase PTP-PEST, tubulin and several uncharacterised serine/threonine kinases (Côté, Turner, & Tremblay, 1999; Herreros et al., 2000; Christopher E. Turner, 2000).

Paxillin does not exhibit enzyme activity, but the vast array of protein docking sites conserved throughout nature (figure 18) provide a scaffold to facilitate the assembly of multiprotein complexes crucial for cellular signalling.

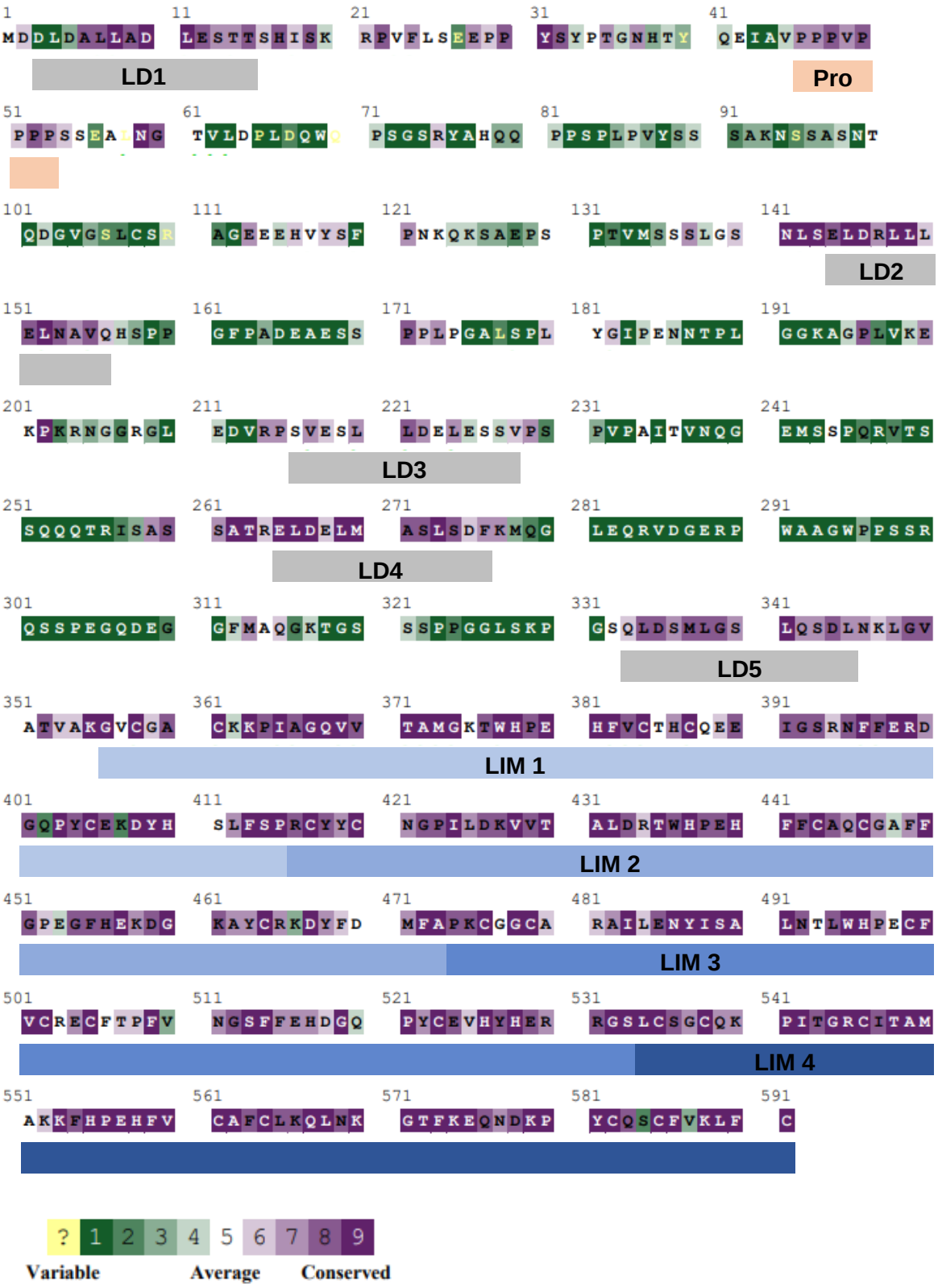

Figure 18. Paxillin sequence coloured according to conservation. The LD motifs, proline-rich region and LIM domains are coloured grey, orange and blue, respectively.

1.7. Paxillin-FAK

Previous data indicate that paxillin and FAK function together to modulate FA dynamics (Hu et al., 2015). It has been shown that paxillin binds to the FAK-Focal Adhesion Targeting (FAT) domain via an interaction involving LD2 and LD4 (Bertolucci, Guibao, & Zheng, 2005a). The FAT domain consists of a right-turn, elongated four-helix bundle maintained by hydrophobic interactions (Arold, Hoellerer, & Noble, 2002). The NMR solution structure (Bertolucci et al., 2005a) reveals that the LD motifs bind simultaneously to opposite faces of the α-helical bundle, with LD2 binding preferentially between helices 1 and 4, and LD4 binding preferentially between helices 2 and 3 (figure 19).

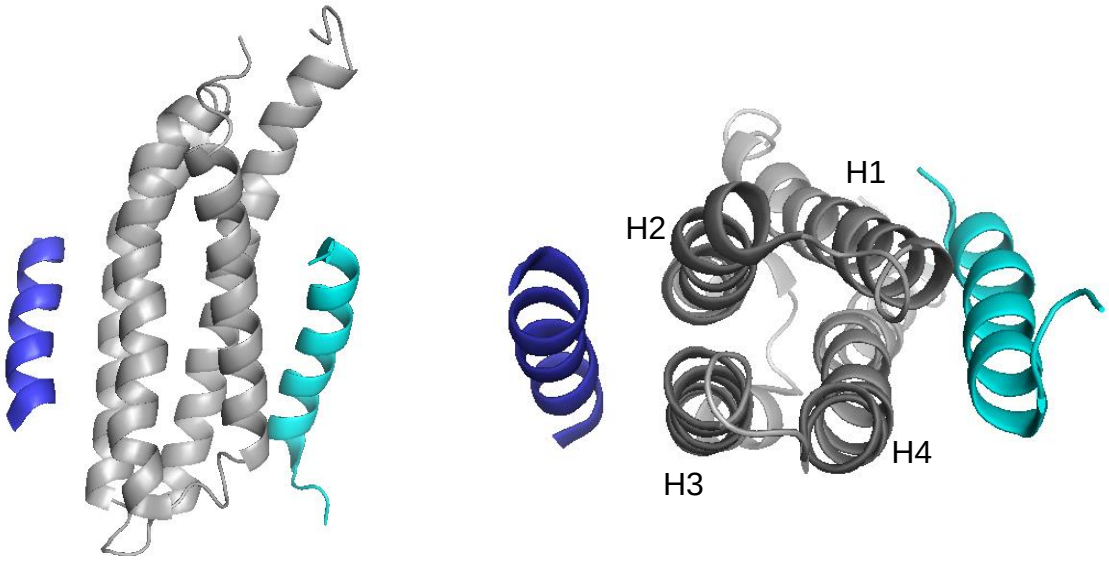

Figure 19. NMR solution structure of the FAK-FAT domain bound to LD2 and LD4 of paxillin. LD2 (cyan) binds within helix 1 (H1) and 4 (H4). LD4 (blue) binds within helix 2 (H2) and 3 (H3).

Binding of both LD motifs is required to form a stable FAK-paxillin complex; an interaction that is necessary but not sufficient to localise FAK to FAs (Cooley, Broome, Ohngemach, Romer, & Schaller, 2000). The roles of FAK in adhesion dynamics

remains unclear, however integrin-activated FAK must by deactivated to promote migration via FA disassembly. Dissociation of the FAK-paxillin complex, most likely through inhibition of one of the LD-binding sites, could trigger FA breakdown, raising the question of whether paxillin is involved in regulating the activation state of FAK.

1.8. Paxillin-Vinculin

Vinculin was the first paxillin binding partner to be identified (C E Turner et al., 1990) and has since been shown to bind paxillin via an interaction between LD2 and the vinculin tail domain (Wood, Turner, Jackson, & Critchley, 1994). Colocalization assays using a truncated vinculin construct lacking the C-terminal tail domain have demonstrated that paxillin is recruited to FAs prior to vinculin, independently of the paxillin-binding site within the vinculin tail (Humphries et al., 2007a). The question therefore remains, what is the function of the paxillin-vinculin complex within adhesion dynamics?

1.9. Paxillin-Talin

Paxillin contains a focal adhesion targeting sequence within the C-terminal LIM region. Of the four LIM domains, LIM 3 has been highlighted as a major contributor in recruitment to FAs, with LIM 2 also playing a minor role (Brown, Perrotta, & Turner, 1996). The mechanisms of this recruitment are yet to be established, however it does not appear to involve FAK or vinculin, since paxillin constructs containing mutations that abrogate FAK and vinculin binding have been shown to localise effectively to FAs (Brown et al., 1996).

N-RAP is a protein found in skeletal and cardiac muscles where it localises at the longitudinal ends of myofibrils (Luo et al., 1997). It comprises an N-terminal LIM domain connected to a C-terminal region with sequence homology to the actin-binding

protein nebulin, and serves as a mechanical linkage between the terminal actin filaments of myofibrils and protein complexes located beneath the sarcolemma. N-RAP has been shown to bind talin with high-affinity; an interaction involving the N-terminal LIM domain (Luo, Herrera, & Horowits, 1999).

Using image correlation analysis, talin and paxillin have been shown to colocalise almost identically with a C-terminally truncated vinculin construct, vin880. Colocalization of endogenous paxillin and talin have also been detected using antibodies (Humphries et al., 2007a). Vin880 lacks the paxillin-binding site within the C-terminal tail domain, and thus supports the notion that paxillin recruitment to FAs occurs independently of vinculin. Additionally, FAK is absent from vin880-induced FAs, indicating that paxillin recruitment occurs via another protein. Colocalization of talin and paxillin, and binding of talin to the LIM domain of N-RAP, raises the possibility that paxillin recruitment occurs via a talin-LIM-mediated mechanism.

1.10. Project Aims

The overarching aim of this project is to provide clarity on the role(s) of paxillin in focal adhesions. This project aims to explore the function(s) of paxillin within focal adhesion dynamics, and how such functions are regulated. Using *in-vitro* biochemical and biophysical methods, the recruitment of paxillin to adhesion sites, the interactions of paxillin with talin, vinculin and FAK, and the regulation of paxillin activity were investigated.

2. Materials and Methods

2.1 Cell culture

2.1.1 Protein expression in *E. coli*

All protein constructs were expressed in *BL21 (DE3) E. coli* cells and grown in Lysogeny-Broth (LB) medium at 37°C. Plasmid selection was achieved by the addition of ampicillin or kanamycin from filter sterilised 1000x stocks, to give a final concentration of 50 µg/ml.

2.1.2 *E. coli* transformation

40 µl aliquots of competent *E. coli* cells were thawed on ice. 1-2 µl of plasmid DNA was added to the cells and incubated on ice for 30 minutes. Cells were heat shocked for 90 seconds at 42°C and then put back on ice for 2 minutes. 100 µl of LB was added and the cells allowed to recover for 1 hour at 37°C before being plated onto an LB plate containing appropriate antibiotic selection. A 5 ml overnight starter culture was set up using a single colony. 4 ml was used to inoculate 750 ml of fresh LB medium. 750 µl was added to 500 µl of filter sterilised glycerol (50%) and stored at -80°C.

Cells were grown at 37°C, 150 rpm shaking, until the cell density reached an OD_{600} of 0.5-0.7. Protein expression was then induced by addition of Isopropyl β-D-1-thiogalactopyranoside (IPTG) (Melford) to a final concentration of 0.1 mg/ml. Cells were induced for 2 hours at 37°C, 3 hours at 37°C, or overnight at 18°C as appropriate (table 1) and then harvested by centrifugation at 6000 rpm for 15 minutes. Cell pellets were resuspended in appropriate buffer for protein purification and frozen in liquid nitrogen for storage at -20°C.

Table 1. Induction conditions.

Construct	Induction Time (hours)	Induction Temperature (ºC)
Full length vinculin	2	37
VD1-4	2	37
VtΔLinker	3	37
^{15}N- VtΔLinker	20	18
Paxillin LD1-5	2	37
Paxillin LIM1-4	20	18
Paxillin LIM1-2	20	18
Paxillin LIM3-4	20	18

2.1.3 Production of calcium competent cells

A 5 ml overnight culture starter was set up from a single colony, and then used at 1:100 dilutions to inoculate 50 ml of fresh LB medium containing no antibiotic selection. Cells were grown at 37ºC until the cell density reached an OD_{600} of 0.5-0.7. The culture was cooled on ice for 10 minutes and then harvested by centrifugation at 4000 rpm for 10 minutes at 4ºC. Cells were resuspended in 10 ml of chilled $CaCl_2$-glycerol (0.1 M $CaCl_2$, 10% w/v glycerol, filter sterilised) and incubated on ice for 15 minutes. Cells were collected by centrifugation at 3000 rpm for 10 minutes at 4ºC. The supernatant was discarded, and the pellet carefully resuspended in 1 ml of chilled $CaCl_2$-glycerol. 40 µl aliquots were frozen in liquid nitrogen and stored at -80ºC.

2.2 Protein purification

2.2.1 His-tagged protein purification

Bacterial pellets were resuspended in 20 mM TRIS, 500 mM NaCl, 20 mM imidazole in the presence of protease inhibitors and frozen in liquid nitrogen for storage at -20^{o}C. Cells were thawed and lysed by 6 cycles of sonication; 30 second pulse, resting on ice for 30 second intervals. Lysates were centrifuged at 18,000 rpm for 20 minutes at 4^{o}C. The soluble fraction was retained, and the insoluble pellet discarded.

His-tagged proteins have a high affinity for Ni-NTA resin and can therefore be isolated from cell lysates using nickel-affinity chromatography (Spriestersbach, Kubicek, Schäfer, Block, & Maertens, 2015). The soluble cell lysate is passed through the Ni-NTA affinity column, allowing the his-tagged proteins to bind. The column is washed with Ni-NTA buffer A (20 mM TRIS, 500 mM NaCl, 20 mM imidazole, pH 8) to remove non-specific binders. The his-tagged protein is eluted from the column by a gradient of increasing imidazole, achieved by titrating in Ni-NTA buffer B (20 mM TRIS, 500 mM NaCl, 500 mM imidazole, pH 8). His-tagged proteins were purified using AKTA FPLC at room temperature. Eluted protein fractions were identified using absorbance at 280 nm and confirmed by SDS-PAGE on a 10% gel stained with Coomassie blue.

2.2.2 Buffer exchange: dialysis

Protein was dialysed using Thermo Scientific SnakeSkin dialysis tubing (7000 MWCO) overnight on a stirrer at 4^{o}C, in 100x volume of buffer.

His-tagged proteins to be purified further by ion exchange chromatography were dialysed into Q Buffer A (20 mM TRIS, 50 mM NaCl, pH 8) or S Buffer A (20 mM phosphate, 50 mM NaCl, pH 6.5) as determined by the isoelectric point calculated using ProtParam (https://web.expasy.org/protparam/). The his-tag was removed by cleavage with TEV protease.

2.2.3 Buffer exchange: pd-10 desalting column

PD-10 desalting columns (GE Healthcare) contain Sephadex G-25 resin which allow rapid buffer exchange. The column is first equilibrated with 25 ml buffer and then loaded with 2.5 ml protein sample. The protein is eluted with 3.5 ml buffer and collected.

2.2.4 Ion exchange chromatography

Ion exchange chromatography separates ionisable molecules based on their total charge, and can be used as a subsequent purification step following Ni-NTA affinity chromatography. The pH at which a protein has no net charge is its isoelectric point, and is calculated from the primary sequence of a protein, using ProtParam (https://web.expasy.org/protparam/). If the pI < 7, a negatively charged cation exchange resin is used to capture the protein. If the pI > 7, a positively charged anion exchange resin is used. The protein is then eluted using a salt gradient.

Table 2. Principles of Ion Exchange Chromatography.

	Cation Exchanger (Q column)	**Anion Exchanger (S column)**
pI	+	-
Charge of resin	-	+
Wash Buffer	20 mM TRIS, 50 mM NaCl, pH 8	20 mM phosphate, 50 mM NaCl, pH 6.5
Elution Buffer	20 mM TRIS, 1 M NaCl, pH 8	20 mM phosphate, 1 M NaCl, pH 6.5

Eluted protein fractions were confirmed by SDS-PAGE on a 10% gel stained with Coomassie blue. Pooled fractions were dialysed into appropriate buffer, divided into aliquots and frozen in liquid nitrogen for storage at -20^{o}C.

2.2.5 GST-tagged protein purification

Bacterial pellets were resuspended in 20 mM HEPES, 100 mM NaCl, 1 mM $ZnSO_4$ in the presence of protease inhibitors and frozen in liquid nitrogen for storage at -20^oC. Cells were thawed and lysed by 6 cycles of sonication; 30 second pulse, resting on ice for 30 second intervals. Lysates were centrifuged at 18,000 rpm for 20 minutes at 4^oC. The soluble fraction was incubated with glutathione Sepharose beads (Thermo Scientific) on a rocker for 2 hours at room temperature, followed by centrifugation at 4000 rpm for 5 minutes at 4^oC. The supernatant was removed, and the protein-bound beads were washed in 20 mM HEPES, 100 mM NaCl, 1 mM $ZnSO_4$ and then centrifuged at 4000 rpm for 3 minutes. This wash-spin cycle was repeated 5 times. After the final spin, the protein-bound beads were resuspended in 1 mL 20 mM HEPES, 100 mM NaCl, 1 mM $ZnSO_4$. The GST-tagged proteins were left bound to the beads for use in GST pulldown experiments.

2.2.6 SDS-PAGE

SDS-PAGE gels were cast in pre-made gel cassettes using the recipe in Table 3.

Table 3. SDS-PAGE gel recipe.

Separating Gel 10 %		**Stacking Gel 4 %**	
40 % Acrylamide/BIS	6.0 ml	**40 % Acrylamide/BIS**	1.5 ml
Separating Gel Buffer	9.4 ml	**Stacking Gel Buffer**	4.2 ml
10 % SDS	250 µl	**10 % SDS**	125 µl
50 % Sucrose	4.0 ml	**Water**	5.8 ml
Water	4.8 ml	**TEMED**	5.0 µl
TEMED	6.25 µl	**Catalyst**	1.0 ml
Catalyst	625 µl		

Separating Gel Buffer:

1 M TRIS-HCl, pH 8.8

Stacking Gel Buffer:

0.375 M TRIS-HCl, pH 6.8

Catalyst:

100 mg Ammonium Persulfate in 2 ml of water

The separating gel was poured into the gel cassette, overlaid with degassed water and allowed to polymerise for 1 hour. The water was removed and the cassette filled with stacking gel. The comb was immediately inserted and the stacking gel allowed to polymerise for 1 hour.

5x SDS loading buffer was added to all protein samples and heated at 95^{o}C for 5 minutes before being loaded into the wells. Gels were run at 200 V for approximately 40 minutes.

2.3 Biochemical Assays

2.3.1 Fluorescence Polarisation

Polarised light describes a light wave that is vibrating within a single plane. When a fluorescently labelled ligand (typically <1500 Da) is excited by polarised light, the emitted light is largely depolarised due to rapid tumbling of the ligand during the lifetime of its excited state. If the fluorescently labelled ligand is bound to a larger protein (typically > 10 kDa), the emitted light is largely polarised due to the reduced tumbling rate of the complex. Thus, the degree of polarisation is inversely proportional to the rate of molecular tumbling. This property of fluorescence

polarisation (FP) provides a technique to measure protein-ligand binding (Moerke, 2009).

Peptides were coupled to a thiol-reactive fluorescein dye via the C-terminal cysteine. Stock solutions were made in phosphate-buffered saline (PBS; 137 mM NaCl, 27 mM KCl, 100 mM Na_2HPO_4, 18 mM KH_2PO_4, pH 7.4), 1mM TCEP and 0.05% Triton X-100. Excess dye was removed using a PD-10 desalting column (GE Healthcare). Titrations were performed in PBS using a black 96-well plate. A constant fluorescein-coupled peptide concentration of 1 µM was used, with increasing concentration of protein, to a final volume of 100 µL. Fluorescent polarisation measurements were recorded on a BMGLabTech CLARIOstar plate reader at 25^{o}C and analysed using GraphPad Prism. K_d values were calculated with nonlinear curve fitting using a one-site total binding model.

2.3.2 Microscale Thermophoresis

Thermophoresis describes the directed motion of molecules through a temperature gradient, and is dependent on molecule size, charge, hydration shell and conformation. Microscale thermophoresis monitors the directed movement of fluorescent molecules through microscopic temperature gradients in microlitre volumes, enabling precise quantification of the binding events of virtually any molecule, independent of size or nature (Jerabek-Willemsen et al., 2014). The temperature gradient is generated by an infrared laser and the directed movement of molecules through this gradient is quantified using an intrinsic fluorophore. The thermophoresis of a protein differs significantly to that of a protein-ligand complex, due to changes in size, charge and solvation entropy induced upon binding, thereby

providing a highly sensitive technique for measuring protein-protein interactions (Seidel et al., 2013).

Paxillin LD1-5 was coupled to an equimolar amount of NT-647 dye (RED-tris-NTA, NanoTemper) via its C-terminal his-tag in a one-step coupling reaction (Tschammer et al., 2016). Titrations were performed in PBS. A constant RED-tris-NTA coupled paxillin LD1-5 concentration of 100 nM was used, with increasing concentration of protein, to a final volume of 20 µl. Prepared samples were loaded into Monolith NT.115 capillaries (NanoTemper) and measurements were recorded on a Monolith NT.115 at 25^{o}C, excited under red light with medium MST power and 100% excitation power. The data was analysed using MO.Affinity Analysis software and fitted using the K_d fit model.

2.3.3 Size Exclusion Chromatography with Multi-Angle Light Scattering

Size Exclusion Chromatography (SEC) separates molecules based on their hydrodynamic volume and size. Samples are passed through a matrix of porous beads that lack reactivity or adsorptive properties. Large molecules cannot diffuse into the pores and are eluted first. Smaller molecules are able to penetrate the pores and have a longer retention time prior to elution. Multi-angle light scattering (MALS) is used in conjunction with SEC to determine the absolute molecular weight, independent of the protein conformation, size and elution position.

Size Exclusion Chromatography with Multi-Angle Light Scattering (SEC-MALS) was performed using a Superdex-200 size-exclusion chromatography column (GE healthcare) at a 0.75 mL min^{-1} flow rate in PBS. 200 µl samples were run consisting of 50 µM of each protein, incubated at a 1:1 or 1:1:1 ratio (table 4) at room

temperature for 30 minutes. Elution was monitored by a Malvern Viscotek SEC-MALS-9 (Malvern Panalytical, Malvern, UK).

Table 4. Protein incubation ratios.

1:1	1:1:1
Paxillin LD1-5 : Full length vinculin	Paxillin LD1-5 : VD1-4 : VtΔLinker
VD1-4 : VtΔLinker	
Paxillin LD1-5 : VD1-4	
Paxillin LD1-5 : VtΔLinker	

2.3.4 GST Pulldowns

Proteins tagged to glutathione S-transferase (GST) were purified as described in section 2.2.5. The purified GST-tagged, glutathione-attached protein was incubated with 150 µl of the query protein on a rocker for 1 hour at 25^{o}C. The sample was run through a column and the supernatant collected. The beads were washed with 20 mM HEPES, 100 mM NaCl, 1 mM $ZnSO_4$, resuspended, transferred to an eppendorf and centrifuged at 4000 rpm for 5 minutes to form a pellet. The supernatant and pellet were analysed by SDS-PAGE on a 10% gel stained with Coomassie blue.

2.4. Nuclear Magnetic Resonance Spectroscopy

2.4.1. Basic principles of Nuclear Magnetic Resonance Spectroscopy

Nuclear Magnetic Resonance (NMR) is a biophysical technique that utilises the behaviour of atomic nuclei within an applied magnetic field. 2D NMR experiments involve the transfer of magnetisation between a proton and the ^{15}N (or ^{13}C) atomic nucleus it is bonded to. Within a protein, each backbone amide group is in a distinct environment, and therefore gives a distinct peak. If this environment changes, as a result of ligand binding for example, a shift in the peak corresponding to that amide

group is observed, allowing for the characterisation of protein-ligand interactions. Since the naturally occurring nitrogen-14 isotope is not magnetically active, proteins must be grown in minimal media containing ^{15}N as the sole nitrogen source.

2.4.2. ^{15}N-labelled Protein Expression and Purification

^{15}N-labelled VtΔLinker was expressed in M9 minimal media using the recipe in Table 5.

Table 5. M9 minimal media recipe for 1 L preparation.

M9 Solution A		**M9 Solution B**	
Na_2HPO_4	12.5 g	**Glucose**	4.0 g
KH_2PO_4	7.5 g	**BME Vitamins**	10.0 ml
Water	1.0 L	**Water**	10.0 ml
		$MgSO_4$ (1M)	2.0 ml
		$CaCl_2$ (1M)	0.1 ml
		Ampicillin (1 mg/ml)	1.0 ml
		$^{15}NH_4Cl$	1.0 g

Solution B was filter sterilised and added to autoclaved Solution A. An overnight starter culture was set up using a scraping of the VtΔLinker glycerol stock in 10 ml M9 Solution A, 250 µl M9 Solution B. 8 ml was used to inoculate 1 L of M9 minimal media.

Cells were grown at 37°C, 150 rpm shaking, until the cell density reached an OD_{600} of 0.5-0.7. Protein expression was then induced by addition of Isopropyl β-D-1-thiogalactopyranoside (IPTG) to a final concentration of 0.1 mg/ml. Cells were induced overnight at 18°C and then harvested by centrifugation at 6000 rpm for 15 minutes. Cell pellets were resuspended in Ni-NTA Buffer A (20 mM TRIS, 500 mM NaCl, 20 mM imidazole, pH 8) for protein purification and frozen in liquid nitrogen for

storage at -20°C. ^{15}N-VtΔLinker was purified, and buffer exchanged into NMR buffer (16 mM NaH_2PO_4, 6 mM Na_2HPO_4, 50 mM NaCl, 2 mM DTT, pH 6.5) as described in section 2.2 above. 450 µl samples were prepared containing 5% D2O. All NMR experiments were performed on a Bruker 600 MHz spectrometer at 298 K, pH 6.5 and processed using TOPSPIN.

2.5 Molecular Biology Techniques

2.5.1 Primer Design

Primers were designed using ApE software and are listed in table 6.

Table 6. Primer design.

Construct	Vector	Restriction Enzymes		Forward Primer	Reverse Primer
		5'	3'		
VD1-4	*pET-151*	BamHI	XhoI	AAGGATCCCCGGTTTTTCATACCCG	AACTCGAGTTATGCTTCACGCACTTTTGC
VD1	*pET-151*	BamHI	XhoI	AAGGATCCCCGGTTTTTCATACCCG	GGCTCGAGTTACCATGCATCTTCATCCC
VD2	*pET-151*	BamHI	XhoI	AAGGATCCGCAAGCAAAGATACCG	AACTCGAGATTTGCAACTGCACG
VD3	*pET-151*	BamHI	XhoI	AAGGATCCAGCCGTCCGGCAAAAGC	AACTCGAGTTATTCATCTACCAGACCGG
VD4	*pET-151*	BamHI	XhoI	AAGGATCCGCAATTGATACCAAAAGCC	AACTCGAGTTATGCTTCACGCACTTTTGC
VtΔLinker	*pET-151*	BamHI	XhoI	AAGGATCCGAAGAAAAAGATGAAGAATTTCCGG	GGTGCTCGAGTTATTAGCTAGCC
Full length Paxillin	*pGEX-TEV*	BglII	SalI	AAGGATCCATGGACGACCTCGATGCC	AAGTCGACCTAGCAGAAGAGCTTCACG

Paxillin LD1-5	*pET-151*	BamHI	EcoRI	AAGGATCCATGGACGACCTCGATGCC	AAAGAATTCTTAACAGACCCCTTTGGCAACG
Paxillin LIM1-4	*pGEX-TEV*	Sal1	NheI	AAGCTAGCGGAGCCTGCAAGAAGC	AAGTCGACCTAGCAGAAGAGCTTCACG

2.5.2 PCR

50 µl PCR reactions were set up as below:

Component	**Final Volume**	**Final Concentration**
5X GoTaq Flexi Buffer (Promega)	10 µl	1X
$MgCl_2$ solution (Promega)	2 µl	1.0 mM
dNTPs (Invitrogen)	1 µl	100 mM each
Forward primer (IDT)	1 µl	100 µM
Reverse primer (IDT)	1 µl	100 µM
GoTaq G2 Hot Start Polymerase (Promega)	0.5 µl	2.5 u
Template DNA	X µl	100 – 200 ng/µl
dH_2O	to a final volume of 50 µl	

Template DNA was amplified by PCR according to the conditions listed in table 7.

Table 7. PCR conditions.

	Denaturation	Annealing	Elongation	Final extension
VD1-4	30 secs at 92ºC	1 min at 52ºC	30 secs at 68ºC	10 min at 68ºC
VD1	30 secs at 92ºC	1 min at 52ºC	30 secs at 68ºC	10 min at 68ºC
VD2	30 secs at 92ºC	1 min at 52ºC	30 secs at 68ºC	10 min at 68ºC
VD3	30 secs at 92ºC	1 min at 52ºC	30 secs at 68ºC	10 min at 68ºC
VD4	30 secs at 92ºC	1 min at 52ºC	30 secs at 68ºC	10 min at 68ºC
VtΔLinker	30 secs at 92ºC	1 min at 52ºC	30 secs at 68ºC	10 min at 68ºC
Full length Paxillin	30 secs at 92ºC	1 min at 60ºC	90 secs at 68ºC	10 min at 68ºC
Paxillin LD1-5	30 secs at 92ºC	1 min at 60ºC	1 min at 68ºC	10 min at 68ºC
Paxillin LIM1-4	30 secs at 92ºC	1 min at 57ºC	40 secs at 68ºC	10 min at 68ºC

Amplification was confirmed by agarose gel electrophoresis, and the PCR product purified using a QIAquick Gel Extraction Kit (Qiagen – 28704) according to the manufacturer's instructions.

2.5.3 Agarose Gel Electrophoresis

1 % w/v agarose was dissolved in 0.5x TAE by heating in a microwave, and then poured into casting trays with appropriately sized well combs. Ethidium bromide was added to a final concentration of 0.5 µg/ml and the gels allowed to set. Prior to

loading, 5x loading buffer was added to each sample. Gels were run at 50 V for approximately 30 minutes, and imaged using a UV transilluminator.

2.5.4 Restriction Digests

100 µl restriction digests were set up according to the restriction enzymes:

Component	**Final Volume**	**Final Concentration**
Restriction Enzyme 10X Buffer	10 µl	1X
DNA	X µl	1.0 - 2.0 µg/µl
Restriction Enzyme		
BamHI, 20 u/µl (NEB)	1 µl	20 u
XhoI, 10 u/µl (Promega)	2 µl	20 u
SalI, 10 u/µl (Promega)	2 µl	20 u
EcoRI, 12 u/µl (Promega)	1.7 µl	20 u
BglII, 10 u/µl (Promega)	2 µl	20 u
dH_2O	to a final volume of 100 µl	

Restriction digests were incubated at 37^{o}C for two hours. The desired DNA fragment was cut out from an agarose gel and purified using a QIAquick Gel Extraction kit (Qiagen – 28704) according to the manufacturer's instructions.

2.5.5 Ligations

10 µl ligation reactions were set up as below:

Component	Final Volume	Final Concentration
T4 DNA Ligase, 3 u/µl (Promega)	1 µl	3 u
10X Ligase Buffer (Promega)	1 µl	1X
Purified insert DNA	X µl	50 – 250 ng/µl
Purified vector DNA	X µl	50 – 250 ng/µl
dH_2O	to a final volume of 10 µl	

Insert and vector DNA was ligated at a 1:1 molar ratio, determined by absorbance at 260 nm, measured using a NanoDrop. Ligations were incubated at 4^{o}C overnight.

2.5.6 *E. coli* Transformation

DNA was transformed as described in section 2.1.2.

2.5.7 Plasmid DNA Preparation

Plasmid DNA from *E. coli* DH10β cells was extracted using a QIAprep spin Miniprep Kit (Qiagen – 27106) according to the manufacturer's instructions.

2.5.8 Test Digest

10 µl test digests were set up according to the restriction enzyme:

Component	Final Volume	Final Concentration
Restriction Enzyme 10X Buffer	1 µl	1X
Miniprepped DNA	X µl	100 - 200 ng/µl
Restriction Enzyme		
BamHI, 20 u/µl (NEB)	1 µl	20 u
XhoI, 10 u/µl (Promega)	2 µl	20 u
SalI, 10 u/µl (Promega)	2 µl	20 u
EcoRI, 12 u/µl (Promega)	1.7 µl	20 u
BglII, 10 u/µl (Promega)	2 µl	20 u
dH_2O	to a final volume of 10 µl	

Test digests were incubated at 37°C for 2 hours and then run on an agarose gel. Successful ligation was then confirmed by Sanger sequencing (Valencia, Pervaiz, Husami, Qian, & Zhang, 2013).

3. Results

Chapter 1: Functions of the N-terminal LD region of paxillin.

Introduction

Paxillin associates with focal adhesions and provides a scaffold to which diverse cytoskeletal and signalling proteins are recruited. Studies have shown that the individual LD motifs located at the N-terminal region of paxillin provide binding sites for multiple ligands including the cytoplasmic actin-binding protein vinculin (C E Turner et al., 1990), and the non-receptor tyrosine kinase FAK (Bertolucci, Guibao, & Zheng, 2005b)

This chapter explores the binding characteristics of paxillin with various vinculin subdomains, and with the focal adhesion targeting domain of FAK; providing evidence that the five LD motifs functioning cooperatively to amplify binding affinities and tether multiple ligands in proximity.

3.1.1 Paxillin binds to the tail domain of vinculin.

An association between the LD2 motif of paxillin (residues 141-153) and the tail domain of vinculin (residues 879-1066) has previously been reported (Brown et al., 1996; C E Turner et al., 1990; C E Turner & Miller, 1994). To explore this interaction further, mouse VtΔLinker (residues 879-1066, 21,189 Da) was sub-cloned into *pET-151* and expressed in *E. coli* as described in sections 2.4 and 2.1.1. The linker region was omitted to reduce the risk of proteolytic cleavage. The construct was first purified by Ni-NTA affinity chromatography, and then by ion exchange chromatography using an anion exchanger, as described in section 2.2.

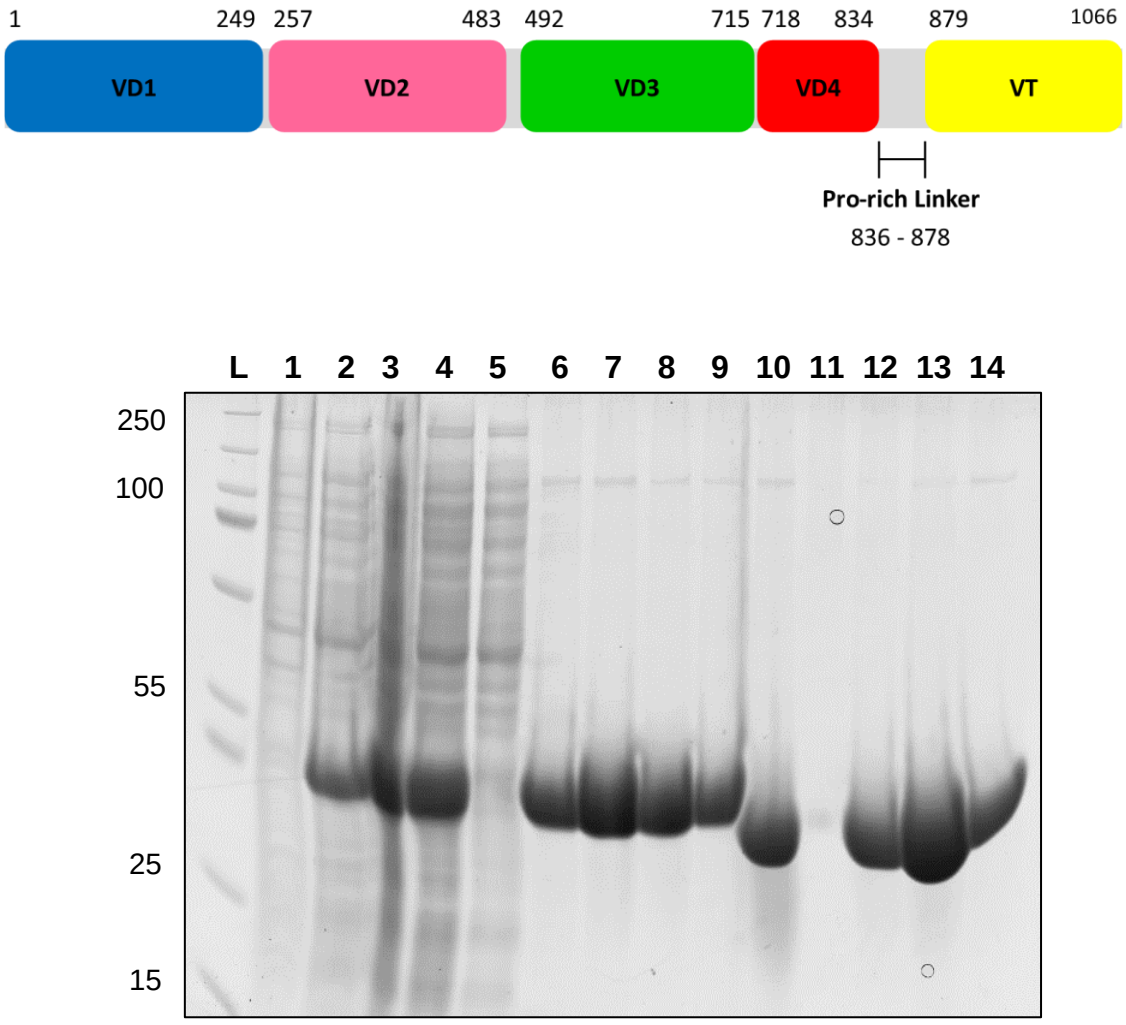

Figure 20. Expression and purification of VtΔLinker. (A) Domain organisation of full-length vinculin. VtΔLinker corresponds to residues 879-1066 at the C-terminal end. **(B)** A coomassie stained SDS-PAGE gel of the expression and purification of VtΔLinker using Ni-NTA affinity and anion exchange chromatography. L; ladder (kDa), 1; pre-induction, 2; post induction, 3; after sonication, 4; after spinning, 5; Ni-NTA flow-through, 6; Ni-NTA fraction 1, 7; Ni-NTA fraction 2, 8; Ni-NTA fraction 3, 9; Ni-NTA fraction 4, 10; after TEV cleavage, 11; S-column flow-through, 12; S-column fraction 1, 13; S-column fraction 2, 14; S-column fraction 3. Fractions 1, 2 and 3 eluted during anion exchange chromatography were pooled, exchanged into appropriate buffer, concentrated and used for future experiments.

Fluorescence polarisation (FP) was first utilised to confirm whether paxillin binds VtΔLinker via LD2. The five LD peptides were coupled to fluorescein via the C-terminal cysteine: LD1 (3-22)C; LD2 (141-153)C; LD3 (214-228)C; LD4 (262-274)C; LD5 (331-352)C. As previously demonstrated using coprecipitation assays and western blots

(Brown et al., 1996; C E Turner et al., 1990), we were able to confirm using FP that LD2 binds to the vinculin tail (figure 21). The affinity of the interaction is weak, and thus could not be accurately calculated using GraphPad.

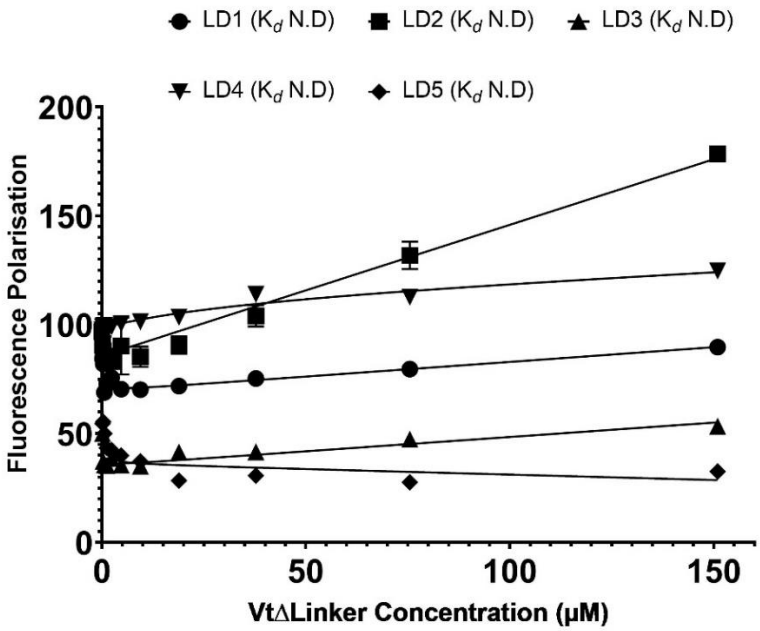

Figure 21. Paxillin LD2 binds VtΔLinker with weak affinity. Binding of fluorescein-labelled paxillin LD1 (3-22)C, LD2 (141-153)C, LD3 (214-228)C, LD4 (262-274)C and LD5 (331-352)C to VtΔLinker, measured using a fluorescence polarisation assay. All measurements were performed in triplicate. Dissociation constants are indicated in the legend. ND; not determined.

Binding of LD2 to the vinculin tail domain was also confirmed by Nuclear Magnetic Resonance (NMR) using ^{15}N-labelled-VtΔLinker expressed in M9 minimal media. 2D TROSY NMR spectra were obtained for ^{15}N-VtΔLinker (figure 22A) and ^{15}N-VtΔLinker: LD2 (at an excess of 1:3) (figure 22B). Overlaying the spectra indicated subtle shift peaks indicative of a weak binding interaction, consistent with the FP data above (figure 21).

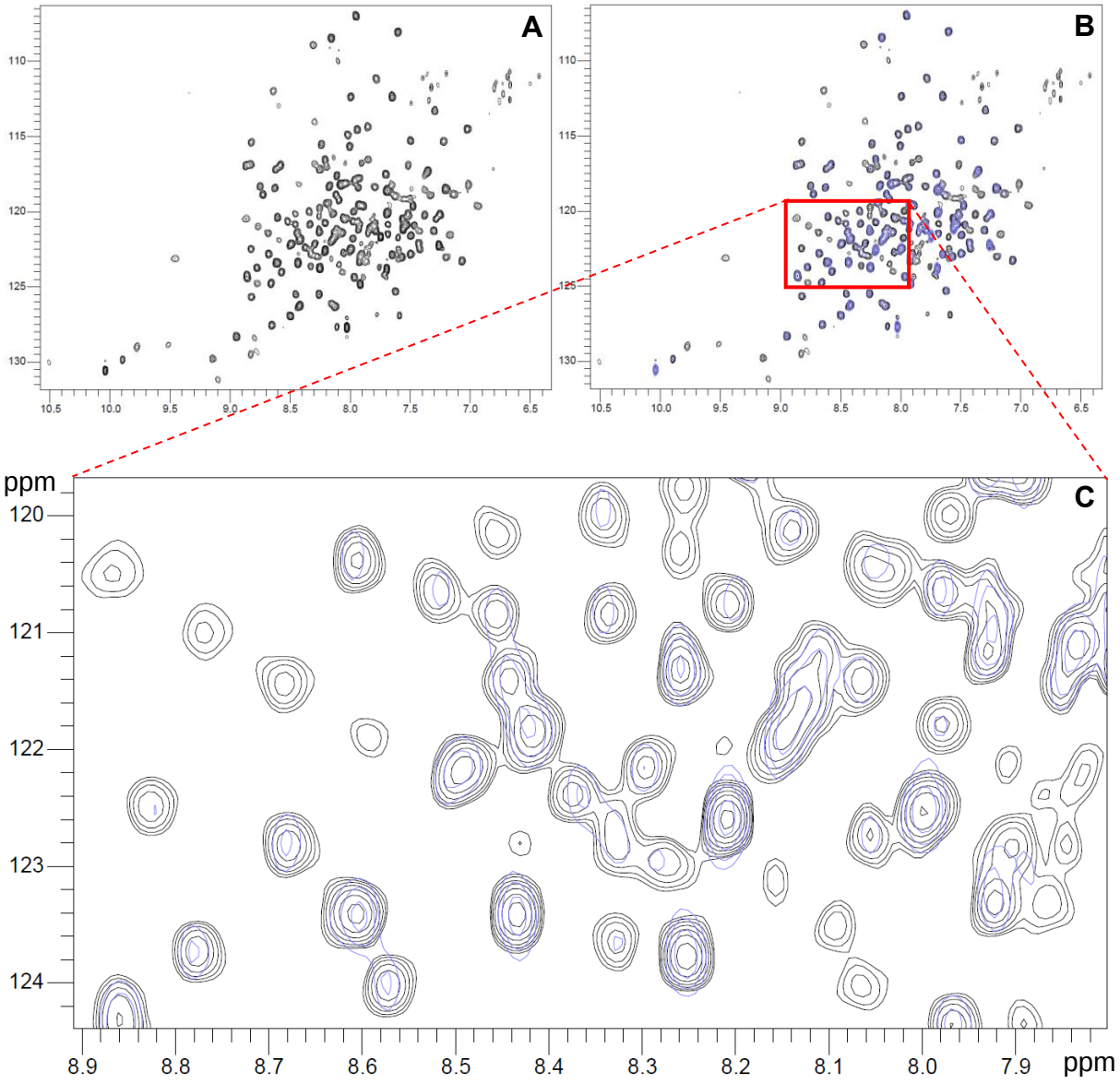

Figure 22. ^{15}N-VtΔLinker chemical shifts induced by paxillin LD2. TROSY spectra of ^{15}N-VtΔLinker (black) **(A)** overlaid with ^{15}N-VtΔLinker: LD2 (blue) **(B)**. Regions of the overlaid spectra are enlarged to allow identification of peak changes **(C)**.

3.1.2. Paxillin binds to the head domain of vinculin.

Having confirmed that paxillin binds to the vinculin tail domain, we next wanted to explore whether the N-terminal head domain (VD1-4) is also involved in paxillin binding. To do this, VD1-4 (residues 1-835, 90,843 Da) was sub-cloned into *pET-151* and expressed in *E. coli* as described in sections 2.5 and 2.1.1. The construct was first

purified by Ni-NTA affinity chromatography, and then by ion exchange chromatography using a cation exchanger, as described in section 2.2. Due to the size of VD1-4, a two-hour induction at 37ºC was selected to limit proteolytic cleavage. However, protein cleavage could not be eliminated completely (figure 23).

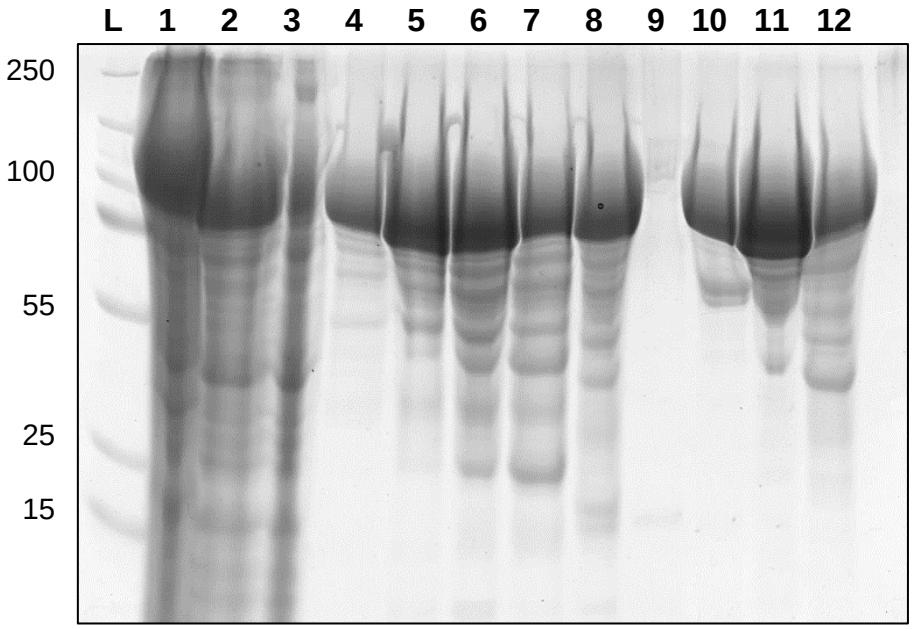

Figure 23. Expression and purification of VD1-4. A coomassie stained SDS-PAGE gel of the expression and purification of VD1-4 using Ni-NTA affinity and cation exchange chromatography. L; ladder (kDa), 1; after sonication, 2; after spinning, 3; Ni-NTA flow-through, 4; Ni-NTA fraction 1, 5; Ni-NTA fraction 2, 6; Ni-NTA fraction 3, 7; Ni-NTA fraction 4, 8; after TEV cleavage, 9; Q-column flow-through, 10; Q-column fraction 1, 11; Q-column fraction 2, 12; Q-column fraction 3. Fraction 1 eluted during cation exchange chromatography was buffer exchanged into appropriate buffer, concentrated and used for future experiments. Fractions 2 and 3 were disregarded due to the degree of proteolytic cleavage.

Having confirmed that paxillin binds VtΔLinker via LD2, we were also able to determine, using FP, that paxillin binds VD1-4 via LD1, LD2 and LD4. In each case, the binding affinity is weak and thus could not be accurately calculated using GraphPad (figure 24).

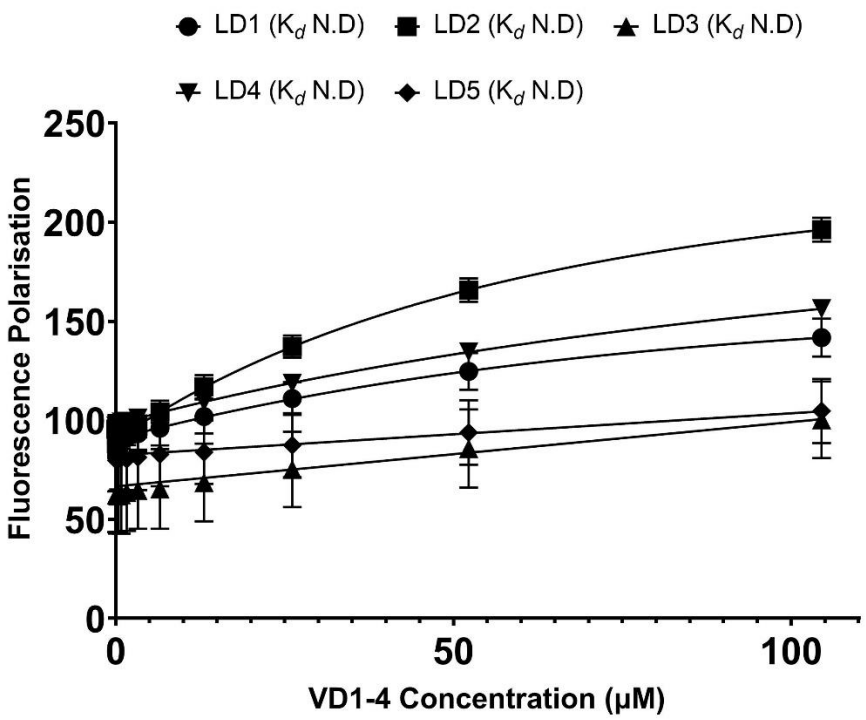

Figure 24. Multiple paxillin LD motifs bind VD1-4 with weak affinity. Binding of fluorescein-labelled paxillin LD1 (3-22)C, LD2 (141-153)C, LD3 (214-228)C, LD4 (262-274)C and LD5 (331-352)C to VD1-4, measured using a fluorescence polarisation assay. All measurements were performed in triplicate. Dissociation constants are indicated in the legend. ND; not determined.

3.1.3. The paxillin LD motifs function cooperatively to enhance binding.

Having observed that the paxillin-vinculin interaction involves multiple paxillin LD motifs, we next wanted to explore whether the LD motifs may function cooperatively, in which binding is enhanced when all five motifs are present and in proximity with one another. To do this, paxillin LD1-5 (residues 1-345, 36,459 Da) was sub-cloned into *pET-151* and expressed in *E. coli* as described in sections 2.5 and 2.1. Due to the unstructured nature of this region, an additional boiling step at 95^{o}C for 10 minutes was introduced prior to freezing, and a two-hour induction at 37^{o}C was selected to limit proteolytic cleavage. However, cleavage could not be eliminated completely (figure 25). It was later found that not cleaving the His-tag also improved protein stability (data

not shown). The construct was purified by Ni-NTA affinity chromatography and then by ion exchange chromatography using a cation exchanger, as described in section 2.2.

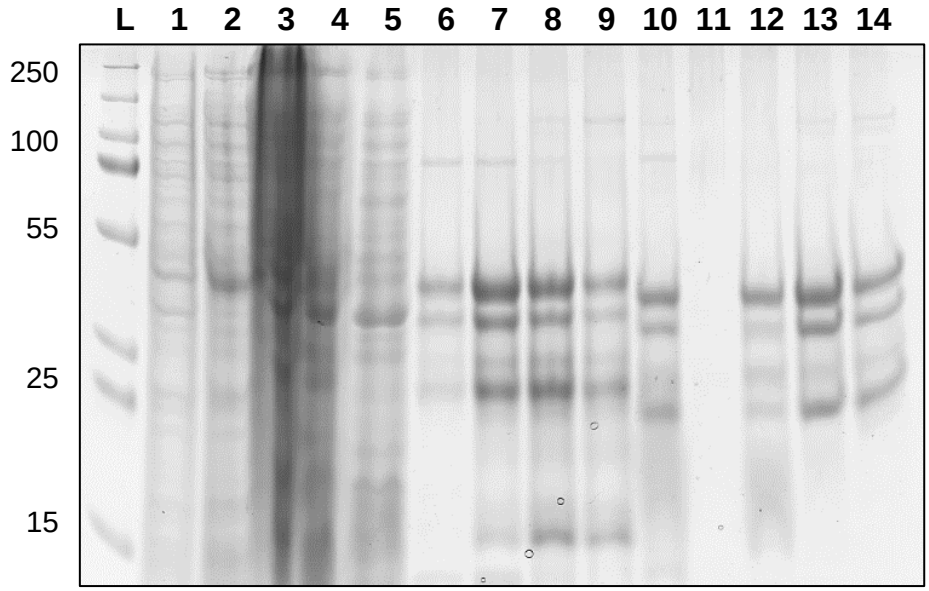

Figure 25. Expression and purification of paxillin LD1-5. A coomassie stained SDS-PAGE gel of the expression and purification of paxillin LD1-5 using Ni-NTA affinity and cation exchange chromatography. L; ladder (kDa), 1; pre-induction, 2; post induction, 3; after sonication, 4; after spinning, 5; Ni-NTA flow-through, 6; Ni-NTA fraction 1, 7; Ni-NTA fraction 2, 8; Ni-NTA fraction 3, 9; Ni-NTA fraction 4, 10; after TEV cleavage, 11; Q-column flow-through, 12; Q-column fraction 1, 13; Q-column fraction 2, 14; Q-column fraction 3. Fraction 1 eluted during cation exchange chromatography was exchanged into appropriate buffer, concentrated and used for future experiments. Fractions 2 and 3 were disregarded due to the degree of proteolytic cleavage.

The size of paxillin LD1-5 made it incompatible with FP experiments. Instead, microscale thermophoresis (MST) was used to investigate whether paxillin binds VtΔLinker and VD1-4 with higher affinity when all five LD motifs are present and in proximity. Un-cleaved paxillin LD1-5 was coupled to an equimolar amount of NT-647 dye via the C-terminal his-tag and titrated against increasing concentrations of VtΔLinker and VD1-4. MST analysis revealed an increase in the affinity of paxillin for

both VtΔLinker and VD1-4 when multiple LD motifs can bind simultaneously (figure 26).

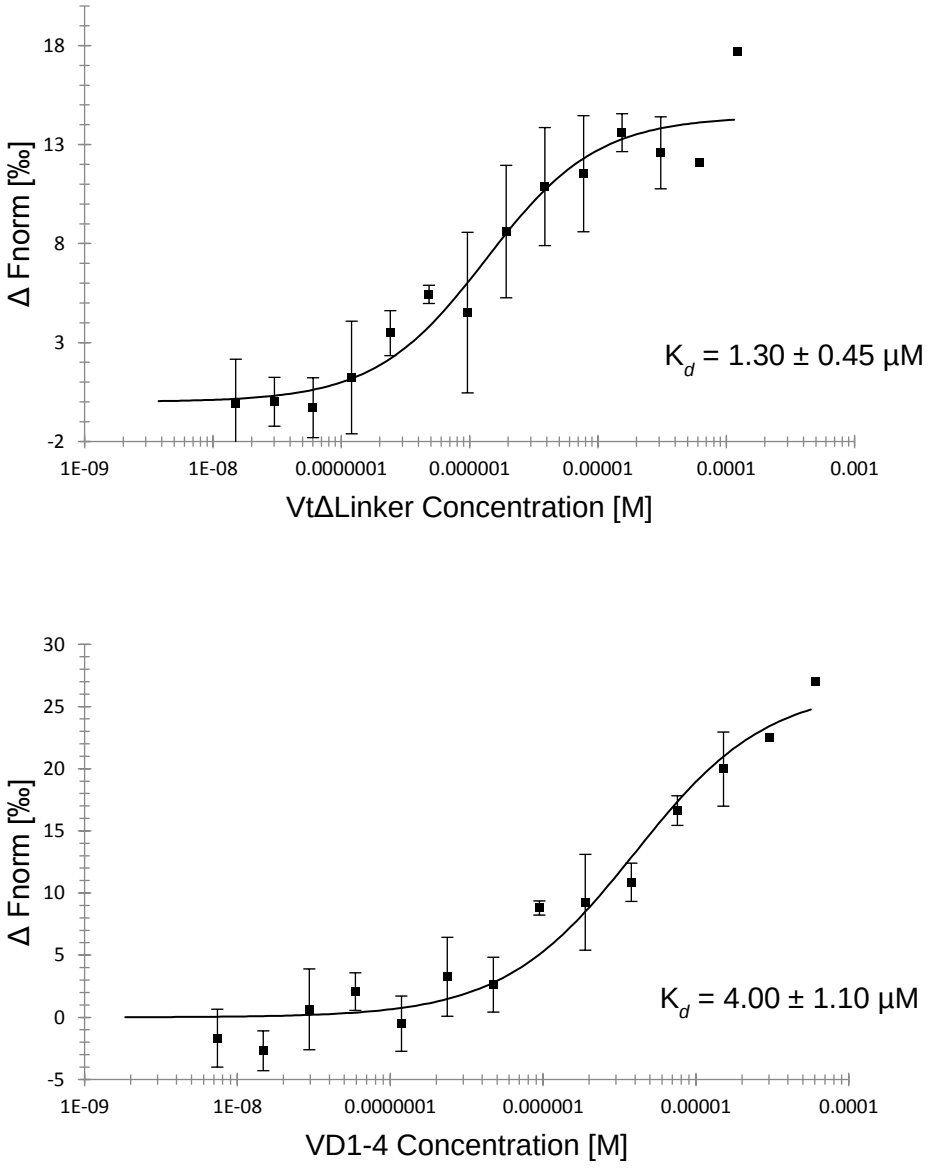

Figure 26. Paxillin LD1-5 binds VtΔLinker and VD1-4 with greater affinity compared to individual LD peptides. MST analysis of His-tagged paxillin LD1-5 binding to VtΔLinker (top panel) and VD1-4 (bottom panel). All measurements were performed in triplicate. Dissociation constants ± standard errors are indicated in the legend.

Binding of paxillin LD1-5 to VtΔLinker was also confirmed by NMR using ^{15}N-labelled-VtΔLinker expressed in M9 minimal media. 2D TROSY NMR spectra were obtained

for ^{15}N-VtΔLinker and ^{15}N-VtΔLinker: Paxillin LD1-5 (at an excess of 1:3). Overlaying the spectra indicated both shifts and loss of peaks indicative of binding (figure 27), consistent with both the MST and FP data above.

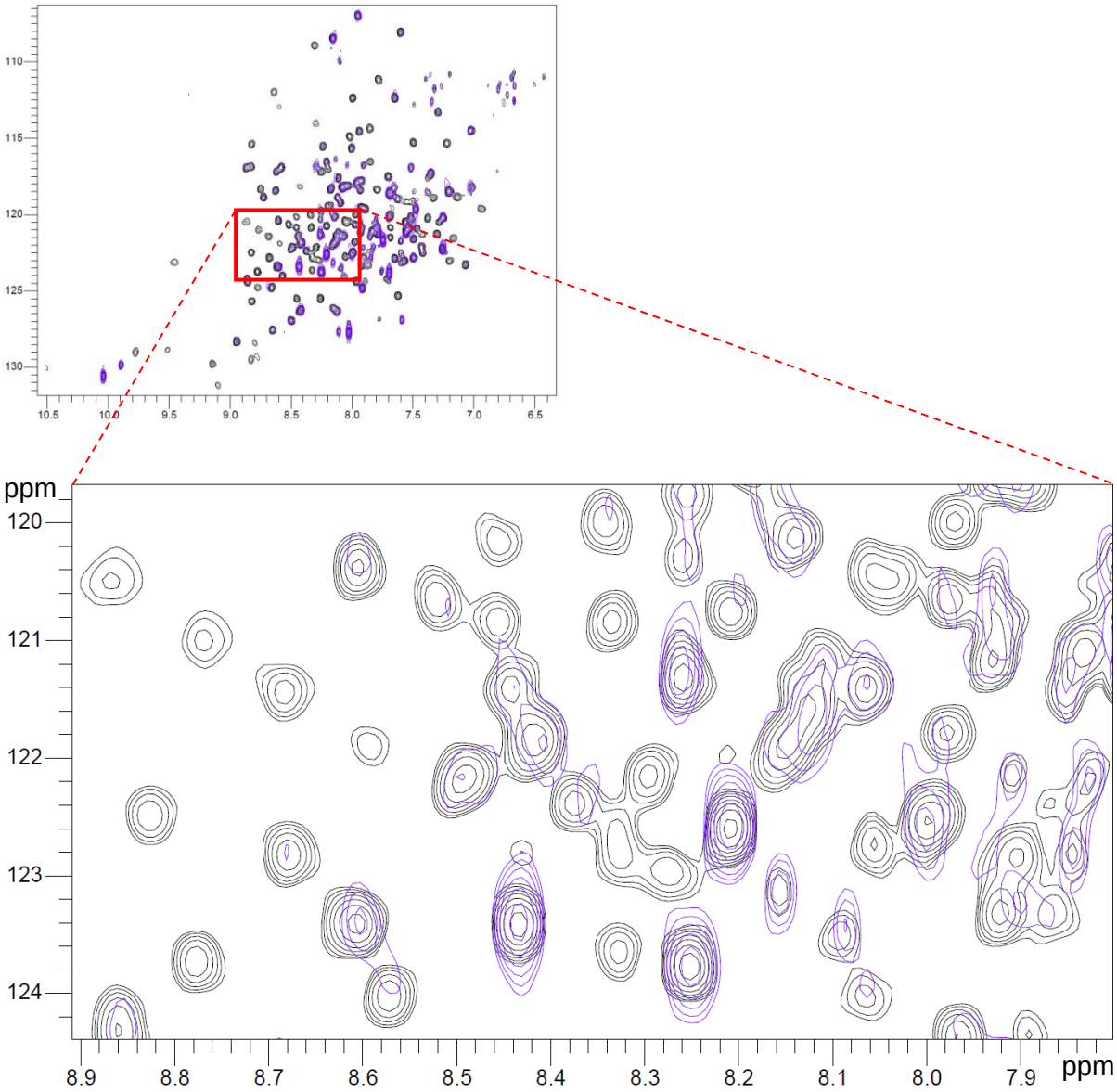

Figure 27. ^{15}N-VtΔLinker chemical shifts induced by paxillin LD1-5. 2D TROSY spectra of ^{15}N-VtΔLinker (black) overlaid with ^{15}N-VtΔLinker: Pax LD1-5 (purple). Regions of the overlaid spectra are enlarged to allow identification of peak changes.

Binding of paxillin LD1-5 to VD1-4 was also confirmed using size exclusion chromatography with multi-angle light scattering (SEC-MALS). The VD1-4 sample had

previously been flash-frozen, and consequently did not give a clean signal, most likely due to the instability demonstrated during the purification process. However, a shift in the VD1-4: Pax LD1-5 peak indicative of formation of a larger complex was still observed (figure 28).

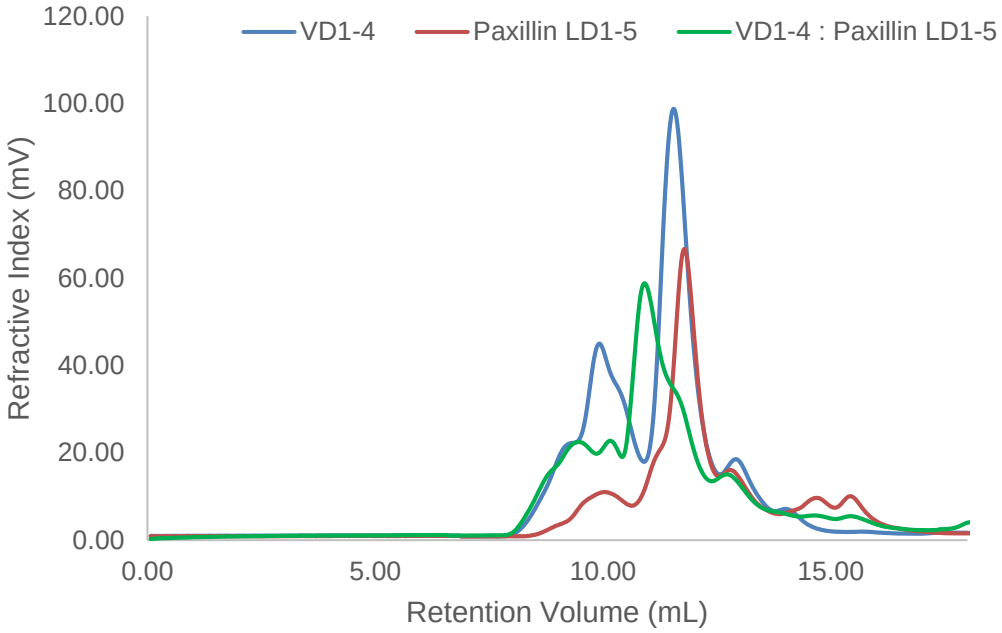

Figure 28. Paxillin LD1-5 binds VD1-4. Paxillin LD1-5 (red) and VD1-4 (blue) were analysed on a gel filtration column. Paxillin LD1-5 was incubated with an equimolar concentration of VD1-4 for 30 minutes at room temperature and analysed (green).

The protein eluted in 0.75 ml fractions and was analysed by SDS-PAGE (data not shown). However, the protein was too dilute to be observed clearly.

3.1.4. Paxillin binds full-length vinculin with high affinity.

Since paxillin LD1-5 can bind both the vinculin head and tail domains, we next wanted to explore the affinity of paxillin for full-length (FL) vinculin (residues 1-1066, 116.7 kDa). To do this, DNA encoding FL-vinculin was transformed into and expressed in *BL21 (DE3) E. coli* cells as described in sections 2.1.1 and 2.1.2. Due to protein size, a two-hour induction at 37ºC was selected to limit proteolytic cleavage. However,

cleavage could not be eliminated completely (figure 29). The protein was purified by Ni-NTA affinity chromatography and then by ion exchange chromatography using a cation exchanger, as described in section 2.2.

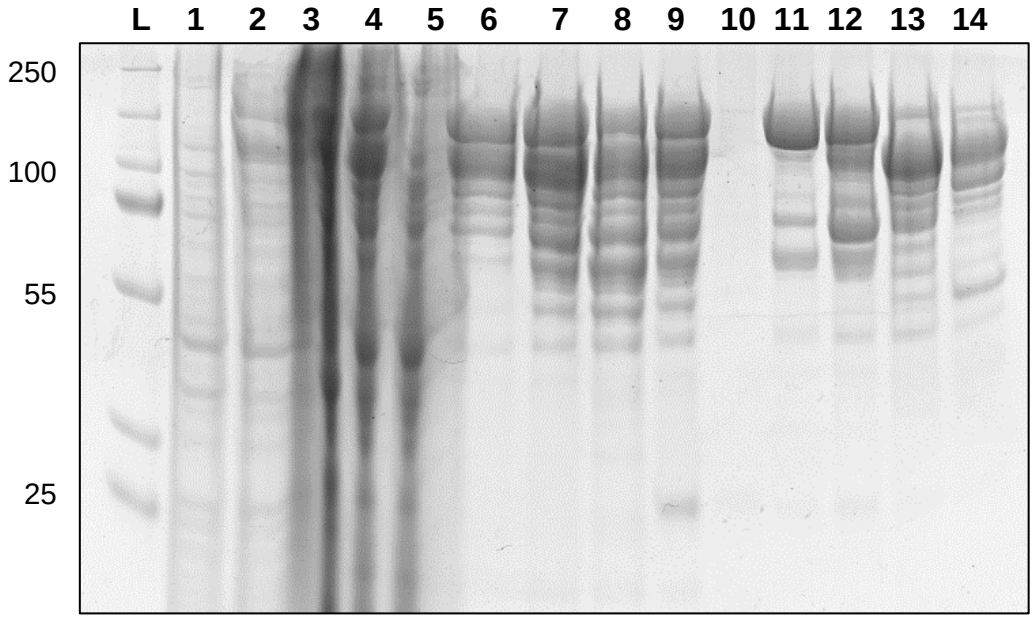

Figure 29. Expression and purification of full-length vinculin. A coomassie stained SDS-PAGE gel of the expression and purification of FL-vinculin using Ni-NTA affinity and cation exchange chromatography. L; ladder (kDa), 1; pre-induction, 2; post induction, 3; after sonication, 4; after spinning, 5; Ni-NTA flow-through, 6; Ni-NTA fraction 1, 7; Ni-NTA fraction 2, 8; Ni-NTA fraction 3, 9; after TEV cleavage, 10; Q-column flow-through, 11; Q-column fraction 1, 12; Q-column fraction 2, 13; Q-column fraction 3, 14; Q-column fraction 4. Fraction 1 eluted from cation exchange chromatography was exchanged into appropriate buffer, concentrated and used for further experiments. Fractions 2, 3 and 4 were disregarded due to the degree of proteolytic cleavage.

MST was used to investigate the binding affinity of paxillin LD1-5 for FL-vinculin. Un-cleaved paxillin LD1-5 was coupled to an equimolar amount of NT-647 dye via the C-terminal his-tag and titrated against an increasing concentration of FL-vinculin. MST analysis of his-tagged paxillin LD1-5 binding to FL-vinculin revealed a 72-fold and 23-fold increase in affinity compared to VD1-4 and VtΔLinker, respectively (figure 30). It is important to add that the calculated binding constant may have been affected by

contributions from the degradation products of FL-vinculin to the concentration calculation.

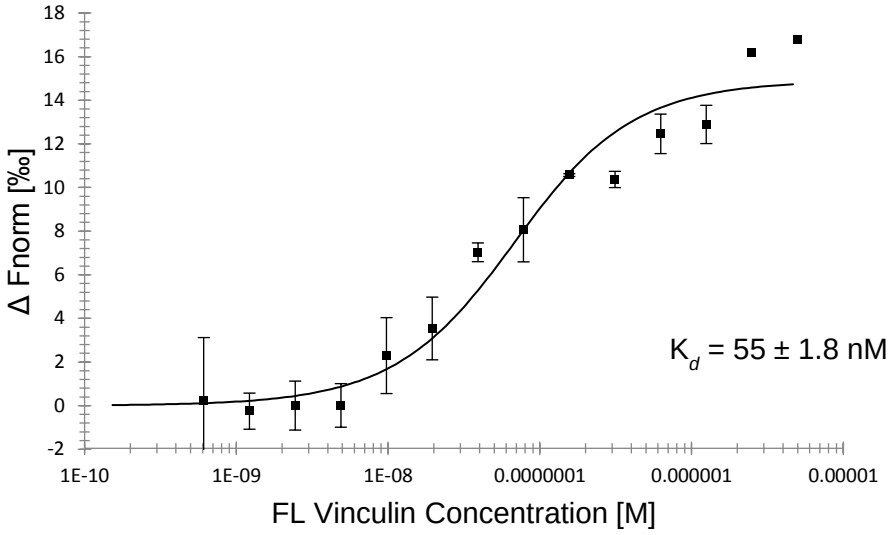

Figure 30. Paxillin LD1-5 binds full-length vinculin with high affinity. MST analysis of His-tagged paxillin LD1-5 binding to full-length vinculin. All measurements were performed in triplicate. Dissociation constants ± standard errors are indicated in the legend.

Binding of paxillin LD1-5 to FL-vinculin was also confirmed using SEC-MALS, indicated by a shift and broadening of the vinculin: paxillin LD1-5 peak indicative of formation of a larger complex (figure 31).

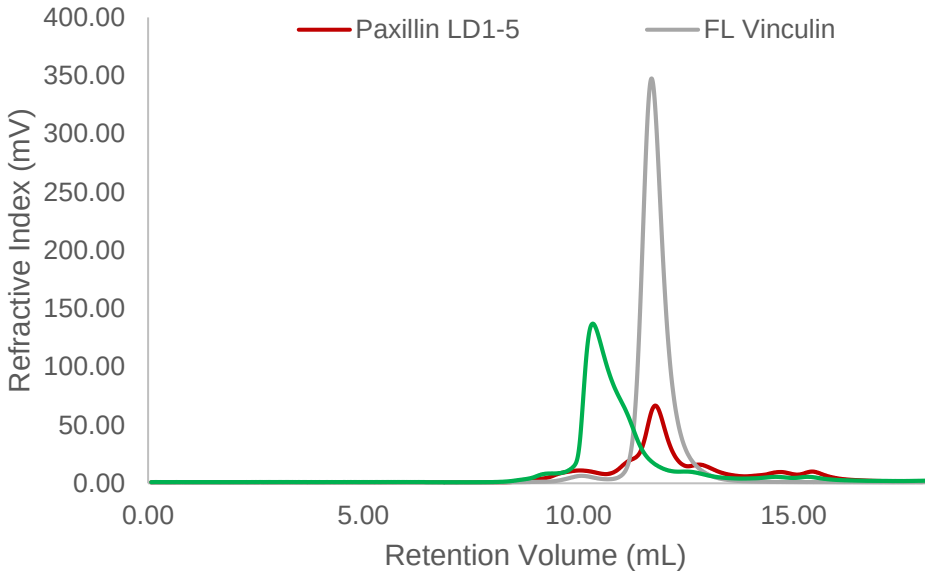

Figure 31. Paxillin LD1-5 binds full-length vinculin. Paxillin LD1-5 (red) and FL-vinculin (grey) were analysed on a gel filtration column. Paxillin LD1-5 was incubated with an equimolar concentration of FL-vinculin for 30 minutes at room temperature and analysed (green).

The protein eluted in 0.75 ml fractions and was analysed by SDS-PAGE (data not shown). However, the protein was too dilute to be observed clearly.

3.1.5. Paxillin engages the head and tail domains of vinculin simultaneously.

Crystal structures of FL-vinculin has revealed that an interface exists between the N-terminal head domain and C-terminal tail domain (Bakolitsa et al., 2004; Borgon, Vonrhein, Bricogne, Bois, & Izard, 2004b; Izard et al., 2004). The unstructured proline-rich linker tethering the two domains together is highly flexible and facilitates conformational changes in the α-helical bundles which control the ligand-binding affinity of vinculin. FL-vinculin has been shown to exist in two conformations: 1) an autoinhibited conformation in which VD1, 3 and 4 of the head domain engage the vinculin tail domain, consequently masking numerous ligand binding sites, and 2) an

open conformation in which these binding sites are exposed following dissociation of the head domain from the tail domain.

The ability of the vinculin head domain (VD1-4) to associate with the tail domain (VtΔLinker) was confirmed by SEC-MALS.

SEC-MALS analysis revealed a reduction in the VtΔLinker peak and a shift in the VD1-4 peak following incubation of the two domains, indicating formation of a head-tail complex (figure 32). Unexpectedly, the VD1-4 : VtΔLinker complex eluted later than VD1-4, possibly due to protein loss through aggregation during the incubation period.

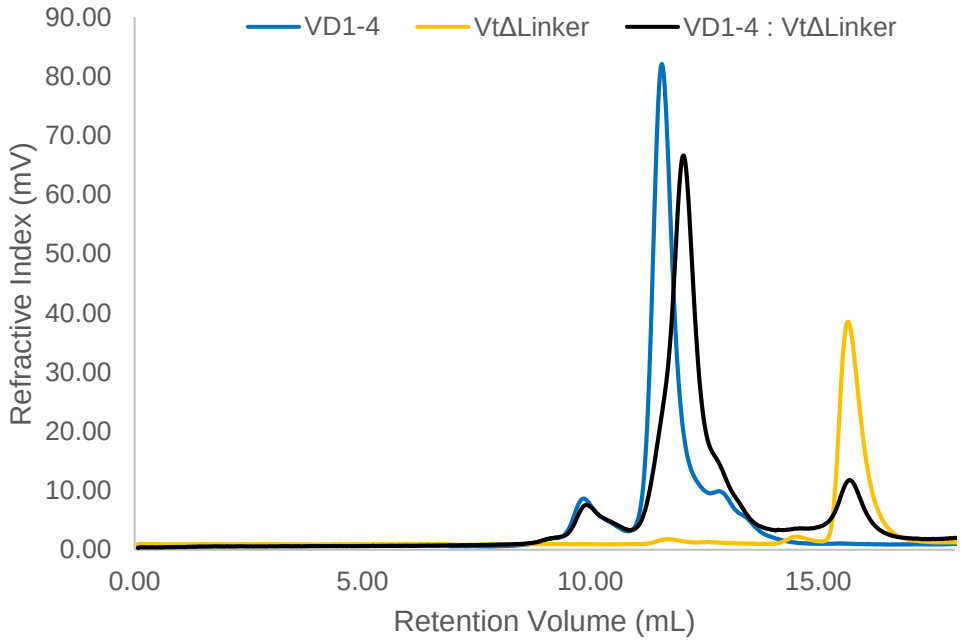

Figure 32. VD1-4 binds VtΔLinker. VD1-4 (blue) and VtΔLinker (orange) were analysed on a gel filtration column. VD1-4 was incubated with an equimolar concentration of VtΔLinker for 30 minutes at room temperature and analysed (black).

The protein eluted in 0.75 ml fractions and was analysed by SDS-PAGE (data not shown). However, the protein was too dilute to be observed clearly.

NMR experiments confirmed that the autoinhibited conformation involves contributions from VD1 and VD3 of the head domain, but not VD2 (figure 33). The four-helix VD4 bundle could not be sub-cloned into a *pET-151* vector; preventing investigation of this subdomain. Significant peak shifts were observed on addition of VD1, with more subtle shifts on addition of VD3 (both at an excess of 1:3), consistent with the VD1:Vt interface being most significant to maintain the autoinhibited head-to-tail conformation (Miller et al., 2001). As observed in the crystal structures of FL-vinculin, VD1 and VD3, held apart by VD2, form pincers that capture opposite ends of the vinculin tail, with VD2 having no involvement in the interaction (figure 34).

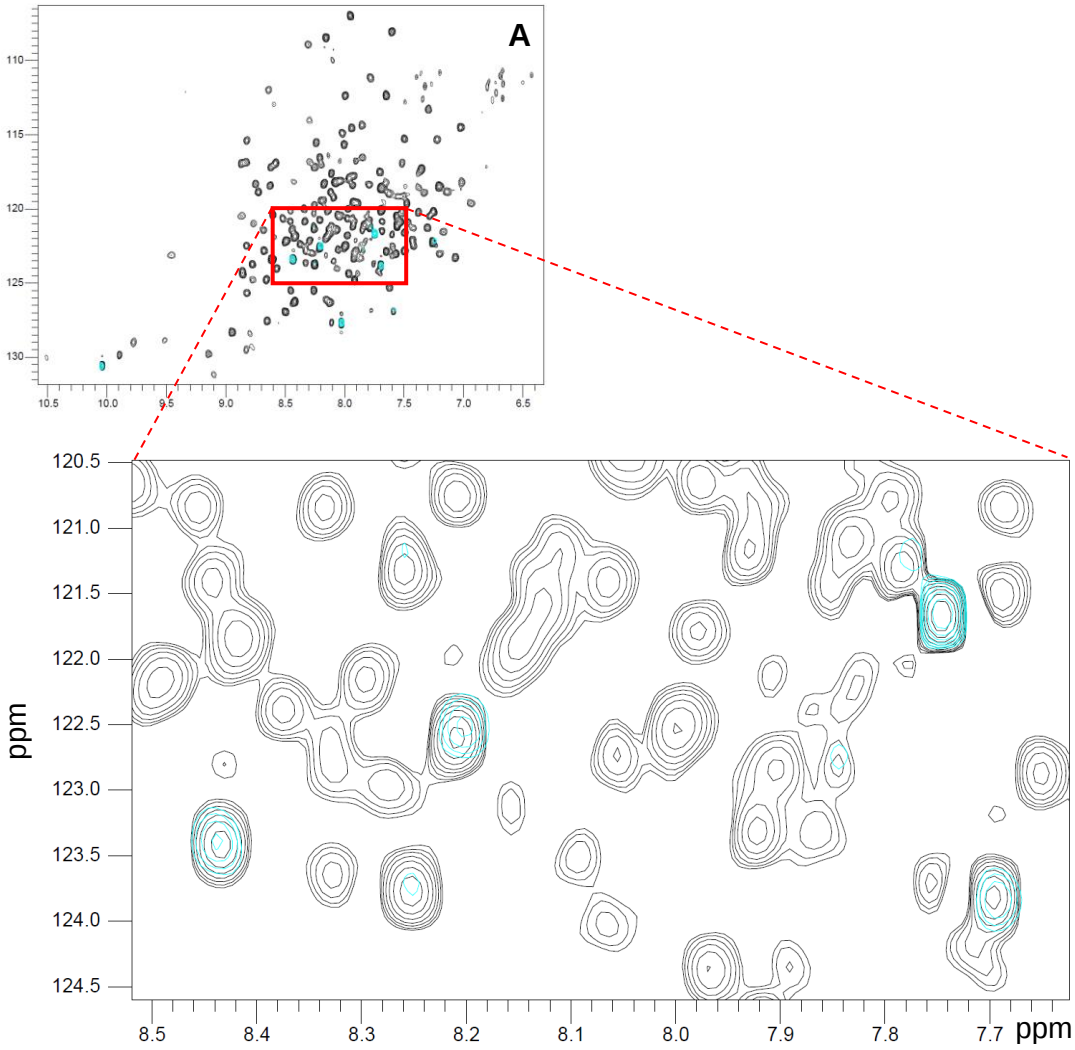

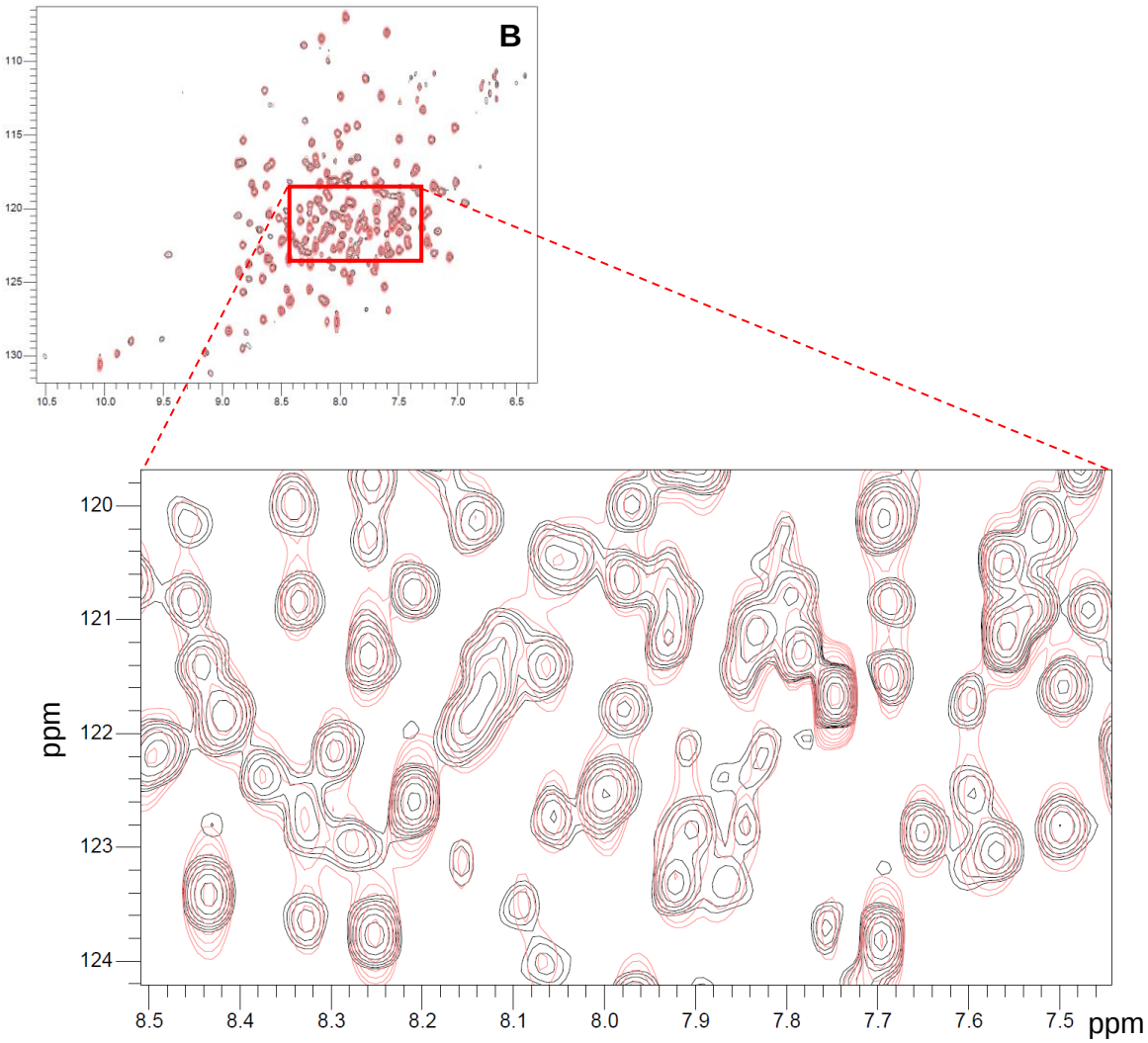
B
110
115
120
125
130
10.5
10.0
9.5
9.0
8.5
8.0
7.5
7.0
6.5
120
121
122
123
124
ppm
8.5
8.4
8.3
8.2
8.1
8.0
7.9
7.8
7.7
7.6
7.5
ppm

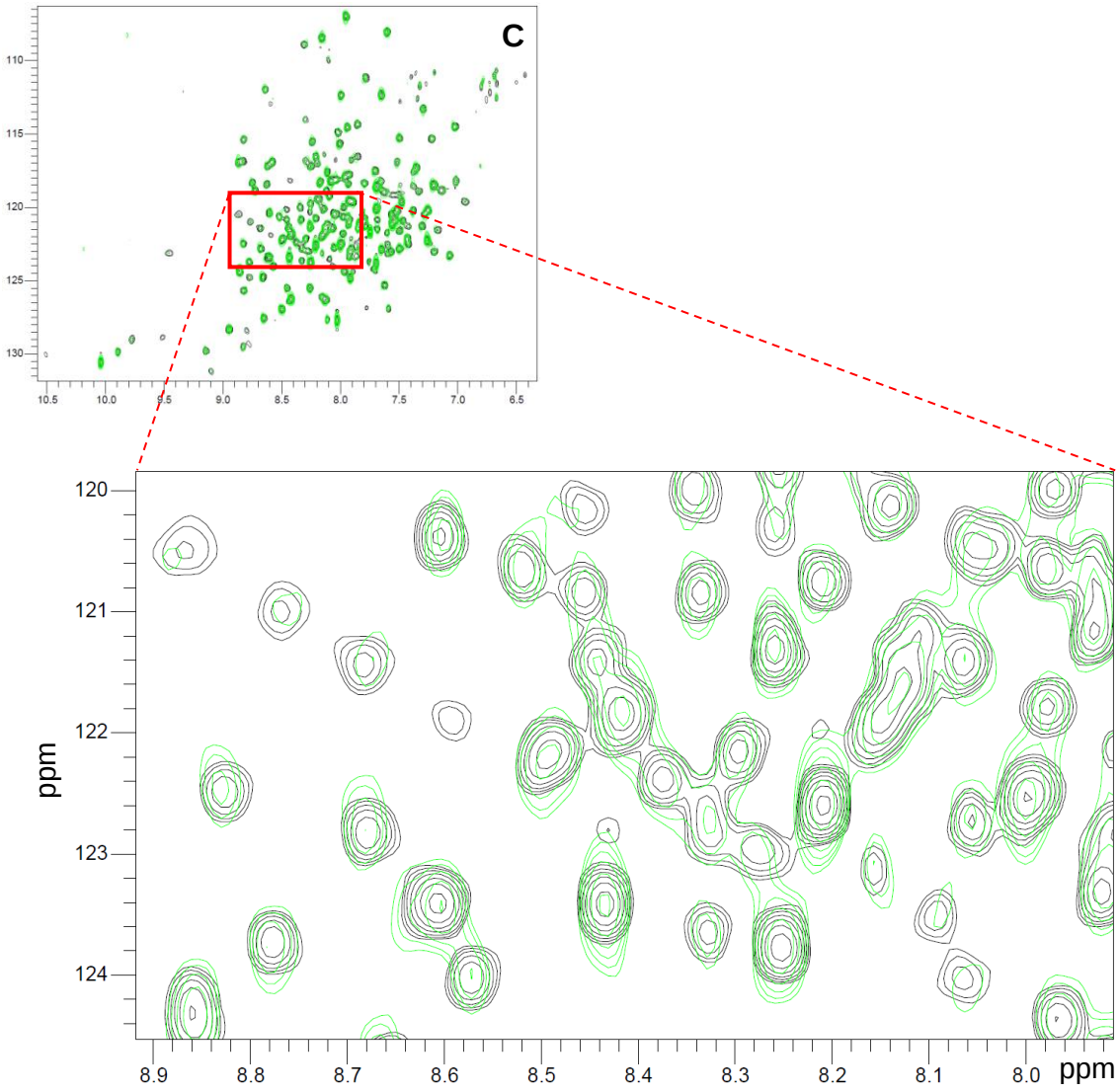

Figure 33. ^{15}N-VtΔLinker chemical shifts induced by VD1 and VD3. 2D TROSY spectra of ^{15}N-VtΔLinker overlaid with ^{15}N-VtΔLinker: VD1 (cyan) **(A)**, ^{15}N-VtΔLinker: VD2 (pink) **(B)** and ^{15}N-VtΔLinker: VD3 (green) **(C)**. Regions of the spectra are enlarged to allow identification of peak changes. VD1 and VD3 were at a 3-fold excess to VtΔLinker, VD2 was at a 2-fold excess.

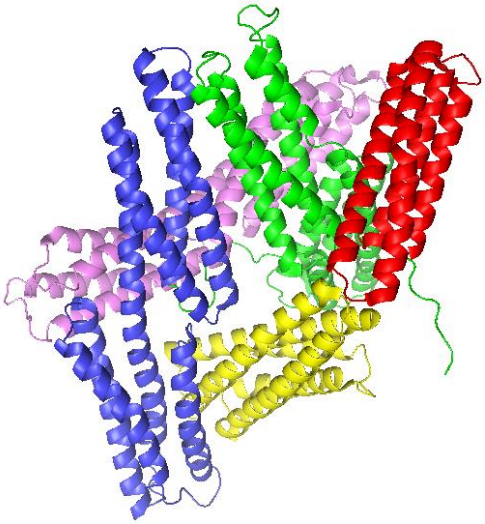

Figure 34. Autoinhibited full-length vinculin. VD1 (blue) and VD3 (green) form pincers that bind opposite ends of the five-helix tail domain (yellow). VD2 (pink) does not bind to the tail domain directly.

Since paxillin LD1-5 was shown to bind both VD1-4 and VtΔLinker, we next asked whether paxillin might facilitate the autoinhibition of FL-vinculin by wrapping around the subdomains, holding them in an inactive, compact conformation. To do this, equimolar amounts of paxillin LD1-5, VD1-4 and VtΔLinker were incubated for 30 minutes at room temperature, and then analysed by SEC-MALS. SDS-PAGE analysis of the eluted protein fraction revealed a tripartite complex involving VD1-4, VtΔLinker and paxillin LD1-5 (figure 35).

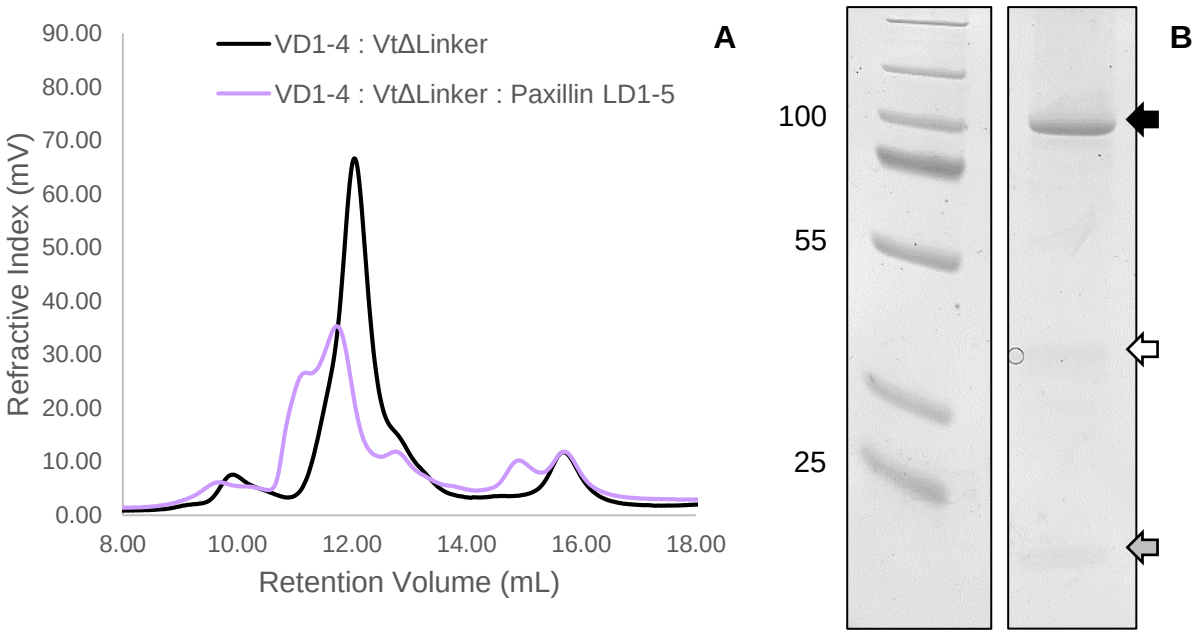

Figure 35. Paxillin LD1-5 binds VD1-4 and VtΔLinker simultaneously. (A) VD1-4 was incubated with an equimolar concentration of VtΔLinker for 30 minutes at room temperature, and then analysed by SEC-MALS (black). Equimolar concentrations of VD1-4, VtΔLinker and paxillin LD1-5 were then incubated and analysed (purple). **(B)** The eluted protein fraction (retention volume 11 mL) was run on an SDS-PAGE gel stained with coomassie blue. Three bands were observed, which correspond to VD1-4 (black arrow), paxillin LD1-5 (white arrow) and VtΔLinker (grey arrow).

3.1.6. Paxillin binds to FAK-FAT with high affinity.

Previous data has shown that paxillin binds to the focal adhesion targeting (FAT) domain of Focal Adhesion Kinase (FAK). This interaction requires the simultaneous binding of both LD2 and LD4 to opposite faces of the four-helix bundle (Bertolucci et al., 2005b).

We used FP to confirm that paxillin does indeed bind FAK-FAT via LD2 (K_d=38.75±9.70μM) and LD4 (K_d=34.57±5.98μM). Furthermore, we also detected weak binding of LD1 (K_d=114.20±10.71μM) (figure 36). Although a binding constant could not be determined for the binding of LD5 to FAK-FAT, fluorescence changes suggest a weak, possibly non-specific interaction.

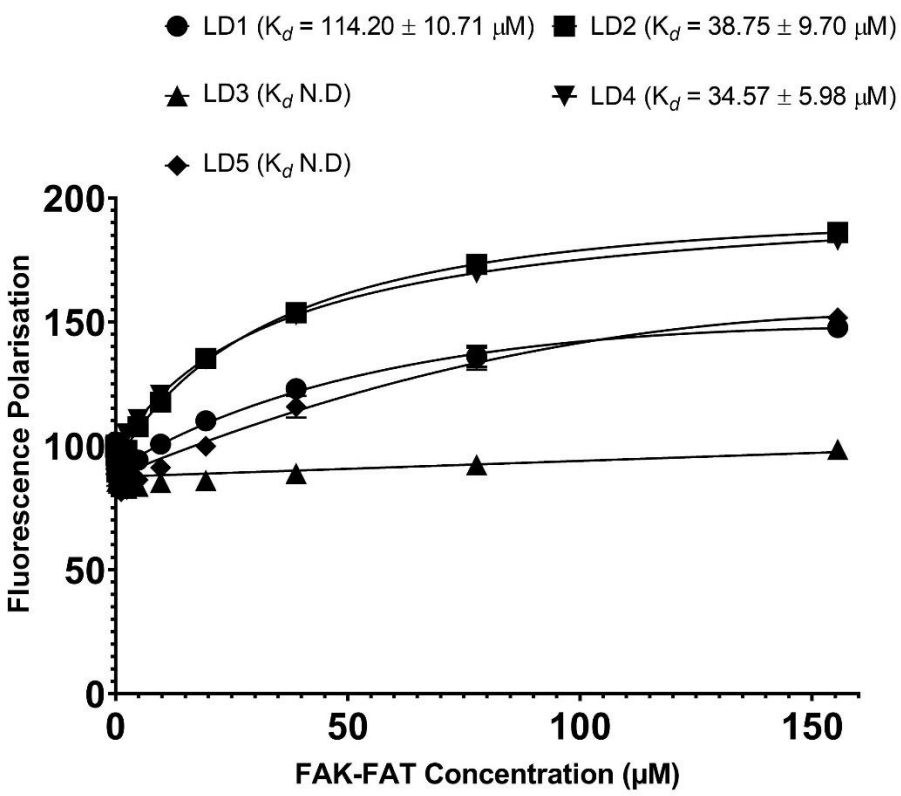

Figure 36. FAK-FAT binds multiple paxillin LD motifs. Binding of fluorescein-labelled paxillin LD1 (3-22)C, LD2 (141-153)C, LD3 (214-228)C, LD4 (262-274)C and LD5 (331-352)C to FAK-FAT, measured using a fluorescence polarisation assay. All measurements were performed in triplicate. Dissociation constants ± standard error are indicated in the legend. ND; not determined.

Having determined that the paxillin LD motifs function cooperatively to enhance the binding affinity for vinculin (see section 3.1.3.), we wanted to investigate whether this is also the case for FAK-FAT. To do this, his-tagged paxillin LD1-5 was titrated against an increasing concentration of FAK-FAT. MST analysis revealed a 1000-fold increase in affinity compared to the individual LD peptides (figure 37), confirming that the LD motifs function cooperatively to enhance the affinity of paxillin for both vinculin and FAK.

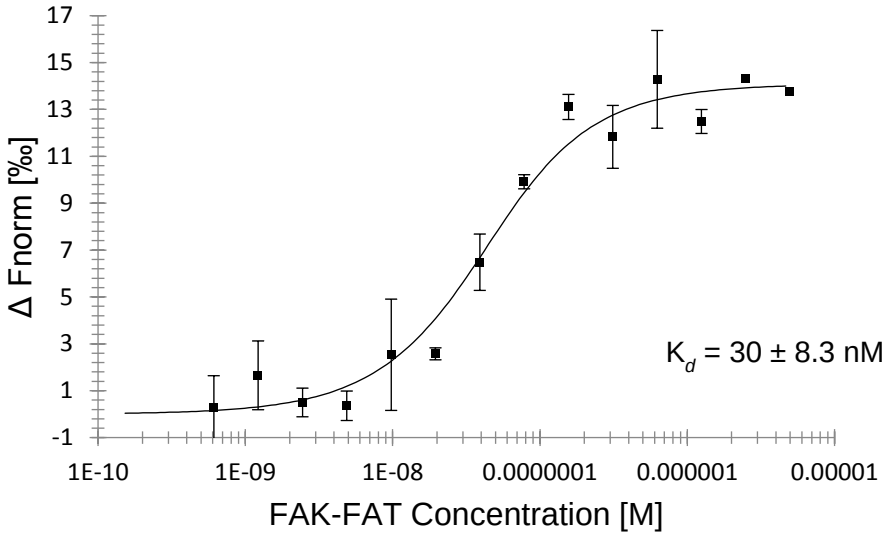

Figure 37. Paxillin LD1-5 binds FAK-FAT with higher affinity compared to individual LD peptides. MST analysis of His-tagged paxillin LD1-5 binding to FAK-FAT. All measurements were performed in triplicate. Dissociation constants ± standard errors are indicated in the legend.

Chapter 2: Functions of the C-terminal LIM region of paxillin.

Introduction

LIM domains are zinc-binding structures that coordinate two zinc ions via conserved cysteine and histidine residues, with a secondary structure comprised of both beta sheets and alpha helices. Paxillin contains four LIM domains (LIM 1-4), organised in tandem at the C-terminal end of the protein (figure 38).

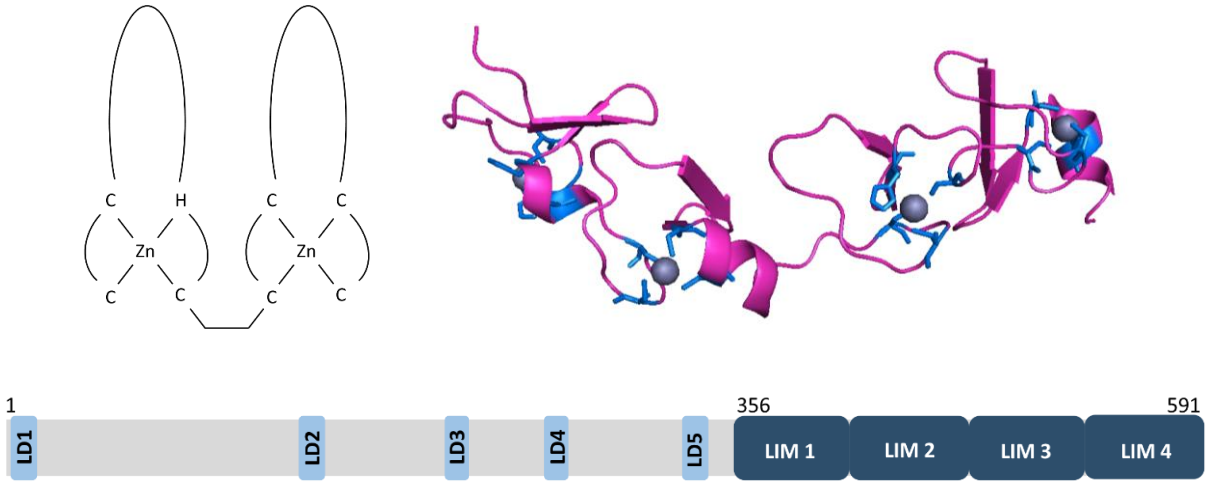

Figure 38. LIM domain structure.
Each LIM domain coordinates two zinc ions (grey spheres) via seven conserved cysteine residues (blue sticks) and one conserved histidine residue (blue sticks) (Gill, 1995). The four LIM domains of paxillin are located in tandem at the C-terminus.

Due in part to the complexity of the LIM domain structure, the role of the paxillin LIM domains in facilitating paxillin activity has not been well studied biochemically. However, the four paxillin LIM domains are thought to function as a modular protein binding site and have been implicated in recruitment to focal adhesions (Brown et al., 1996) and possible regulation of paxillin activity via autoinhibition (Böttcher et al., 2017a). Direct interactions with the tyrosine phosphatase PTP-PEST, tubulin and several uncharacterised serine/threonine kinases have been established (Côté et al., 1999; Herreros et al., 2000; Christopher E. Turner, 2000), and a link with the

mechanosensitive scaffold protein talin has been identified (Zacharchenko, Qian, Goult, Critchley, et al., 2016).

This chapter aims to investigate the role of the LIM domains in coordinating paxillin function. Using GST pulldown experiments, we investigate the biochemical evidence to support a paxillin-talin interaction, and explore the possibility that paxillin activity is regulated via an autoinhibited mechanism, similar to that employed by numerous other focal adhesion-associated proteins.

3.2.1. Expression and purification of paxillin LIM fragments.

Paxillin LIM 1-4 (residues 356-591, 27 kDa) was not soluble in a *pET-151* vector and was instead sub-cloned into a *pGEX-TEV* vector containing a 26 kDa N-terminal glutathione *S*-transferase (GST) solubility tag (figure 39).

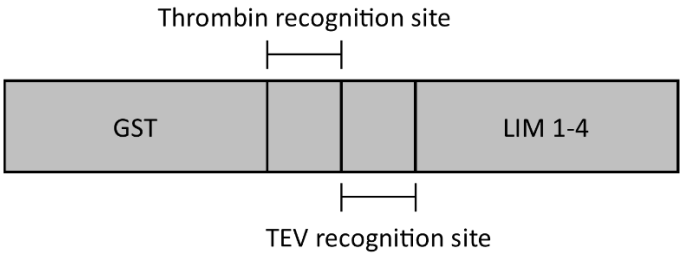

Figure 39. GST-LIM 1-4 construct.

The construct was expressed in *E. coli,* as described in section 2.1.1, and purified by batch chromatography using glutathione beads, as described in section 2.2.5 (figure 40). 1 mM $ZnSO_4$ was added to the buffer to ensure the key structural zincs were not lost, and thus facilitate correct protein folding. The protein was used in pulldown experiments and so was not cleaved from the GST tag, giving a final molecular weight of approximately 53 kDa.

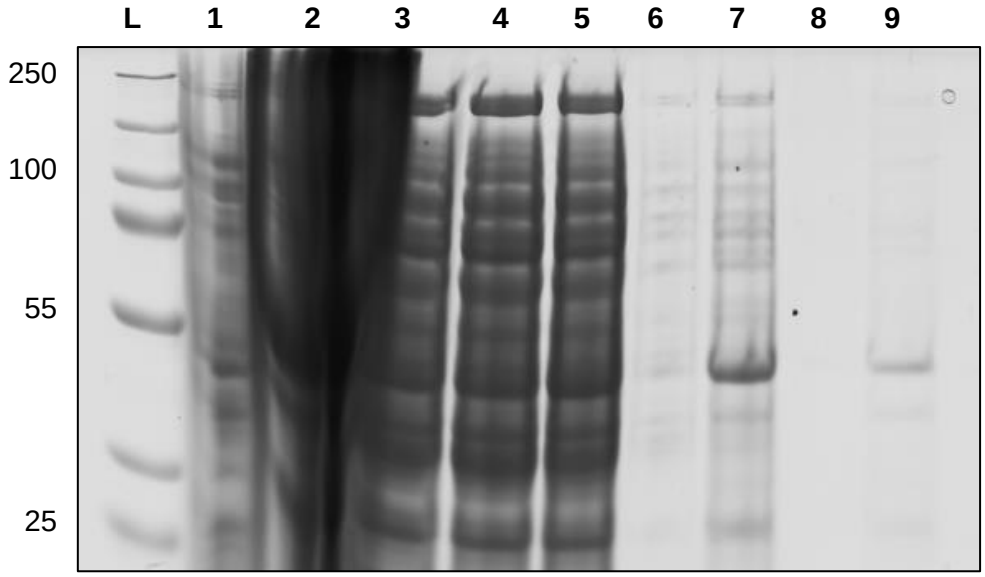

Figure 40. Expression and purification of GST-tagged LIM 1-4. A coomassie stained SDS-PAGE gel of the expression and purification of LIM 1-4 using batch chromatography with glutathione beads. Following sonication, the soluble fraction was incubated with glutathione beads, prior to five wash-spin cycles with 20 mM HEPES, 100 mM NaCl, 1 mM $ZnSO_4$. L; ladder (kDa), 1; post induction, 2; after sonication, 3; after spinning, 4; SN after spin 1, 5; beads after spin 1, 6; SN after wash 1, 7; beads after wash 1, 8; SN after wash 5, 9; beads after wash 5.

LIM 1-2 (residues 356-473, 13.5 kDa) in a *pGST-1* vector (Sheffield, Garrard, & Derewenda, 1999) (figure 41) was kindly provided by Prof Jun Qin and Dr Liang Zhu of the Lerner Research Institute, Cleveland.

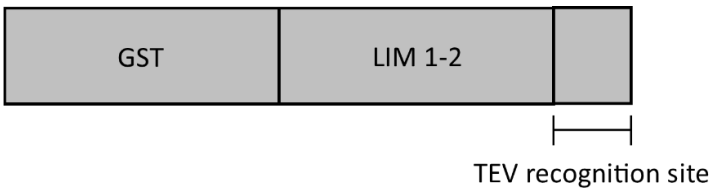

Figure 41. GST-LIM 1-2 construct.

The construct was transformed into *BL21 DE3 E. coli* cells, expressed, and purified by batch chromatography using glutathione beads, as described in sections 2.1.2 and 2.2.5 (figure 42). The protein was used in pulldown experiments and so was not cleaved from the GST tag, giving a final molecular weight of approximately 39.5 kDa.

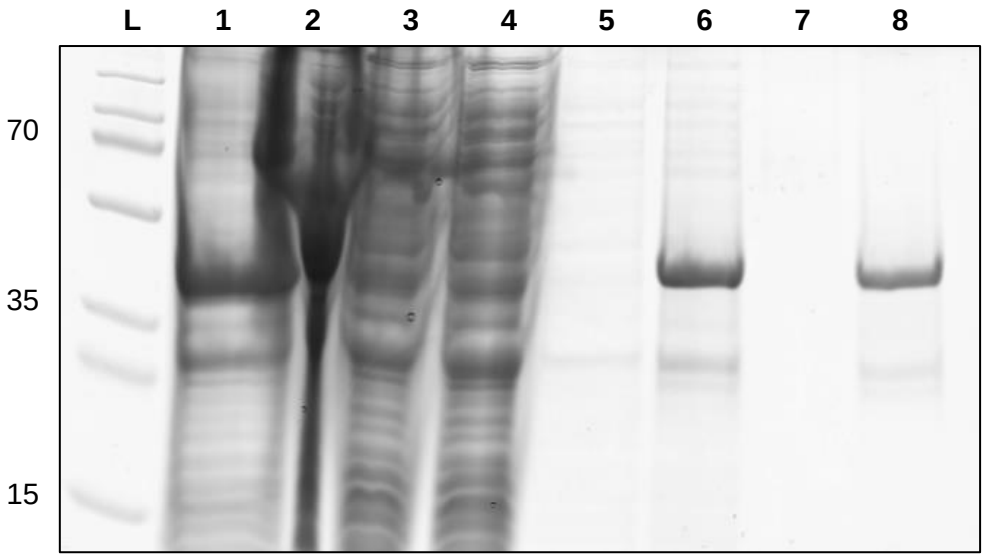

Figure 42. Expression and purification of GST-tagged LIM 1-2. A coomassie stained SDS-PAGE gel of the expression and purification of LIM 1-2 using batch chromatography with glutathione beads. Following sonication, the soluble fraction was incubated with glutathione beads, prior to five wash-spin cycles with 20 mM HEPES, 100 mM NaCl, 1 mM $ZnSO_4$. L; ladder (kDa), 1; post induction, 2; after sonication, 3; SN after spin 1, 4; beads after spin 1, 5; SN after wash 1, 6; beads after wash 1, 7; SN after wash 5, 8; beads after wash 5.

LIM 3-4 (residues 474-591) in a *pGST-1* vector was also provided by Dr Liang Zhu. The construct was transformed, expressed and purified in the same manner as LIM 1-2, however GST-tagged LIM 3-4 (approximately 39.5 kDa) could not be purified using batch chromatography (figure 43).

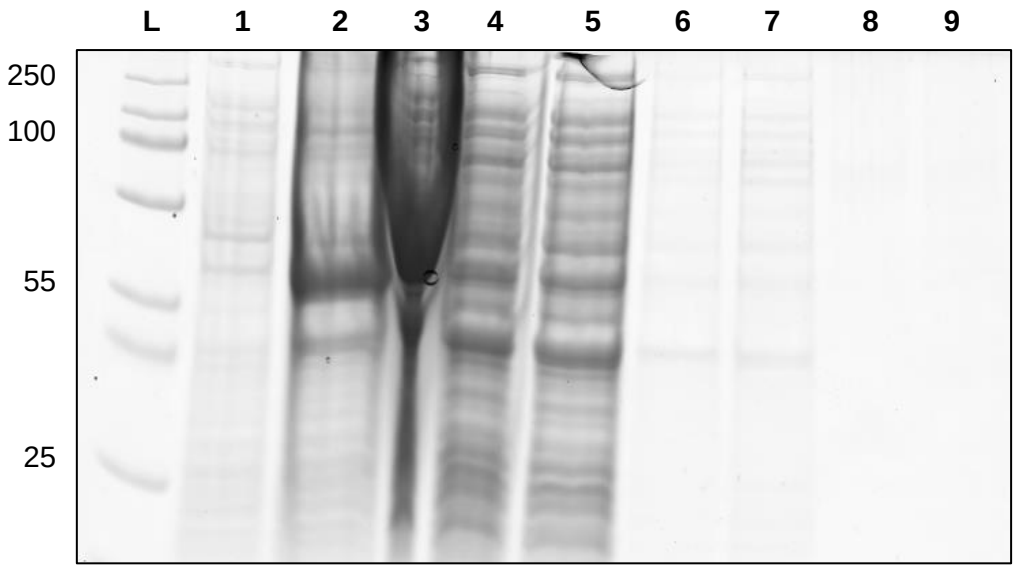

Figure 43. Expression and purification of GST-tagged LIM 3-4. A coomassie stained SDS-PAGE gel of the expression and purification of LIM 3-4 using batch chromatography with glutathione beads. Following sonication, the soluble fraction was incubated with glutathione beads, prior to five wash-spin cycles with 20 mM HEPES, 100 mM NaCl, 1 mM $ZnSO_4$. L; ladder (kDa), 1; pre-induction, 2; post induction, 3; after spinning, 4; SN after spin 1, 5; beads after spin 1, 6; SN after wash 1, 7; beads after wash 1, 8; SN after wash 5, 9; beads after wash 5.

3.2.2. Paxillin binds talin via the LIM domains.

The C-terminal LIM domains of paxillin, particularly LIM 2 and 3, have been implicated in recruitment to FAs via the focal adhesion targeting sequence (Brown et al., 1996). Furthermore, mitochondrial targeting assays have demonstrated that paxillin and talin colocalise (Atherton et al., 2019), and reduced FA localisation of paxillin in cells expressing a talin mutant lacking the R8 rod domain has been observed (Zacharchenko, Qian, Goult, Jethwa, et al., 2016a). These observations, in addition to high affinity talin-binding to the LIM domain of the muscle protein N-RAP, suggests a mechanism of paxillin recruitment involving an interaction between talin and paxillin, potentially through the paxillin LIM domain(s).

To confirm, using biochemical techniques, whether talin does indeed bind paxillin, we first utilised FP to determine whether this interaction involves the paxillin LD motifs.

Fluorescein-coupled LD 1-5 peptides were tested against F0-F3, R1-R4, R4-R8, R7-R8 and R9-R12 of talin and none were found to bind to the helical talin bundles (figure 44).

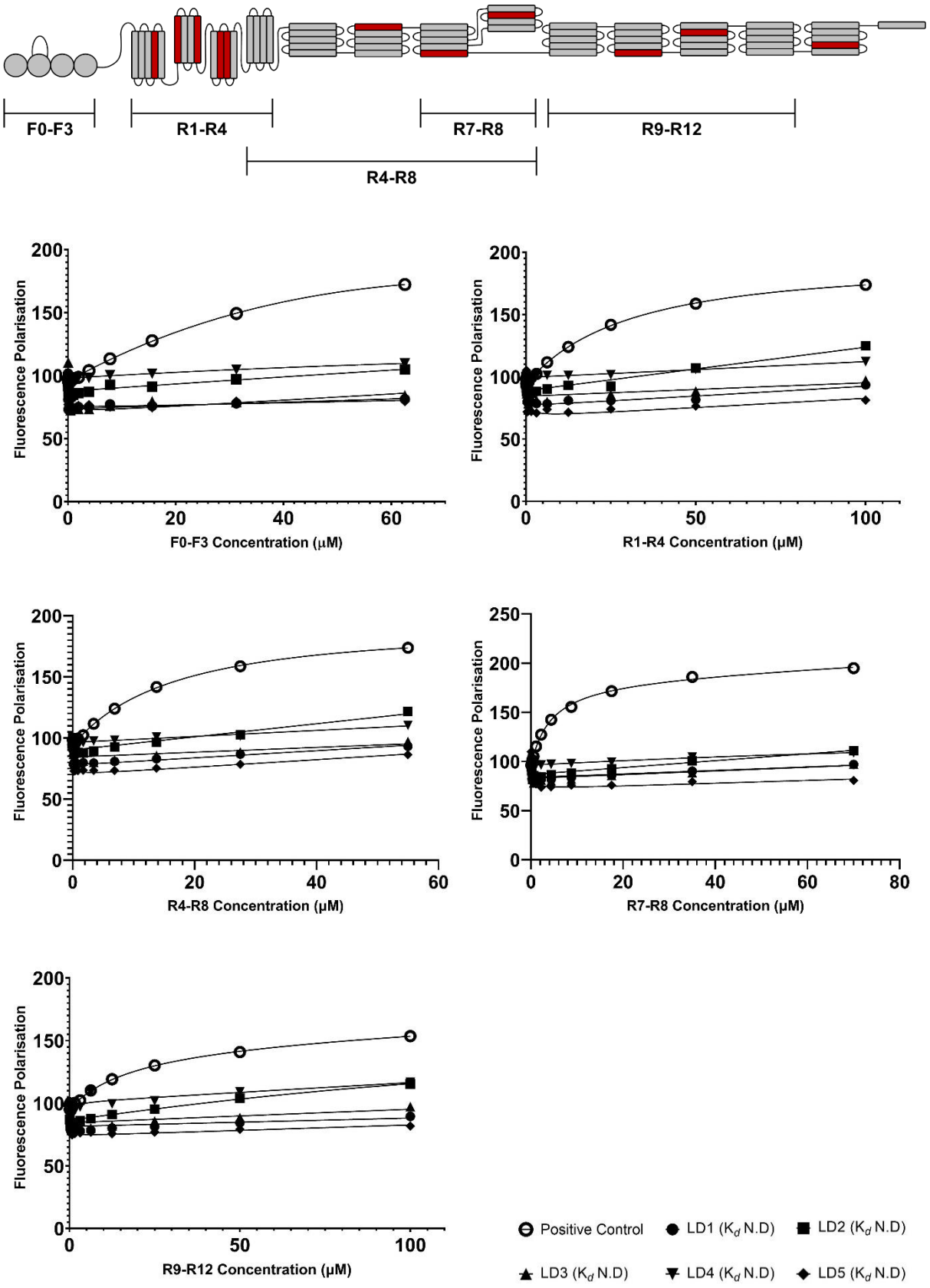

Figure 44. Talin does not bind paxillin via the LD motifs. Binding of fluorescein-labelled paxillin LD1 (3-22)C, LD2 (141-153)C, LD3 (214-228)C, LD4 (262-274)C and LD5 (331-352)C to F0-F3, R1-R4, R4-R8, R7-R8 and R9-R12 of talin, measured using

a fluorescence polarisation assay. Alpha-integrin and RIAM were used as positive controls for the talin head domain and rod bundles, respectively. Organisation of the talin bundles within the full-length structural schematic are indicated. Dissociation constants are indicated in the legend. ND; not determined.

We next asked whether paxillin binds talin via the LIM domains. To explore the involvement of the LIM domains in talin-mediated focal adhesion targeting, GST-pulldown experiments were performed using full-length talin (residues 1-2541, 269,821 Da), R1-R3 (residues 482-911, 44,224 Da), R4-R8 (residues 913-1653, 76,706 Da) and R9-R12 (residues 1655-2294, 67,305 Da) (figure 45). In each case, the bead-bound GST-tagged LIM protein was incubated with the target protein for one hour before being passed through a column. The supernatant (SN), containing any proteins that did not bind to the paxillin LIMs, was collected. The beads were then washed, resuspended in buffer and spun down to form a pellet (P). Proteins that did interact with the paxillin LIMs were bead-bound and present in the pellet.

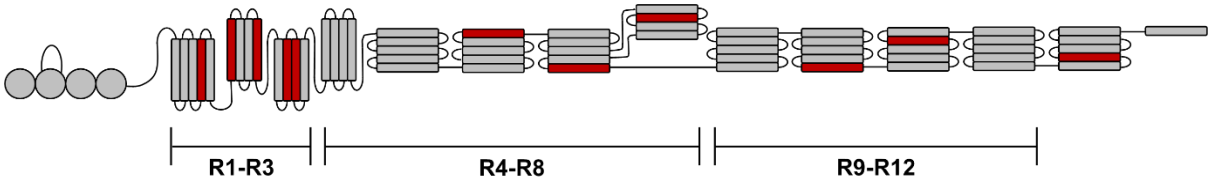

Figure 45. Talin rod domain regions used in GST pulldowns.

To first determine if a binding interaction exists between talin and the paxillin LIM domains, GST-LIM 1-2 was incubated with full-length talin and was found to pull down talin on three separate occasions (figure 46). GST-LIM 1-2 was selected over GST-LIM 1-4 due to greater protein yield following purification.

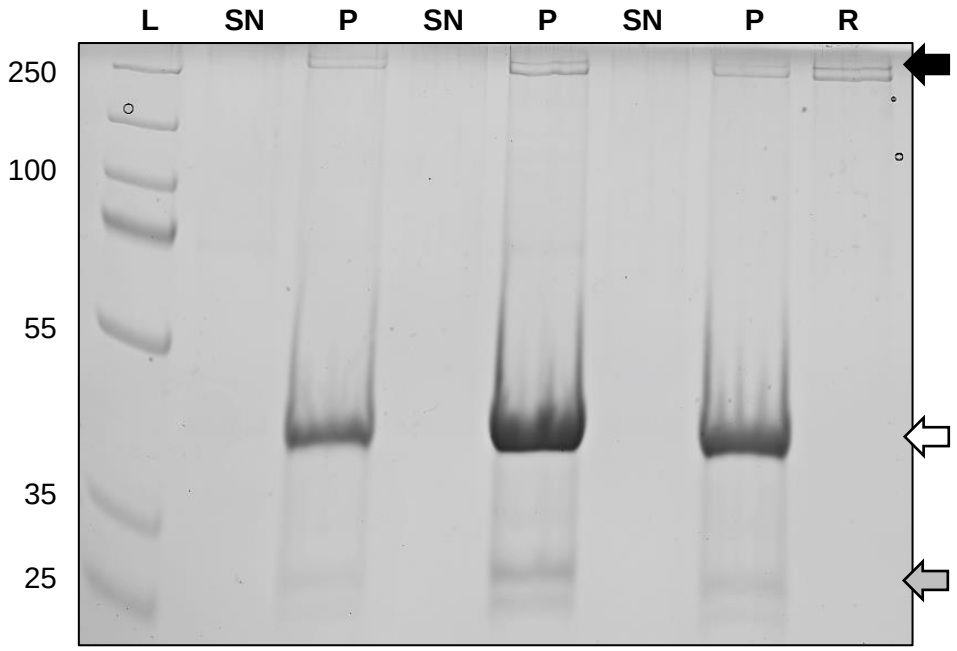

Figure 46. GST-pull down of GST-LIM1-2 with full length talin. A coomassie stained SDS-PAGE gel of GST-LIM 1-2 (white arrow) pulling down full length talin (black arrow), performed in triplicate. Due to the size of full-length talin, a sample of talin alone was run as a reference (R). The band at ~26 kDa (grey arrow) corresponds to the GST-tag. L; ladder (kDa), SN; supernatant P; pellet.

Having confirmed that talin binds the paxillin LIM domains, we next wanted to isolate which region(s) of talin facilitates this interaction. To do this, the pulldown experiments were repeated with R1-R3, R4-R8 and R9-R12, each at an initial concentration of 30 µM. To determine whether any result was due to the glutathione beads rather than the LIM protein, R1-R3, R4-R8 and R9-R12 were incubated with the beads in the absence of the paxillin LIM, as a control. Cleavage of the GST-tagged LIM construct with TEV protease would yield the isolated LIM protein and the GST tag. Incubation of the GST with the talin rod regions would provide an additional control to investigate any effect of the GST, however the paxillin LIM protein could not be identified in either the supernatant or bead-bound following TEV cleavage (data not shown). The inability to

cleave the LIM protein from the GST tag also prevented determination of the protein concentration.

In the case of R1-R3, saturation was observed in both the supernatant and the pellet, and so the experiment was repeated at 5 μM, 10 μM and 15 μM protein concentrations (figure 47). Most of the protein was present in the supernatant, with some being captured in the pellet by the glutathione beads, concluding that paxillin does not bind talin via R1-R3.

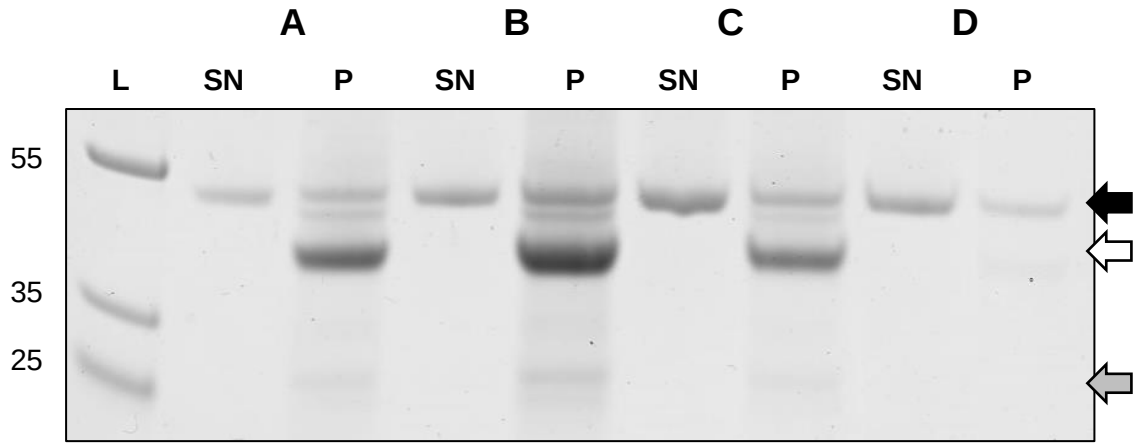

Figure 47. GST-pull down of GST-LIM1-2 with talin R1-R3. A coomassie stained SDS-gel of GST-LIM 1-2 (white arrow) incubated with R1-R3 (black arrow) at 5 μM **(A)**, 10 μM **(B)** and 15 μM **(C)** concentrations. 10 μM R1-R3 was incubated with glutathione beads in the absence of GST-LIM 1-2 as a control **(D)**. The band at ~26 kDa (grey arrow) corresponds to the GST-tag. L; ladder (kDa), SN; supernatant, P; pellet.

In the case of R4-R8, aggregation was observed immediately following incubation with GST-LIM 1-2 and GST-LIM 1-4, and so it was not possible to determine whether an interaction exists between the two protein domains. Aggregation was most likely a result of the buffer (HEPES, NaCl, $ZnSO_4$) since all of the protein was present in the pellet of the control sample (R4-R8 incubated with glutathione beads in the absence of the GST-tagged paxillin LIM domains) (figure 48).

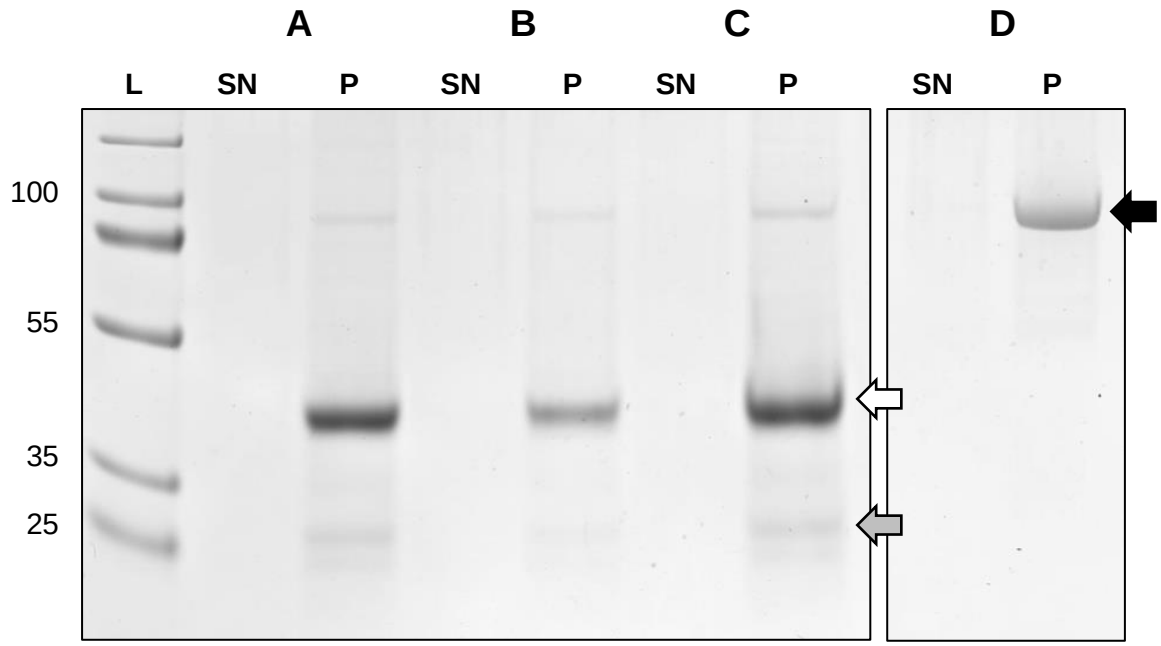

Figure 48. GST-pull down of GST-LIM1-2 with talin R4-R8. A coomassie stained SDS-PAGE gel of GST-LIM 1-2 (white arrow) incubated with 30 μM R4-R8 (black arrow), performed in triplicate **(A-C)**. R4-R8 was incubated with glutathione beads in the absence of GST-LIM 1-2 as a control **(D)**. The band at ~26 kDa (grey arrow) corresponds to the GST-tag. L; ladder (kDa), SN; supernatant, P; pellet.

In the case of R9-R12, saturation was observed in both the supernatant and the pellet and so the experiment was repeated at 5 μM R9-R12 concentration (figure 49). Most of R9-R12 was captured by GST-LIM 1-2 within the pellet, with some present in the supernatant. As with the R1-R3 control, some of R9-R12 was captured by the glutathione beads within the control sample. However, since significantly more protein was present in the pellet compared to the supernatant, it was concluded that paxillin binds talin via R9-R12.

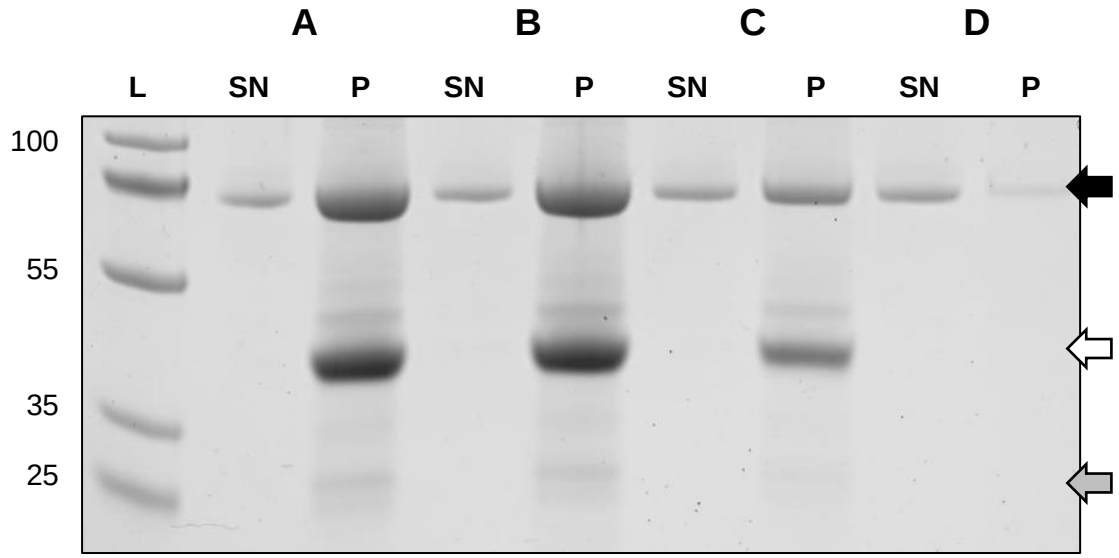

Figure 49. GST-pull down of GST-LIM1-2 with talin R9-R12. A coomassie stained SDS-PAGE gel of GST-LIM 1-2 (white arrow) incubated with 5 μM R9-R12 (black arrow), performed in triplicate **(A-C)**. R9-R12 was incubated with glutathione beads in the absence of GST-LIM 1-2 as a control **(D)**. The band at ~26 kDa (grey arrow) corresponds to the GST-tag. L; ladder (kDa), SN; supernatant, P; pellet.

Binding of paxillin to the R9-R12 bundle of talin was also confirmed by pulldown experiments with GST-LIM 1-4 (figure 50).

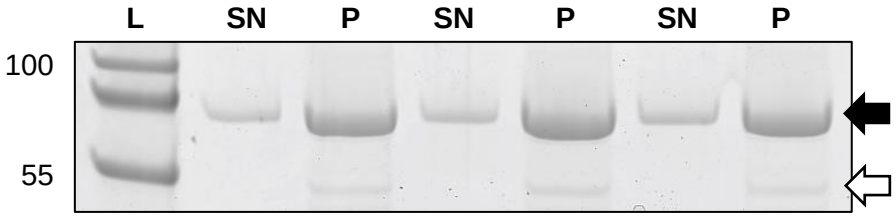

Figure 50. GST-pull down of GST-LIM1-4 with talin R9-R12. A coomassie stained SDS-PAGE gel of GST-LIM 1-4 (white arrow) incubated with 5 μM R9-R12 (black arrow), performed in triplicate. L; ladder (kDa), SN; supernatant, P; pellet.

The ability of LIM 1-2 to bind talin R9-R12 independently of LIM 3-4 suggests that the LIM domains can function as discrete binding platforms, rather than a modular protein

binding site. Additionally, engagement of talin via LIM 1-2 suggests that LIM 3-4 are not involved in this interaction, and are instead available to bind other targets.

3.2.3. The C-terminal LIM domains bind the N-terminal LD region of paxillin.

It has recently been revealed that intraprotein cross-links exists between the N-terminal LD region and C-terminal LIM region of paxillin (Böttcher et al., 2017a) (figure 51), suggesting that regulation of paxillin activity may occur via an autoinhibitory mechanism similar to that of talin, vinculin and FAK (see introduction).

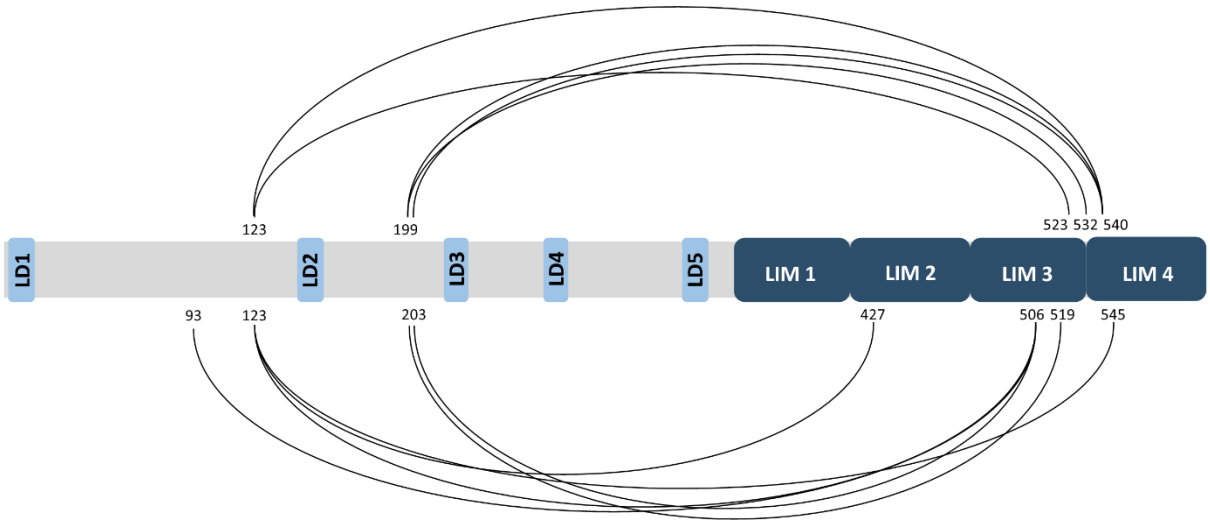

Figure 51. Intraprotein cross-links within paxillin. 32 intraprotein cross-links were identified between the N-terminal LD region and the C-terminal LIM region of paxillin. Residue positions are indicated.

To explore whether the LIM domains facilitate paxillin regulation, GST-pulldown experiments were performed using paxillin LD1-5. GST-LIM 1-2 and GST-LIM 1-4 were incubated with 30 μM paxillin LD1-5 for one hour before being passed through a column. The supernatant (SN) was collected. The beads were then washed, resuspended in buffer and spun down to form a pellet (P). If the N-terminal LD region bound to the C-terminal LIM region, it would be bead-bound and present in the pellet.

If there was no interaction between the two protein regions, paxillin LD1-5 would be present in the supernatant.

Based on the detection of only a single cross-link between the LD region and LIM 1-2 (figure 51), it was assumed that LIM 1-2 would not pull down paxillin LD-1-5. Following incubation with GST-LIM 1-2, a band at approximately 40 kDa was observed in the supernatant on every occasion (figure 52). GST-LIM 1-2 (39.5 kDa) and paxillin LD1-5 (36 kDa) are similar in size and therefore run to a similar point on an SDS-gel. Consequently, it was not possible to determine the identity of this band from SDS-gel analysis alone.

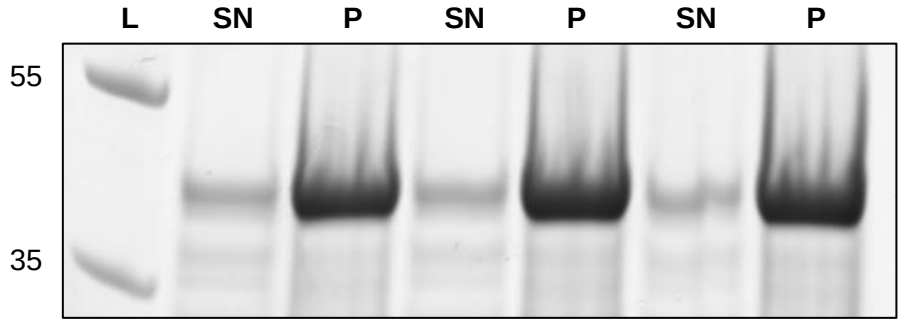

Figure 52. GST-pull down of GST-LIM1-2 with paxillin LD1-5. A coomassie stained SDS-PAGE gel of GST-LIM 1-2 incubated with 30 μM paxillin LD1-5, performed in triplicate. L; ladder (kDa), SN; supernatant, P; pellet.

Of the 32 intraprotein cross-links detected, 31 involved LIM 3-4. It was therefore hypothesised that LIM 1-4 would successfully pulldown paxillin LD1-5. In two of the three experiments performed, paxillin LD1-5 (36 kDa) was captured by GST-LIM 1-4 (53 kDa) within the pellet (figure 53B and C). However, a clear band corresponding to GST-LIM 1-4 could not be seen on the gel, although this was a characteristic of other pulldown experiments performed using GST-LIM 1-4 (data not shown) and may be a result of the low protein yields following batch purification.

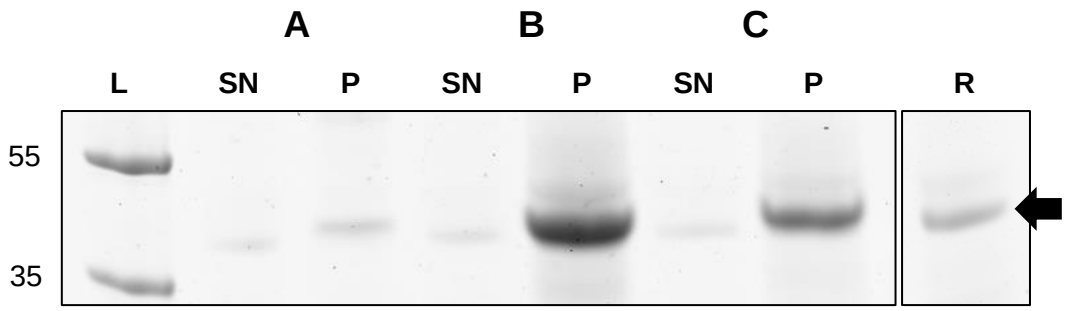

Figure 53. GST-pull down of GST-LIM1-4 with paxillin LD1-5. A coomassie stained SDS-PAGE gel of GST-LIM 1-4 incubated with 30 μM paxillin LD1-5 (black arrow), performed in triplicate **(A-C)**. Due to the instability of the unstructured LD region, LD1-5 was run alone as a reference (R). L; ladder (kDa), SN; supernatant, P; pellet.

The ability of LIM 1-4 to pull-down paxillin LD1-5 provide early indications that paxillin activity may be regulated via an autoinhibitory interface between the N-terminal LD region and the C-terminal LIM domains. Based on the intraprotein crosslinks currently identified, combined with the revelation that LIM 1-2 engage talin R9-R12, it is likely that LIM 3-4 are responsible for the interaction with the LD region, however further experimental optimisation is required to confirm this.

4. Discussion and Conclusions

This study explored the interactions between the focal adhesion-associated proteins paxillin, vinculin and talin. Biochemical and biophysical techniques were used to characterise these interactions and unveil novel functions of paxillin beyond simply a protein scaffold.

4.1. A novel interaction between paxillin and the vinculin head domain.

It had previously been established using gel-blot assays that ^{125}I-labelled paxillin binds to the C-terminal region of vinculin (C E Turner et al., 1990). Using transfection experiments, the paxillin-binding site was localised to a stretch of 50 amino acids spanning residues 979-1028, corresponding to the vinculin tail domain (Wood et al., 1994). Truncation and deletion mutagenesis characterised this interaction further by localising the vinculin-binding site on paxillin to a stretch of 21 amino acids spanning residues 143-164 (Brown et al., 1996). Sequencing of full-length paxillin has since enabled the mapping of this region to the second LD motif located at the N-terminal region.

Using FP and NMR, we have confirmed that paxillin LD2 binds to the vinculin tail domain. Furthermore, FP and SEC-MALS analysis revealed a novel additional interaction between the vinculin head domain (VD1-4) and the paxillin LD motifs 1, 2 and 4. In each case, binding of the individual LD motifs was weak and thus could not be assigned an equilibrium dissociation constant (K_d).

4.2. LD motifs can function cooperatively to enhance binding affinity.

Despite the limitations of FP to investigate only protein-peptide interactions, MST enabled us to explore the interaction between vinculin and the whole 36 kDa N-

terminal LD region of paxillin. Binding of paxillin to the vinculin head domain was found to involve three of the five LD motifs, with each motif binding weakly. It was therefore hypothesised that the affinity of paxillin for vinculin would increase if all three motifs could bind simultaneously. As hypothesised, paxillin LD1-5 bound to the vinculin head domain with μM affinity. Surprisingly, paxillin LD1-5 also bound to the vinculin tail domain with μM affinity, despite only LD2 being implicated in the interaction.

In addition to binding vinculin, we confirmed that paxillin binds to the α-helical focal adhesion targeting domain of FAK by direct interactions with LD2 (K_d=38.75±9.70μM) and LD4 (K_d=34.57±5.98μM). Weak binding of LD1 was also detected (K_d=114.20±10.71μM), although the contribution from LD1 to the paxillin-FAK complex is yet to be established. Having determined that the paxillin LD motifs function cooperatively to enhance the affinity for vinculin, MST analysis revealed that the same is true for FAK. Paxillin LD1-5 bound to the FAK-FAT domain with nanomolar affinity and 1000-fold greater than LD2 and LD4 alone. In conclusion, in addition to providing discrete binding platforms, evidence presented here suggests that the five LD motifs can function cooperatively to strengthen paxillin-mediated interactions.

4.3. Paxillin may facilitate the autoinhibition of vinculin.

Vinculin can exist in either a low-affinity autoinhibited conformation characterised by head-to-tail association, or in an open and ligand-accessible conformation. Unlike endogenous full-length vinculin, vinculin constructs that either lack the C-terminal tail domain (vin880, vin258) or are constitutively active (vinT12) cannot form head-to-tail associations and have been shown to induce a dramatic increase in FA size, number, and residency time, in addition to delaying the turnover rate of talin and integrin (Humphries et al., 2007b).

MST analysis revealed that paxillin has greater affinity for full-length vinculin, and binds with 72-fold higher affinity compared to the head domain, and 23-fold higher affinity compared to the tail domain. Furthermore, VD1-4, VtΔLinker and paxillin LD1-5 eluted as a tripartite complex involving the three protein domains, as evidenced by SDS-PAGE of the fractions eluted from size exclusion chromatography.

Cell adhesion is highly dynamic and requires the continual switching of proteins between their active and inactive states. How paxillin and vinculin cooperate together to regulate adhesion dynamics is still not clear. For example, paxillin has been shown to colocalise with vin880, yet YFP-vin880 expressed in paxillin-deficient cells can still induce FAs similar in size and number as those in wild-type cells (Humphries et al., 2007b). These observations suggest that 1) paxillin is not required at the initial stages of FA formation, and 2) paxillin is recruited downstream of the vinculin-talin interaction and independently of the paxillin-binding site within the vinculin tail. Additionally, unlike talin and integrin, the turnover rate of paxillin is not affected in vin880, vin258 or vinT12-mutant cells, suggesting that paxillin only transiently associates with the core integrin-talin-vinculin complex (Humphries et al., 2007b). Together, these observations suggest a mechanism whereby, subsequent to vinculin activation and talin-actin cross-linking, paxillin is somehow recruited to the core adhesion complex where, as the data in this thesis suggests, it transiently engages both the head and tail domains of vinculin.

Fluorescence Resonance Energy Transfer (FRET) describes the distance-dependent transfer of energy from an excited donor fluorophore to an acceptor fluorophore within several nanometres. Although determined statistically insignificant, FRET measurements of a vinculin conformation sensor were reduced in the absence of paxillin (Case et al., 2015), suggesting that the vinculin head and tail domains exist in

a more open conformation in the absence of paxillin. Since vinculin can only engage exposed VBS within the talin rod following head-to-tail dissociation, it suggests that the paxillin LD motifs bind to the open vinculin conformation.

Simultaneous engagement of the vinculin head and tail domains by multiple paxillin LD motifs subsequent to vinculin activation suggests a mechanism of facilitated autoinhibition, in which paxillin regulates the vinculin autoinhibition status and thus regulates binding of talin and actin to vinculin that ultimately promotes mechanical linkages. Based on the hypothesis that paxillin facilitates the autoinhibition of vinculin by influencing its conformational state, paxillin LD1, 2 and 4 were modelled onto the solved structure of full-length, autoinhibited human vinculin (figure 11A) (Borgon et al., 2004).

4.3.1. Proposed model of the paxillin-vinculin interaction.

It was previously established, and has since been confirmed during this study, that paxillin LD2 directly engages the vinculin tail domain. Consequently, the predicted binding interface and orientation of LD2 on the vinculin tail was modelled, using the alignment tool in PyMOL in addition to manual adjustment, and subsequently enabled us to predict potential LD4 and LD1 vinculin-binding sites.

The four-helical FAT domain of FAK and the five-helical tail domain of vinculin share similar topology and have both been shown to bind the LD2 motif of paxillin. Both domains are right-turn bundles, with helices 1-4 of FAK-FAT sharing three-dimensional similarities with helices 2-5 of the vinculin tail (figure 54).

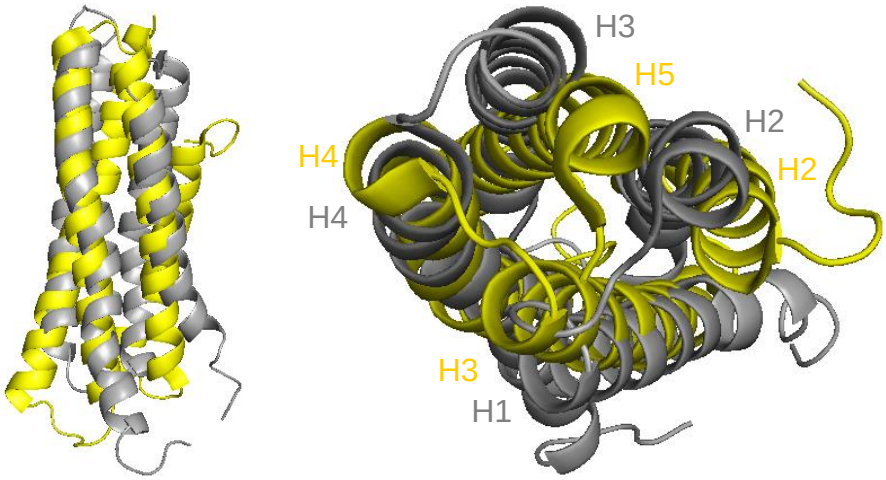

Figure 54. Topographical similarities of the FAK-FAT and vinculin tail domains. Helices 1-4 of the FAK-FAT domain (grey) were overlaid with helices 2-5 of the vinculin tail domain (yellow). Helices are numbered accordingly.

LD2 binds preferentially to a hydrohobic pocket between helix 1 and helix 4 of FAK-FAT, stabilised via a salt bridge between E144 of paxillin and K23 on helix 1 of FAK-FAT (figure 55).

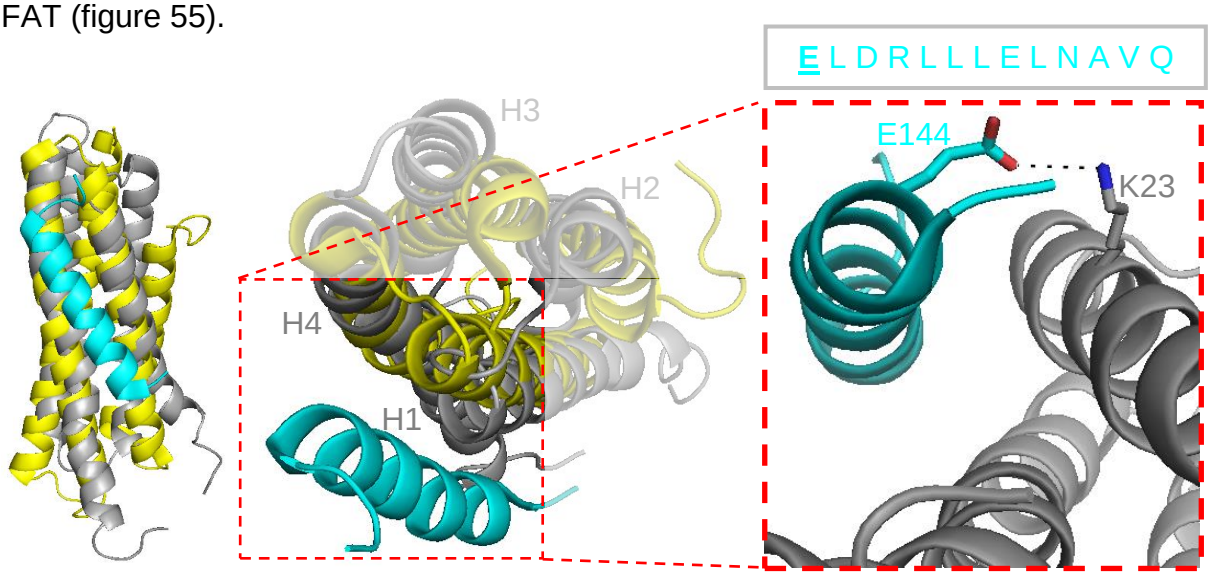

Figure 55. Strutural characteristics of the binding interface between paxillin LD2 and FAK-FAT. LD2 (cyan) docks against helices 1 and 4 of the FAK-FAT domain (grey), stabilised by a salt bridge (black dashed line) between E144 of paxillin and K23 of FAK-FAT. Helices are numbered 1-4. The position of E144 within the LD2 motif is highlighted.

Based on the topographical similarities between FAK-FAT and the vinculin tail (Vt) domains, LD2 was initally modelled to an interface formed by helices 3 and 4 of Vt. The helical motif was then adjusted to permit formation of a salt bridge between D145 of paxillin and a optimally positioned lysine, K996 of vinculin. Surface analysis confirmed that this binding site is accessible in the full-length vinculin structure, and orients LD2 in an N-C terminal position (figure 56). Binding of LD2 in proximity to VD1 may facilitate weak interactions and thus account for fluorescence changes observed during the FP assay (section 3.2.2).

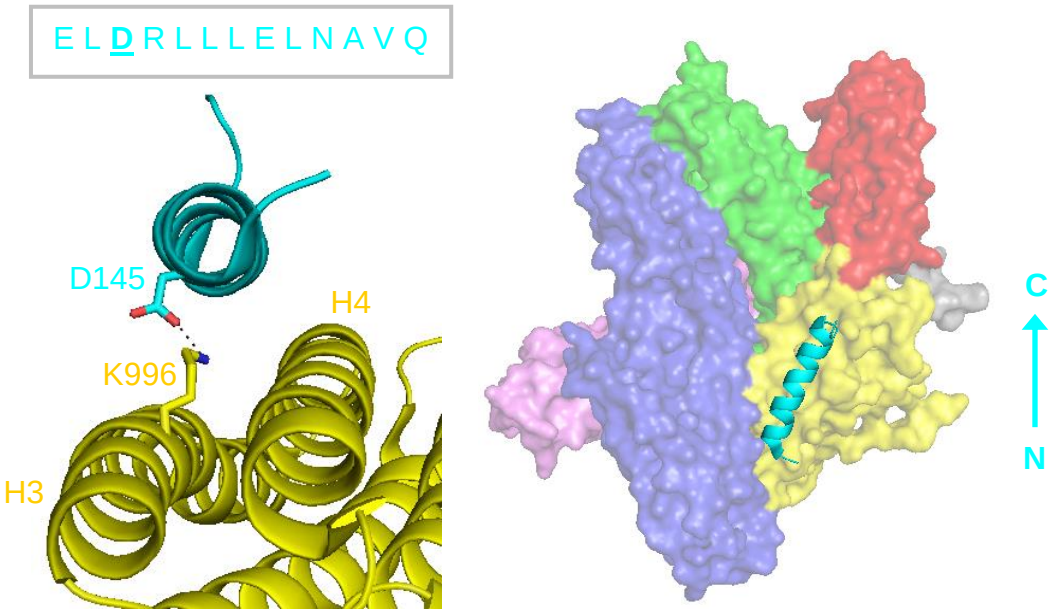

Figure 56. Proposed binding interface between paxillin LD2 and Vt. LD2 (cyan) was modelled to dock against helices 3 and 4 of Vt (yellow), stabilised by a salt bridge (black dashed line) between D145 of paxillin and K996 of Vt. This binding interface is accessible, and orients LD2 in an N-C terminal position. Helices 3 and 4 are indicated. The position of D145 within the LD2 motif is highlighted.

Due to the orientation of the proposed LD2-binding site, it suggested that LD4 might bind to a region of vinculin structurally sequential to Vt. Similarly to FAK-FAT and characteristic of LD-binding sites, VD4 is a four-helix bundle and so was the most likely

candidate. Overlaying the crystal structures of VD4 and FAK-FAT revealed striking topographical similarities between the two (figure 57).

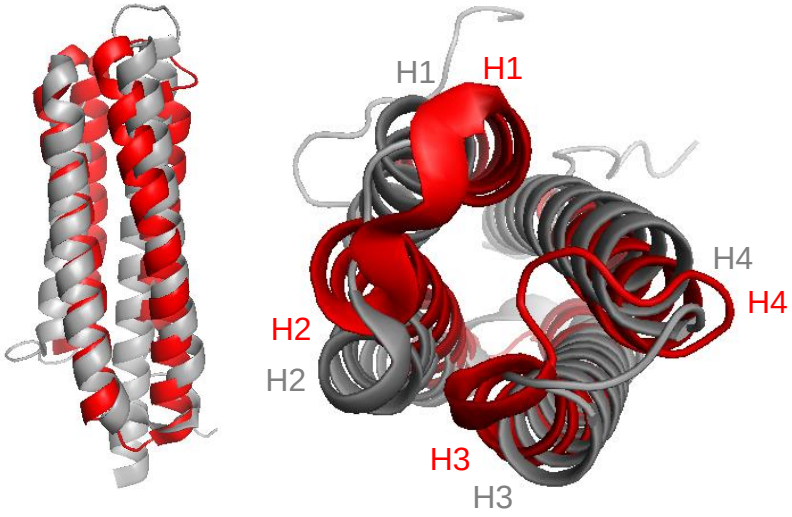

Figure 57. Topographical similarities of FAK-FAT and VD4. Helices 1-4 of the FAK-FAT domain (grey) were overlaid with helices 1-4 of VD4 (red). Helices are numbered accordingly.

LD4 binds preferentially to a hydrophobic pocket between helix 2 and helix 3 of FAK-FAT, directly opposite the LD2-binding interface (figure 58).

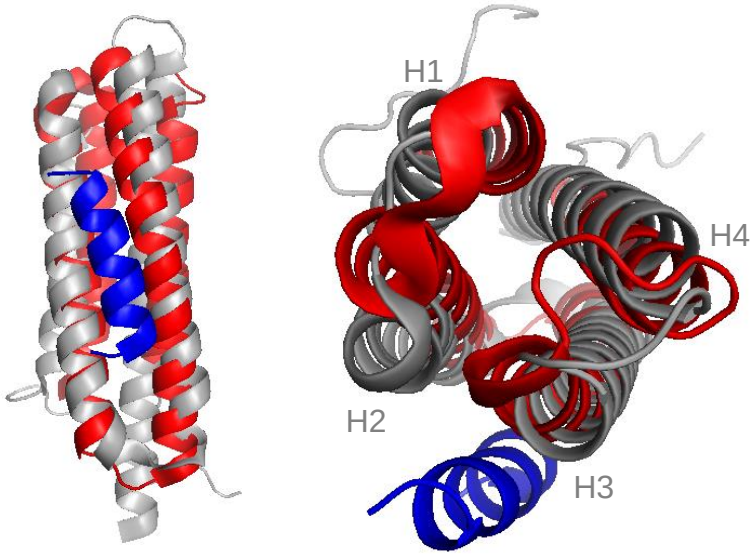

Figure 58. Strutural characteristics of the binding interface between paxillin LD4 and FAK-FAT. LD4 (blue) docks against helices 2 and 3 of the FAK-FAT domain (grey). No salt bridge is identified in the crystal structure, suggesting stabilisation of the interaction occurs via hydrophobic interactions.

Based on the topographical similarities between FAK-FAT and VD4, we were able to model a putative LD4 binding site onto the interface formed by helices 2 and 3 of VD4 with orientation as determined by LD2. No salt bridge could be determined, but hydrophobicity analysis suggests that the interaction is stabilised by hydrophobic interactions. Surface analysis confirmed that this binding site is accessible in the full-length vinculin structure, and orients LD4 in an N-C terminal position (figure 59).

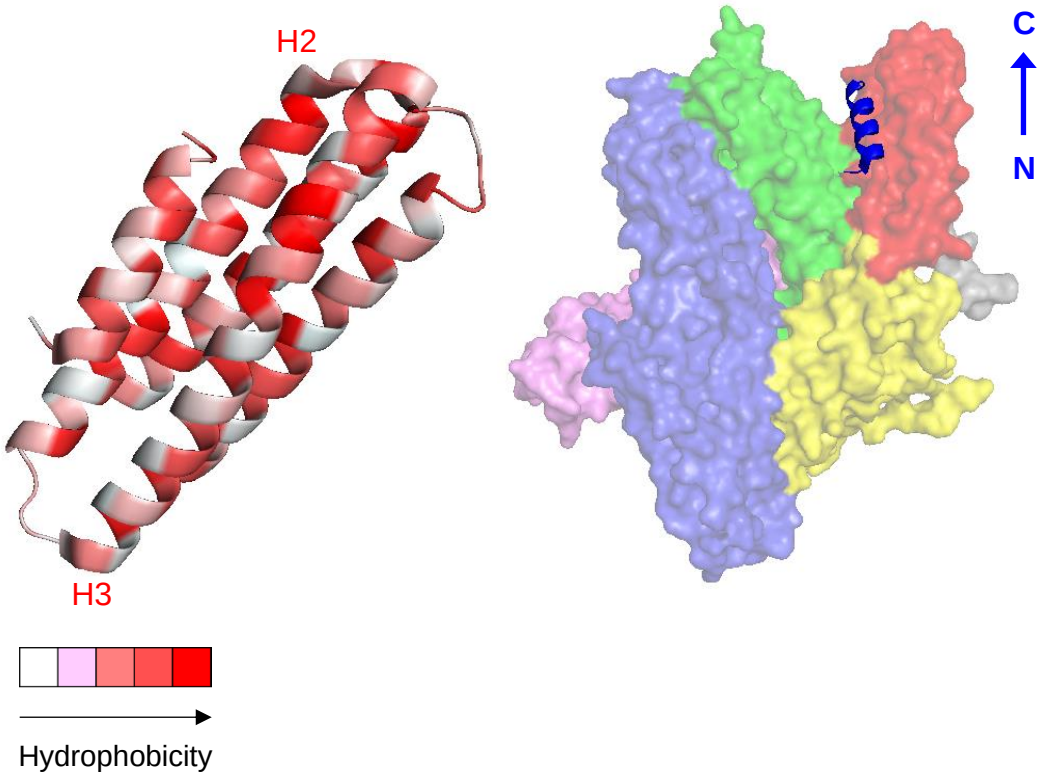

Figure 59. Proposed binding interface between paxillin LD4 and VD4.
LD4 was modelled to dock against helices 2 and 3 of VD4, stabilised by hydrophobic interactions (hydrophobic residues shown in red). This binding interface is accessible, and orients LD4 (blue ribbon) in an N-C terminal position. Helices 2 and 3 are indicated.

Since LD1 is adjacent in sequence to LD2, it was assumed that the LD1-binding interface would be limited to the proximity of the LD2 on the vinculin tail domain. Unlike VD4, VD1 contains two four-helix bundles connected by a long, centrally shared α-helix, and as such has two potential paxillin binding regions; helices 1-4 and helices

4-7. The four-helix FAK-FAT domain was again used to align with these two regions (figure 60).

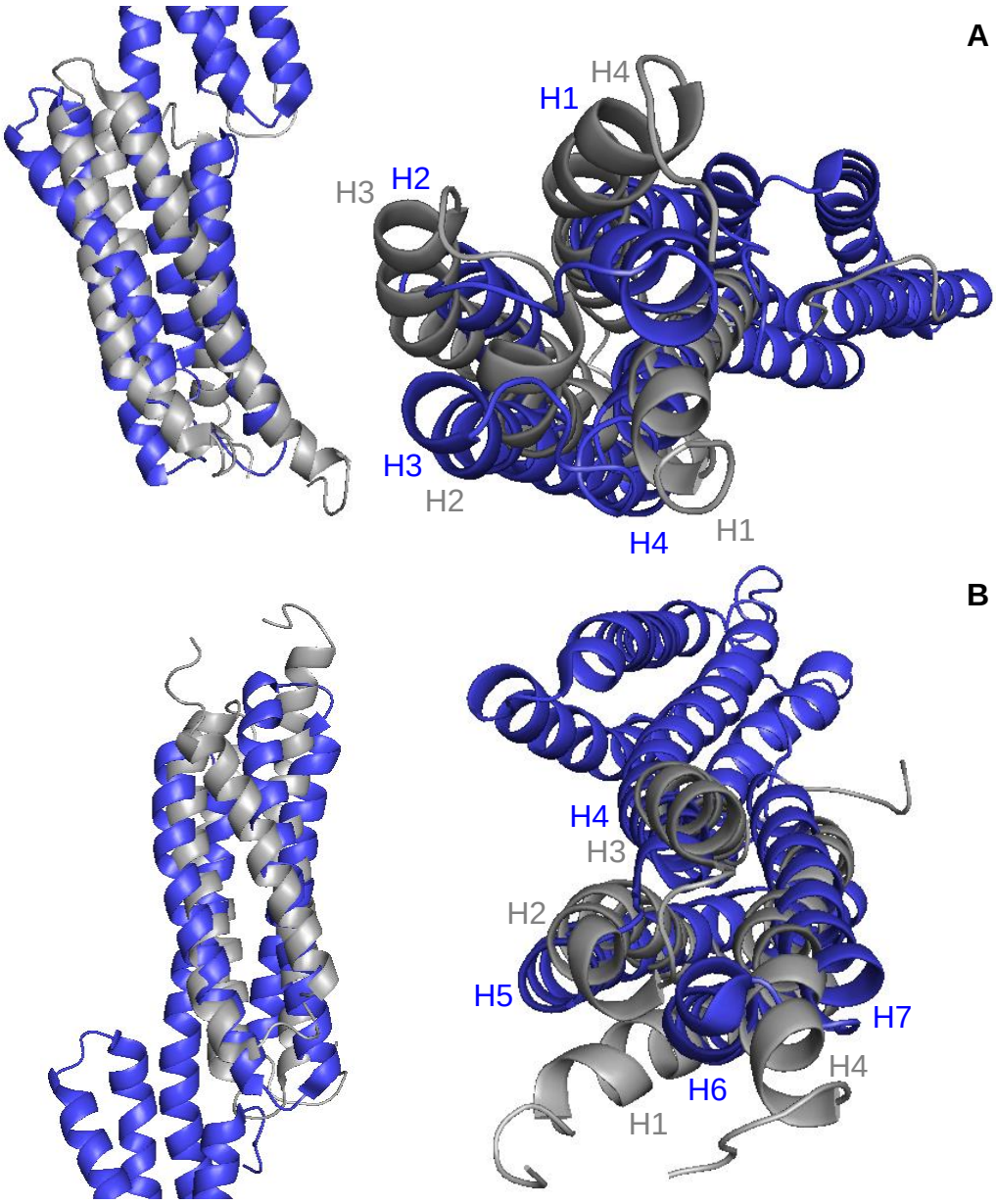

Figure 60. Topographical similarities of FAK-FAT and VD1. Helices 1-4 of the FAK-FAT domain (grey) were overlaid with helices 1-4 **(A)** and 4-7 **(B)** of VD1 (blue). Helices are numbered accordingly.

The four-helix bundle formed by helices 4 to 7 appeared to align more closely with the FAK-FAT domain compared to the bundle formed by helices 1-4, with greater similarities in helix length and angle. Analysis of the hydrophobicity of VD1 highlights

a hydrophobic interface formed within the C-terminal bundle, with helices 5 and 6 accessible on the surface. Modelling of LD1 against helices 5 and 6 in an orientation dictated by LD2 permits formation of a salt bridge between D10 of paxillin and K199 of helix 6 of VD1. Surface analysis confirmed that this binding site is accessible in the full-length vinculin structure, and orients LD1 in a C-N terminal position (figure 61).

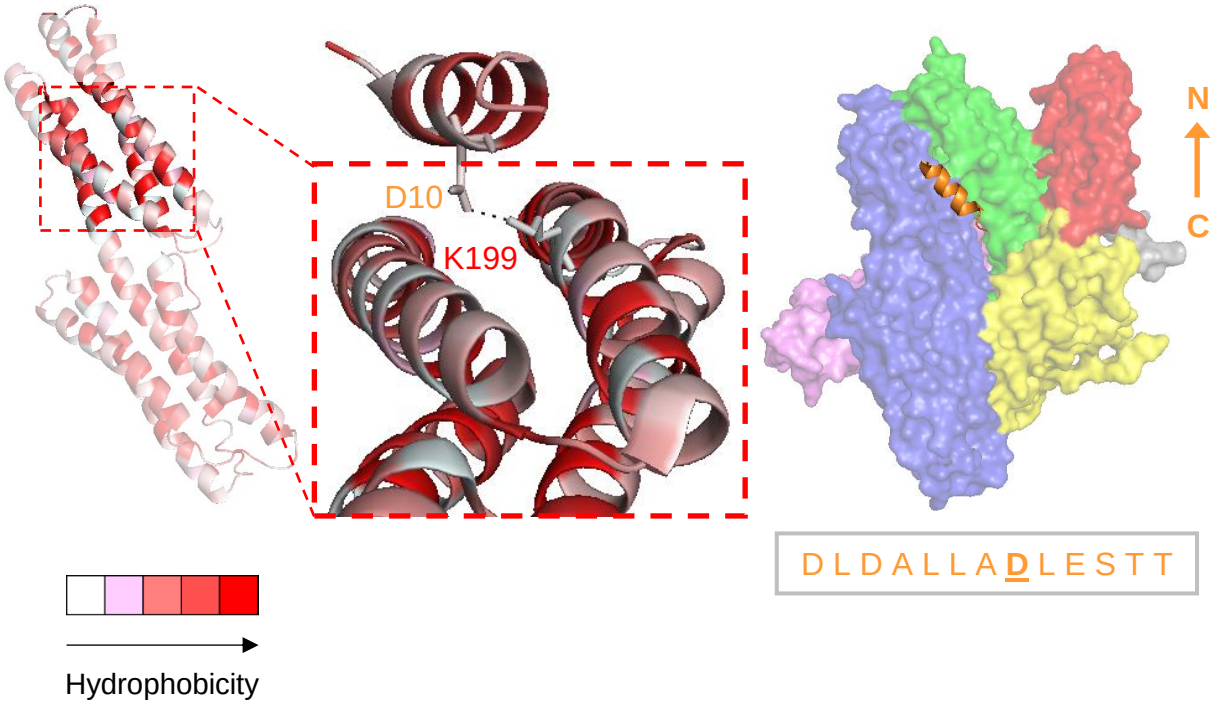

Figure 61. Proposed binding interface between paxillin LD1 and VD1. LD1 (orange) was modelled to dock against the hydrophobic core (hydrophobic residues shown in red) within helices 5 and 6 of VD1, stabilised by a salt bridge (shown as a black dashed line) between D10 of paxillin and K199 of helix 6. This binding interface is accessible, and orients LD1 in a C-N terminal position. The position of D10 within the LD1 motif is highlighted.

4.3.2. Proposed model of the paxillin facilitated autoinhibition of full-length vinculin.

Therefore, this detailed analysis of the putative binding sites between the multiple paxillin and vinculin interactions, enables us to build a proposed model of full-length vinculin bound by paxillin, which involves interactions of LD1, LD2 and LD4 with VD1,

Vt and VD4, respectively (figure 62). In this model, paxillin binds across the VD1-Vt interface, facilitating vinculin autoinhibition.

Cell motility is highly dynamic and requires the continual assembly and disassembly of adhesion complexes. Paxillin is recruited to the core adhesion scaffold downstream of FA maturation. Once at the adhesion site, paxillin only transiently associates with vinculin and/or talin. We have shown that multiple paxillin LD motifs can simultaneously engage the head and tail domains of vinculin, and this interaction has been hinted to hold the two vinculin domains in closer proximity. These factors combined suggest a regulatory role of paxillin, in which downstream recruitment of paxillin functions to disrupt the core adhesion complex by promoting closure of the open vinculin conformation and thus contributing to the disassembly of cell adhesions.

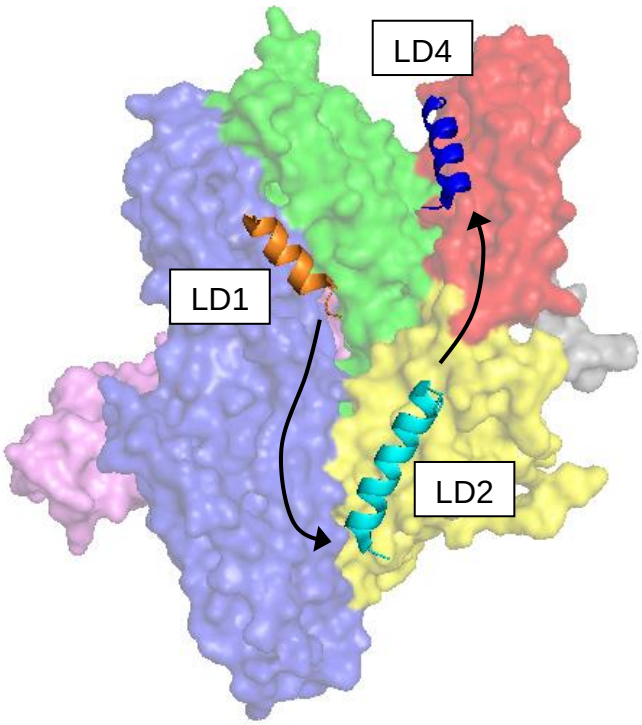

Figure 62. Proposed model of the vinculin-paxillin interaction. Surface model of LD1 (orange), LD2 (cyan) and LD4 (blue) of paxillin bound to VD1 (blue), Vt (yellow) and VD4 (red) of vinculin, respectively. The N-C terminal direction of the LD motifs is indicated by arrows.

4.4. Paxillin LIM domains are implicated in focal adhesion targeting.

Due in part to the complexity of the LIM domain structure, the role(s) of protein LIM domains has not been well studied biochemically. Insolubility of the paxillin LIM domains both in *pET-151* and when cleaved from glutathione *S*-transferase limited our biochemical investigations into how the four consecutive domains facilitate paxillin activity. However, GST-pulldown experiments have provided early indications that the LIM domains may function as discrete binding sites, capable of regulating the activation state of paxillin and recruiting paxillin to sites of cell-ECM adhesion.

Despite colocalizing with vinculin, paxillin recruitment to FAs is not impaired in assays using truncated vinculin constructs lacking the previously identified C-terminal paxillin-binding site (Humphries et al., 2007b). Although, in light of the data presented in this study whereby paxillin engages with the vinculin head, it remains to be established whether paxillin will be recruited in a vinculin null background. Additionally, paxillin constructs containing mutations that abrogate FAK binding localise effectively to FAs (Brown et al., 1996). Clearly, paxillin recruitment occurs via another mechanism.

Although limited, the current understanding of LIM domain function(s) suggests a role in focal adhesion targeting. The muscle-associated protein N-RAP is thought to serve as a mechanical linkage between the terminal actin filaments of myofibrils and protein complexes located beneath the sarcolemma (Luo et al., 1999). Interestingly, N-RAP comprises an N-terminal LIM domain which has been shown to bind talin with high affinity, and this interaction is suggested to target N-RAP to the cell membrane (Luo et al., 1999). The case for talin as the unknown protein responsible for paxillin recruitment is strengthened further by the observation that the two proteins colocalise almost identically both *in-vitro* and *in-vivo* (Humphries et al., 2007b).

Talin has already been proposed to recruit paxillin to FAs, although the N-terminal LD motifs, rather than the C-terminal LIM domains, were implicated in this interaction (Zacharchenko, Qian, Goult, Jethwa, et al., 2016b). In contrast to the FP data presented here in section 3.2.3, NMR demonstrated a 168±7.74μM affinity interaction between talin R8 and paxillin LD1. Although this interaction could not be identified in our study, it is interesting that reduced FA localisation of paxillin is observed in cells expressing a talin mutant lacking the R8 rod domain.

4.4.1. A novel interaction between talin and the paxillin LIM domains.

Of the three rod regions, R1-R3, R4-R8 and R9-R12, investigated, talin R9-R12 was identified to bind paxillin LIM 1-2 independently of LIM 3-4. The ability of paxillin LIM 1-2 to engage talin independently of LIM 3-4 suggests that, unlike a modular protein binding site, the four LIM domains can engage specific proteins independently of each other. It is interesting to note that talin R9 is the key helical bundle responsible for talin autoinhibition via direct interaction with F3 within the head domain (Goksoy et al., 2008a; Goult et al., 2009). Binding of paxillin to this region therefore supports a model whereby paxillin is recruited downstream of the activation of talin, possibly after the interaction between activated talin and vinculin, and thus downstream of FA formation. Multiple interactions may exist between paxillin and talin, as has been demonstrated between paxillin and vinculin, which could involve the synergistic engagement of both the paxillin LIM domains and LD motifs with various interfaces across the length of talin. Clearly the interaction between talin and paxillin requires further characterisation, including isolation of the specific talin bundle(s) involved, however GST pulldown assays presented here identify a novel interaction that could be a missing link in paxillin recruitment.

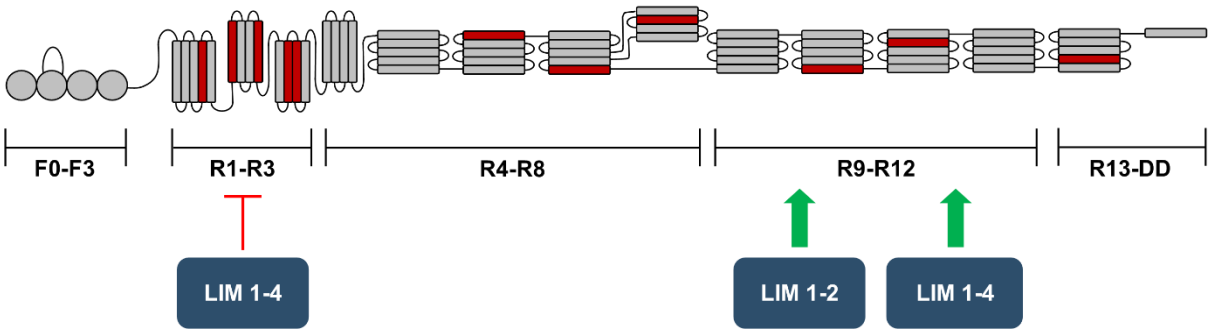

Figure 63. GST-pulldown assays identified an interaction between paxillin LIM 1-2 and talin R9-R12. GST-LIM 1-2 was found to bind talin R9-R12 independently of LIM 3-4. GST-LIM 1-4 was not found to bind talin R1-R3. Whether there are additional interactions between paxillin LIM 1-4 with talin F0-F3, R4-R8 and R13-DD remains to be investigated.

4.5. Paxillin activity may be regulated via an autoinhibitory mechanism involving the C-terminal LIM domains.

Cell adhesion and migration is highly dynamic and requires association and dissociation of specific proteins at a specific time and in a specific cellular location. To facilitate such a multifaceted process, layers of regulation have been uncovered that control protein recruitment, conformational state and binding affinity. One mechanism by which multiple focal adhesion-associated proteins regulate their conformational state and thus activation state is autoinhibition. As demonstrated by talin, vinculin and FAK, proteins can exist in a low-affinity closed conformation by association of intraprotein domains. Disruption of this interface results in protein activation, often by exposure of ligand binding sites (vinculin) or catalytic domains (FAK), for example. Identification of multiple intraprotein cross-links between the N-terminal LD region and C-terminal LIM domains of paxillin (Böttcher et al., 2017) suggest that paxillin activity may too be regulated by this mechanism (figure 51, section 3.2.3).

All but one cross-link was identified to involve LIM 3-4. The identification of a novel interaction between talin R9-R12 and LIM 1-2 in this work revealed that the LIM

domains can function as discrete binding sites. The observation that LIM 1-2 is predominately absent from the detected paxillin cross-links, in addition to the ability of LIM 1-2 to engage talin, suggests a mechanism of paxillin autoinhibition mediated by LIM 3-4.

In support of this hypothesis, GST-LIM 1-4 successfully pulled down paxillin LD1-5 in our GST-pulldown assay. This confirmed that paxillin can autoinhibit by a head-tail interaction, whereby the LD 1-5 directly interacts with the LIM1-4. However, it proved challenging to dissect this interaction further. The results with GST-LIM 1-2 were less clear. Although a band at approximately 40 kDa was observed in the supernatant, identification of this band by SDS-PAGE analysis alone was not possible since GST-LIM 1-2 and paxillin LD1-5 differ by only 3.5 kDa, meaning their respective bands likely overlap on the gel. Further analysis via mass spectrometry is therefore required to determine whether LIM 1-2, in addition to LIM 3-4, engage the N-terminal LD region.

Inability to purify GST-LIM 3-4 limited our biochemical investigations into paxillin regulation. Additionally, cleavage of glutathione *S*-transferase would have allowed further characterisation of the paxillin LIM-LD interaction by more informative results such as FP, MST and structural studies. However, the results presented here provide early indications that paxillin activity is regulated via an autoinhibitory mechanism in which the LIM domains engage the N-terminal region, thus holding paxillin in a low-affinity state in which key ligand-binding sites are hidden (figure 64).

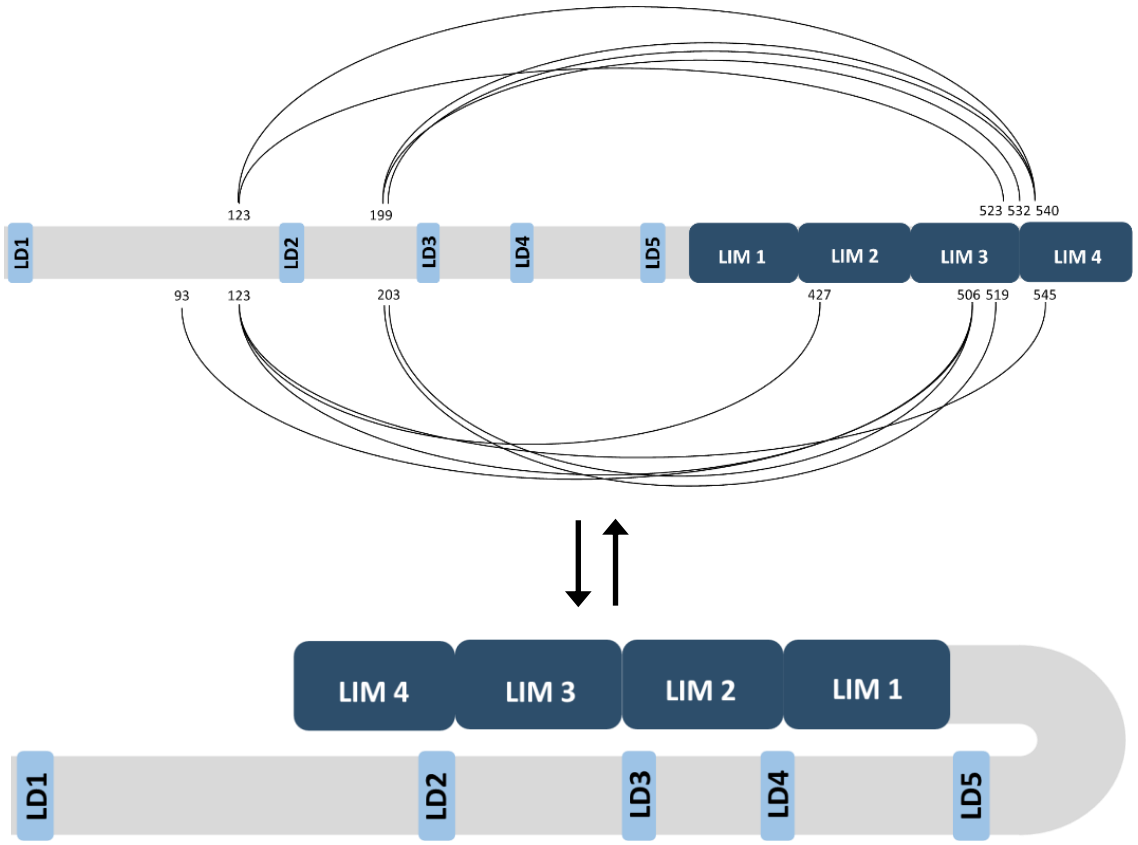

Figure 64. Predicted conformational switching between an open and closed paxillin conformation.

4.6. Future work.

Based on the *in-vitro* data presented in this thesis, we hypothesise that paxillin functions to control the activation state of vinculin. However, this remains to be tested in a cellular context. Constitutively active vinculin is lethal in flies (Maartens et al., 2016). We therefore predict that cooperative binding of the paxillin LD motifs will suppress this lethality by switching vinculin from an active to inactive state, similar to that modelled in figure 62. To test whether this is the case, we plan to cross paxillin LD1-5 with constitutively active vinT12.

Binding of paxillin to the FAK-FAT domain may provide a further layer of regulation controlling the activation state of vinculin. Cooperative, high-affinity binding of multiple

LD motifs to the FAT domain, as presented in section 3.1.6, may function to outcompete and unravel the paxillin-vinculin interaction, thus resulting in more active vinculin. This is something we could validate *in vivo* using cell biology techniques.

The structure of the paxillin-vinculin interaction presented in figure 62 is only a model, and we therefore aim to crystallise this complex, in addition to the structure of the talin-paxillin LIM interaction. Further structural analysis will enable the design of mutations that disrupt both the paxillin-vinculin and paxillin-talin interactions, and which can be tested in a cellular context to try and unpick the complexity of adhesion dynamics.

4.7. Final conclusions.

Within this study, we have presented evidence of multiple new pieces of the puzzle of adhesion assembly. These include;

1. A novel interaction in which multiple paxillin LD motifs simultaneously bind the head and tail domains of vinculin with high-affinity. We propose that through this interaction, paxillin functions to facilitate the autoinhibition of vinculin by regulating its conformational state.

2. A novel interaction between the paxillin LIM domains and talin R9-R12. The biochemical mechanism of paxillin recruitment to focal adhesions is yet to be established. However, from this report we propose that talin might be coordinating paxillin localisation, capable of positioning paxillin in proximity to vinculin. One possibility that arises from this finding is that upon talin activation and exposure of the R9 domain it then serves to recruit paxillin to the adhesion site.

Evidence within this study highlights paxillin as far more than a simple scaffold protein. Instead, we propose a model whereby, subsequent to FA formation via integrin, talin and vinculin, talin-mediated recruitment of autoinhibited paxillin via LIM domains 1 and

2 positions paxillin in proximity with vinculin at the adhesion site. Paxillin activation, possibly by being brought into close proximity with vinculin, or by another mechanism yet to be established, triggers cooperative, high-affinity binding of paxillin LD1, 2 and 4 across the head-tail interface; enabling paxillin to regulate the activation state of vinculin (figure 65).

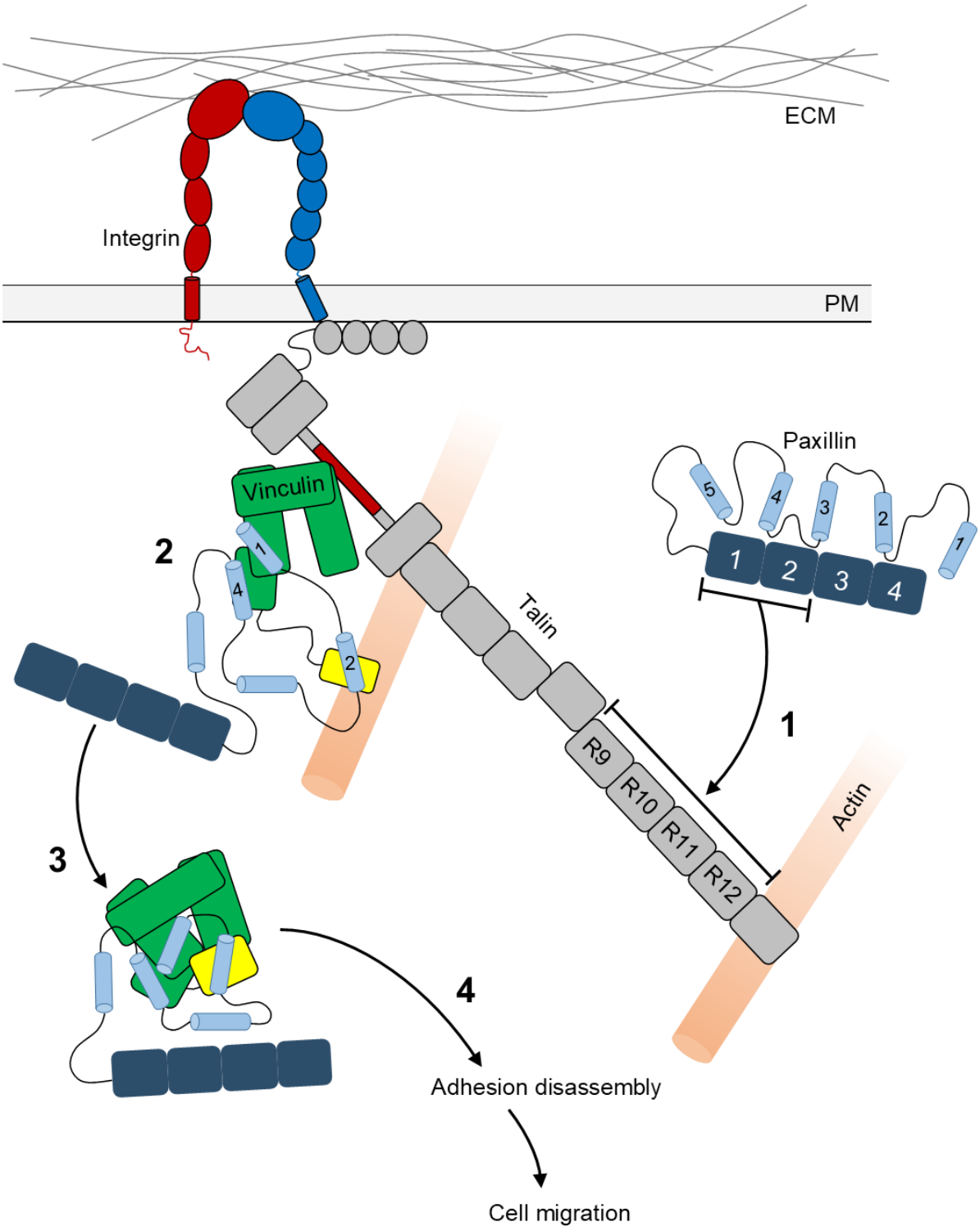

Figure 65. Proposed model of paxillin function within FA dynamics. Binding of talin F3 to the β-integrin tail facilitates integrin activation and subsequent engagement of the ECM. Engagement of actin via talin triggers actomyosin contraction sufficient to expose VBS (red) within the mechanosensitive rod domain. Autoinhibited vinculin (head domain; green, tail domain; yellow) is recruited to the VBS. Affinity of the head and tail domains for talin and actin, respectively, overcomes the autoinhibitory head-tail association and facilitates adhesion strengthening. **(1)** Talin R9-R12 (indicated) recruits autoinhibited paxillin via LIM domains 1 and 2 and positions paxillin in

proximity with vinculin. **(2)** LD1, 2 and 4 of paxillin engage VD1, Vt and VD4 of vinculin, respectively. **(3)** The paxillin-vinculin interaction outcompetes talin and actin and promotes reassociation of the vinculin head and tail domains. **(4)** Loss of vinculin-mediated structural integrity enables rapid turnover and reassembly of the mechanical linkages required for cell migration.

Bibliography

Adair, B. D., & Yeager, M. (2002). Three-dimensional model of the human platelet integrin alpha IIbbeta 3 based on electron cryomicroscopy and x-ray crystallography. *Proceedings of the National Academy of Sciences of the United States of America*, *99*(22), 14059–14064. https://doi.org/10.1073/pnas.212498199

Anthis, N. J., Wegener, K. L., Ye, F., Kim, C., Goult, B. T., Lowe, E. D., … Campbell, I. D. (2009). The structure of an integrin/talin complex reveals the basis of inside-out signal transduction. *The EMBO Journal*, *28*, 3623–3632. https://doi.org/10.1038/emboj.2009.287

Arold, S. T., Hoellerer, M. K., & Noble, M. E. M. (2002). The structural basis of localization and signaling by the focal adhesion targeting domain. *Structure (London, England : 1993)*, *10*(3), 319–327. Retrieved from http://www.ncbi.nlm.nih.gov/pubmed/12005431

Ashok Kumar, T. (2013). CFSSP: Chou and Fasman Secondary Structure Prediction server. *Wide Spectrum*, *1*(9), 15–19. https://doi.org/10.5281/zenodo.50733

Atherton, P., Lausecker, F., Carisey, A., Gilmore, A., Critchley, D., Barsukov, I., & Ballestrem, C. (2019). Force-independent interactions of talin and vinculin govern integrin-mediated mechanotransduction. *BioRxiv*, 629683. https://doi.org/10.1101/629683

Bakolitsa, C., Cohen, D. M., Bankston, L. A., Bobkov, A. A., Cadwell, G. W., Jennings, L., … Liddington, R. C. (2004). Structural basis for vinculin activation at sites of cell adhesion. *Nature*, *430*(6999), 583–586. https://doi.org/10.1038/nature02610

Bate, N., Gingras, A. R., Bachir, A., Horwitz, R., Ye, F., Patel, B., … Critchley, D. R. (2012). Talin contains a C-terminal calpain2 cleavage site important in focal adhesion dynamics. *PloS One*, *7*(4), e34461. https://doi.org/10.1371/journal.pone.0034461

Bertolucci, C. M., Guibao, C. D., & Zheng, J. (2005a). Structural features of the focal adhesion kinase-paxillin complex give insight into the dynamics of focal adhesion assembly. *Protein Science : A Publication of the Protein Society*, *14*(3), 644–652. https://doi.org/10.1110/ps.041107205

Bertolucci, C. M., Guibao, C. D., & Zheng, J. (2005b). Structural features of the focal adhesion kinase-paxillin complex give insight into the dynamics of focal adhesion assembly. *Protein Science*, *14*(3), 644–652. https://doi.org/10.1110/ps.041107205

Borgon, R. A., Vonrhein, C., Bricogne, G., Bois, P. R. J., & Izard, T. (2004a). Crystal structure of human vinculin. *Structure (London, England : 1993)*, *12*(7), 1189–1197. https://doi.org/10.1016/j.str.2004.05.009

Borgon, R. A., Vonrhein, C., Bricogne, G., Bois, P. R. J., & Izard, T. (2004b). Crystal Structure of Human Vinculin. *Structure*, *12*(7), 1189–1197. https://doi.org/10.1016/J.STR.2004.05.009

Böttcher, R. T., Veelders, M., Rombaut, P., Faix, J., Theodosiou, M., Stradal, T. E., … Fässler, R. (2017a). Kindlin-2 recruits paxillin and Arp2/3 to promote membrane protrusions during initial cell spreading. *The Journal of Cell Biology*, *216*(11), 3785–3798. https://doi.org/10.1083/jcb.201701176

Böttcher, R. T., Veelders, M., Rombaut, P., Faix, J., Theodosiou, M., Stradal, T. E., … Fässler, R. (2017b). Kindlin-2 recruits paxillin and Arp2/3 to promote membrane protrusions during initial cell spreading. *The Journal of Cell Biology*, *216*(11), 3785–3798. https://doi.org/10.1083/jcb.201701176

Brown, M. C., Perrotta, J. A., & Turner, C. E. (1996). Identification of LIM3 as the principal determinant of paxillin focal adhesion localization and characterization of a novel motif on paxillin directing vinculin and focal adhesion kinase binding. *The Journal of Cell Biology*, *135*(4), 1109–1123. Retrieved from http://www.ncbi.nlm.nih.gov/pubmed/8922390

Burridge, K., & Connell, L. (1983). A new protein of adhesion plaques and ruffling membranes. *The Journal of Cell Biology*. https://doi.org/10.1083/jcb.97.2.359

Burridge, K., & Feramisco, J. R. (1980). Microinjection and localization of a 130K protein in living fibroblasts: a relationship to actin and fibronectin. *Cell*, *19*(3), 587–595. https://doi.org/10.1016/s0092-8674(80)80035-3

Burridge, K., Turner, C. E., & Romer, L. H. (1992). Tyrosine phosphorylation of paxillin and pp125FAK accompanies cell adhesion to extracellular matrix: a role in cytoskeletal assembly. *The Journal of Cell Biology*, *119*(4), 893–903. https://doi.org/10.1083/jcb.119.4.893

Calderwood, D. A., Zent, R., Grant, R., Rees, D. J. G., Hynes, R. O., & Ginsberg, M. H. (1999). The talin head domain binds to integrin β subunit cytoplasmic tails and regulates integrin activation. *Journal of Biological Chemistry*. https://doi.org/10.1074/jbc.274.40.28071

Case, L. B., Baird, M. A., Shtengel, G., Campbell, S. L., Hess, H. F., Davidson, M. W., & Waterman, C. M. (2015). Molecular mechanism of vinculin activation and nanoscale spatial organization in focal adhesions. *Nature Cell Biology*, *17*(7), 880–892. https://doi.org/10.1038/ncb3180

Chen, H., Choudhury, D. M., & Craig, S. W. (2006). Coincidence of actin filaments and talin is required to activate vinculin. *Journal of Biological Chemistry*, *281*(52), 40389–40398. https://doi.org/10.1074/jbc.M607324200

Choi, C. K., Vicente-Manzanares, M., Zareno, J., Whitmore, L. A., Mogilner, A., & Horwitz, A. R. (2008). Actin and α-actinin orchestrate the assembly and maturation of nascent adhesions in a myosin II motor-independent manner. *Nature Cell Biology*. https://doi.org/10.1038/ncb1763

Cooley, M. A., Broome, J. M., Ohngemach, C., Romer, L. H., & Schaller, M. D. (2000). Paxillin Binding Is Not the Sole Determinant of Focal Adhesion Localization or Dominant-Negative Activity of Focal Adhesion Kinase/Focal Adhesion Kinase-related Nonkinase. *Molecular Biology of the Cell*, *11*(9), 3247–3263. https://doi.org/10.1091/mbc.11.9.3247

Côté, J.-F., Turner, C. E., & Tremblay, M. L. (1999). Intact LIM 3 and LIM 4 Domains of Paxillin Are Required for the Association to a Novel Polyproline Region (Pro

2) of Protein-Tyrosine Phosphatase-PEST. *Journal of Biological Chemistry*, *274*(29), 20550–20560. https://doi.org/10.1074/jbc.274.29.20550

Durrant, T. N., van den Bosch, M. T., & Hers, I. (2017). Integrin αIIbβ3 outside-in signaling. *Blood*, *130*(14), 1607–1619. https://doi.org/10.1182/blood-2017-03-773614

Elliott, P. R., Goult, B. T., Kopp, P. M., Bate, N., Grossmann, J. G., Roberts, G. C. K., … Barsukov, I. L. (2010). The Structure of the Talin Head Reveals a Novel Extended Conformation of the FERM Domain. *Structure*. https://doi.org/10.1016/j.str.2010.07.011

Geiger, B. (1979). A 130K protein from chicken gizzard: Its localization at the termini of microfilament bundles in cultured chicken cells. *Cell*, *18*(1), 193–205. https://doi.org/10.1016/0092-8674(79)90368-4

Geiger, B., Tokuyasu, K. T., Dutton, A. H., & Singer, S. J. (1980). Vinculin, an intracellular protein localized at specialized sites where microfilament bundles terminate at cell membranes. *Proceedings of the National Academy of Sciences of the United States of America*, *77*(7), 4127–4131. https://doi.org/10.1073/pnas.77.7.4127

Gill, G. N. (1995). The enigma of LIM domains. *Structure (London, England : 1993)*, *3*(12), 1285–1289. https://doi.org/10.1016/S0969-2126(01)00265-9

Gingras, A. R., Bate, N., Goult, B. T., Hazelwood, L., Canestrelli, I., Grossmann, J. G., … Critchley, D. R. (2008). The structure of the C-terminal actin-binding domain of talin. *The EMBO Journal*, *27*(2), 458–469. https://doi.org/10.1038/sj.emboj.7601965

Glenney, J. R., & Zokas, L. (1989). Novel tyrosine kinase substrates from Rous sarcoma virus-transformed cells are present in the membrane skeleton. *The Journal of Cell Biology*, *108*(6), 2401–2408. https://doi.org/10.1083/jcb.108.6.2401

Goksoy, E., Ma, Y.-Q., Wang, X., Kong, X., Perera, D., Plow, E. F., & Qin, J. (2008a). Structural Basis for the Autoinhibition of Talin in Regulating Integrin Activation. *Molecular Cell*, *31*(1), 124–133. https://doi.org/10.1016/j.molcel.2008.06.011

Goksoy, E., Ma, Y. Q., Wang, X., Kong, X., Perera, D., Plow, E. F., & Qin, J. (2008b). Structural Basis for the Autoinhibition of Talin in Regulating Integrin Activation. *Molecular Cell*. https://doi.org/10.1016/j.molcel.2008.06.011

Gough, R. E., & Goult, B. T. (2018). The tale of two talins – two isoforms to fine-tune integrin signalling. *FEBS Letters*. https://doi.org/10.1002/1873-3468.13081

Goult, B. T., Bate, N., Anthis, N. J., Wegener, K. L., Gingras, A. R., Patel, B., … Critchley, D. R. (2009). The structure of an interdomain complex that regulates talin activity. *The Journal of Biological Chemistry*, *284*(22), 15097–15106. https://doi.org/10.1074/jbc.M900078200

Goult, B. T., Yan, J., & Schwartz, M. A. (2018). Talin as a mechanosensitive signaling hub. *The Journal of Cell Biology*, *217*(11), 3776–3784. https://doi.org/10.1083/jcb.201808061

Goult, B. T., Zacharchenko, T., Bate, N., Tsang, R., Hey, F., Gingras, A. R., … Barsukov, I. L. (2013). RIAM and vinculin binding to talin are mutually exclusive and regulate adhesion assembly and turnover. *The Journal of Biological Chemistry*, *288*(12), 8238–8249. https://doi.org/10.1074/jbc.M112.438119

Guan, J. L., Trevithick, J. E., & Hynes, R. O. (1991). Fibronectin/integrin interaction induces tyrosine phosphorylation of a 120-kDa protein. *Cell Regulation*, *2*(11), 951–964. https://doi.org/10.1091/mbc.2.11.951

Hemmings, L., Rees, D. J., Ohanian, V., Bolton, S. J., Gilmore, A. P., Patel, B., … Critchley, D. R. (1996). Talin contains three actin-binding sites each of which is adjacent to a vinculin-binding site. *Journal of Cell Science*.

Herreros, L., Rodríguez-Fernandez, J. L., Brown, M. C., Alonso-Lebrero, J. L., Cabañas, C., Sánchez-Madrid, F., … Sánchez-Mateos, P. (2000). Paxillin localizes to the lymphocyte microtubule organizing center and associates with the microtubule cytoskeleton. *The Journal of Biological Chemistry*, *275*(34), 26436–26440. https://doi.org/10.1074/jbc.M003970200

Horton, E. R., Humphries, J. D., James, J., Jones, M. C., Askari, J. A., & Humphries, M. J. (2016). The integrin adhesome network at a glance. *Journal of Cell Science*. https://doi.org/10.1242/jcs.192054

Hu, Y.-L., Lu, S., Szeto, K. W., Sun, J., Wang, Y., Lasheras, J. C., & Chien, S. (2015). FAK and paxillin dynamics at focal adhesions in the protrusions of migrating cells. *Scientific Reports*, *4*(1), 6024. https://doi.org/10.1038/srep06024

Humphries, J. D., Wang, P., Streuli, C., Geiger, B., Humphries, M. J., & Ballestrem, C. (2007a). Vinculin controls focal adhesion formation by direct interactions with talin and actin. *The Journal of Cell Biology*, *179*(5), 1043–1057. https://doi.org/10.1083/jcb.200703036

Humphries, J. D., Wang, P., Streuli, C., Geiger, B., Humphries, M. J., & Ballestrem, C. (2007b). Vinculin controls focal adhesion formation by direct interactions with talin and actin. *The Journal of Cell Biology*, *179*(5), 1043–1057. https://doi.org/10.1083/jcb.200703036

Hynes, R. O. (2002). Integrins: bidirectional, allosteric signaling machines. *Cell*, *110*(6), 673–687. https://doi.org/10.1016/s0092-8674(02)00971-6

Izard, T., Evans, G., Borgon, R. A., Rush, C. L., Bricogne, G., & Bois, P. R. J. (2004). Vinculin activation by talin through helical bundle conversion. *Nature*, *427*(6970), 171–175. https://doi.org/10.1038/nature02281

Janssen, M. E. W., Kim, E., Liu, H., Fujimoto, L. M., Bobkov, A., Volkmann, N., & Hanein, D. (2006). Three-dimensional structure of vinculin bound to actin filaments. *Molecular Cell*, *21*(2), 271–281. https://doi.org/10.1016/j.molcel.2005.11.020

Jerabek-Willemsen, M., André, T., Wanner, R., Roth, H. M., Duhr, S., Baaske, P., & Breitsprecher, D. (2014). MicroScale Thermophoresis: Interaction analysis and beyond. *Journal of Molecular Structure*, *1077*, 101–113. https://doi.org/10.1016/J.MOLSTRUC.2014.03.009

Kanchanawong, P., Shtengel, G., Pasapera, A. M., Ramko, E. B., Davidson, M. W.,

Hess, H. F., & Waterman, C. M. (2010). Nanoscale architecture of integrin-based cell adhesions. *Nature*. https://doi.org/10.1038/nature09621

Kanner, S. B., Reynolds, A. B., Vines, R. R., & Parsons, J. T. (1990). Monoclonal antibodies to individual tyrosine-phosphorylated protein substrates of oncogene-encoded tyrosine kinases. *Proceedings of the National Academy of Sciences*, *87*(9), 3328–3332. https://doi.org/10.1073/pnas.87.9.3328

Karlsson, O., Thor, S., Norberg, T., Ohlsson, H., & Edlund, T. (1990). Insulin gene enhancer binding protein Isl-1 is a member of a novel class of proteins containing both a homeo-and a Cys–His domain. *Nature*, *344*(6269), 879–882. https://doi.org/10.1038/344879a0

Klapholz, B., & Brown, N. H. (2017, August 1). Talin - The master of integrin adhesions. *Journal of Cell Science*. Company of Biologists Ltd. https://doi.org/10.1242/jcs.190991

Luo, G., Herrera, A. H., & Horowits, R. (1999). Molecular interactions of N-RAP, a nebulin-related protein of striated muscle myotendon junctions and intercalated disks. *Biochemistry*, *38*(19), 6135–6143. https://doi.org/10.1021/bi982395t

Luo, G., Zhang, J. Q., Nguyen, T.-P., Herrera, A. H., Paterson, B., & Horowits, R. (1997). Complete cDNA sequence and tissue localization of N-RAP, a novel nebulin-related protein of striated muscle. *Cell Motility and the Cytoskeleton*, *38*(1), 75–90. https://doi.org/10.1002/(SICI)1097-0169(1997)38:1<75::AID-CM7>3.0.CO;2-G

Maartens, A. P., Wellmann, J., Wictome, E., Klapholz, B., Green, H., & Brown, N. H. (2016). Drosophila vinculin is more harmful when hyperactive than absent, and can circumvent integrin to form adhesion complexes. *Journal of Cell Science*, *129*(23), 4354–4365. https://doi.org/10.1242/jcs.189878

McCann, R. O., & Craig, S. W. (1997). The I/LWEQ module: a conserved sequence that signifies F-actin binding in functionally diverse proteins from yeast to mammals. *Proceedings of the National Academy of Sciences of the United States of America*, *94*(11), 5679–5684. https://doi.org/10.1073/pnas.94.11.5679

Miller, G. J., Dunn, S. D., & Ball, E. H. (2001). Interaction of the N- and C-terminal Domains of Vinculin. *Journal of Biological Chemistry*, *276*(15), 11729–11734. https://doi.org/10.1074/jbc.M008646200

Moerke, N. J. (2009). Fluorescence Polarization (FP) Assays for Monitoring Peptide-Protein or Nucleic Acid-Protein Binding. In *Current Protocols in Chemical Biology* (Vol. 1, pp. 1–15). Hoboken, NJ, USA: John Wiley & Sons, Inc. https://doi.org/10.1002/9780470559277.ch090102

Patel, B., Gingras, A. R., Bobkov, A. A., Fujimoto, L. M., Zhang, M., Liddington, R. C., … Critchley, D. R. (2006). The activity of the vinculin binding sites in talin is influenced by the stability of the helical bundles that make up the talin rod. *The Journal of Biological Chemistry*, *281*(11), 7458–7467. https://doi.org/10.1074/jbc.M508058200

Roberts, G. C. K., & Critchley, D. R. (2009). Structural and biophysical properties of the integrin-associated cytoskeletal protein talin. *Biophysical Reviews*, *1*(2), 61–69. https://doi.org/10.1007/s12551-009-0009-4

Schaller, M. D. (2001). Paxillin: a focal adhesion-associated adaptor protein. *Oncogene*, *20*(44), 6459–6472. https://doi.org/10.1038/sj.onc.1204786

Schaller, M. D., Borgman, C. A., Cobb, B. S., Vines, R. R., Reynolds, A. B., & Parsons, J. T. (1992). pp125FAK a structurally distinctive protein-tyrosine kinase associated with focal adhesions. *Proceedings of the National Academy of Sciences*, *89*(11), 5192–5196. https://doi.org/10.1073/pnas.89.11.5192

Seidel, S. A. I., Dijkman, P. M., Lea, W. A., van den Bogaart, G., Jerabek-Willemsen, M., Lazic, A., … Duhr, S. (2013). Microscale thermophoresis quantifies biomolecular interactions under previously challenging conditions. *Methods*, *59*(3), 301–315. https://doi.org/10.1016/j.ymeth.2012.12.005

Shattil, S. J., Kim, C., & Ginsberg, M. H. (2010, April). The final steps of integrin activation: The end game. *Nature Reviews Molecular Cell Biology*. https://doi.org/10.1038/nrm2871

Sheffield, P., Garrard, S., & Derewenda, Z. (1999). Overcoming Expression and Purification Problems of RhoGDI Using a Family of “Parallel” Expression Vectors. *Protein Expression and Purification*, *15*(1), 34–39. https://doi.org/10.1006/prep.1998.1003

Spriestersbach, A., Kubicek, J., Schäfer, F., Block, H., & Maertens, B. (2015). *Purification of His-Tagged Proteins*. *Methods in Enzymology* (Vol. 559). Academic Press. https://doi.org/10.1016/BS.MIE.2014.11.003

Tschammer, N., Weigert, S., Galinec, S., Muller, Y., You, C., Piehler, J., & Breitsprecher, D. (2016). Protein Labeling One-step, purification-free and site-specific labeling of polyhistidine-tagged proteins for MST. *Protein Labeling Application Note NT-MO-29*.

Tumbarello, D. A., Brown, M. C., & Turner, C. E. (2002). The paxillin LD motifs. *FEBS Letters*, *513*(1), 114–118. https://doi.org/10.1016/S0014-5793(01)03244-6

Turner, C. E. (2000). Paxillin and focal adhesion signalling. *Nature Cell Biology*, *2*(12), E231–E236. https://doi.org/10.1038/35046659

Turner, C. E., Glenney, J. R., & Burridge, K. (1990). Paxillin: a new vinculin-binding protein present in focal adhesions. *The Journal of Cell Biology*, *111*(3), 1059–1068. Retrieved from http://www.ncbi.nlm.nih.gov/pubmed/2118142

Turner, C. E., & Miller, J. T. (1994). Primary sequence of paxillin contains putative SH2 and SH3 domain binding motifs and multiple LIM domains: identification of a vinculin and pp125Fak-binding region. *Journal of Cell Science*, *107 (Pt 6)*, 1583–1591. Retrieved from http://www.ncbi.nlm.nih.gov/pubmed/7525621

Valencia, C. A., Pervaiz, M. A., Husami, A., Qian, Y., & Zhang, K. (2013). Sanger Sequencing Principles, History, and Landmarks (pp. 3–11). Springer, New York, NY. https://doi.org/10.1007/978-1-4614-9032-6_1

Wegener, K. L., & Campbell, I. D. (2008). Transmembrane and cytoplasmic domains in integrin activation and protein-protein interactions (Review). *Molecular Membrane Biology*. KLW. https://doi.org/10.1080/09687680802269886

Wood, C. K., Turner, C. E., Jackson, P., & Critchley, D. R. (1994). Characterisation of the paxillin-binding site and the C-terminal focal adhesion targeting sequence

in vinculin. *Journal of Cell Science*, *107 (Pt 2)*, 709–717. Retrieved from http://www.ncbi.nlm.nih.gov/pubmed/8207093

Xiong, J.-P., Stehle, T., Diefenbach, B., Zhang, R., Dunker, R., Scott, D. L., … Amin Arnaout, M. (2001). Crystal Structure of the Extracellular Segment of Integrin αVβ3. *Science*, *294*(5541), 339–345. https://doi.org/10.1126/science.1064535

Yamada, K. M., Collins, J. W., Cruz Walma, D. A., Doyle, A. D., Morales, S. G., Lu, J., … Wang, S. (2019). Extracellular matrix dynamics in cell migration, invasion and tissue morphogenesis. *International Journal of Experimental Pathology*, *100*(3), 144–152. https://doi.org/10.1111/iep.12329

Yamada, K. M., & Geiger, B. (1997). Molecular interactions in cell adhesion complexes. *Current Opinion in Cell Biology*, *9*(1), 76–85. Retrieved from http://www.ncbi.nlm.nih.gov/pubmed/9013677

Yao, M., Goult, B. T., Chen, H., Cong, P., Sheetz, M. P., & Yan, J. (2015). Mechanical activation of vinculin binding to talin locks talin in an unfolded conformation. *Scientific Reports*, *4*(1), 4610. https://doi.org/10.1038/srep04610

Yao, M., Goult, B. T., Klapholz, B., Hu, X., Toseland, C. P., Guo, Y., … Yan, J. (2016). The mechanical response of talin. *Nature Communications*, *7*(1), 11966. https://doi.org/10.1038/ncomms11966

Zacharchenko, T., Qian, X., Goult, B. T., Critchley, D. R., Lowy, D. R., & Barsukov Correspondence, I. L. (2016). LD Motif Recognition by Talin: Structure of the Talin-DLC1 Complex Accession Numbers 5FZT. https://doi.org/10.1016/j.str.2016.04.016

Zacharchenko, T., Qian, X., Goult, B. T., Jethwa, D., Almeida, T. B., Ballestrem, C., … Barsukov, I. L. (2016a). LD Motif Recognition by Talin: Structure of the Talin-DLC1 Complex. *Structure (London, England : 1993)*, *24*(7), 1130–1141. https://doi.org/10.1016/j.str.2016.04.016

Zacharchenko, T., Qian, X., Goult, B. T., Jethwa, D., Almeida, T. B., Ballestrem, C., … Barsukov, I. L. (2016b). LD Motif Recognition by Talin: Structure of the Talin-DLC1 Complex. *Structure*, *24*(7), 1130–1141. https://doi.org/10.1016/j.str.2016.04.016